2021

Behavior of exposed column base plate connection subjected to combined axial load and biaxial bending

Kabir, Md Asif Bin

BEHAVIOR OF EXPOSED COLUMN BASE PLATE CONNECTION SUBJECTED TO COMBINED AXIAL LOAD AND BIAXIAL BENDING

by

Md Asif Bin Kabir

A thesis
submitted to the Faculty of Graduate Studies
in partial fulfilment of the requirements for the
Degree of Master of Science
in

Civil Engineering

Supervisor

Dr. Muntasir Billah

Assistant Professor – Dept. of Civil Engineering

Lakehead University
Thunder Bay, Ontario
May 2021

Author's Declaration Page

I hereby declare that I am the sole author of this thesis. This is a true copy of the thesis, including any required final revisions, as accepted by my examiners. I understand that my thesis may be made electronically available to the public.

Abstract

Column base plate (CBP) connections are one of the most crucial structural components of steel structures that act as a transfer medium for all the forces and moments from the entire building into the foundation. Importance of this type of connection becomes significant when the structure experiences dynamic loading, such as wind or earthquake, which incorporates dynamic effects in the structure that need to be transferred to the foundation. Considerable research efforts have been made over the past few decades on CBP connections, which led to the publication of AISC Design Guide 1 (2006) for CBP design. This design guide is still widely used in the industry. All the previous studies and design guidelines considered only the uniaxial (major axis) bending moment combined with axial load for CBP connection design. However, very often the base plate experiences a bidirectional bending moment from lateral loads during any dynamic loading event. Although, the column is designed and checked under combined axial load and bi-axial bending, when it comes to the base plate connection, only the axial load and major axis bending are considered. Therefore, the objective of this research is to investigate the behavior of CBP connections subjected to combined axial load and biaxial bending through an extensive numerical parametric study, using general purpose finite element software ABAQUS. For this numerical study, an accurate nonlinear finite element (FE) model is developed, considering both geometric and material nonlinearities and validated against experimental results that are available in the literature subjected to monotonic and uniaxial cyclic loading. Validation results show that the developed FE model can effectively simulate force transfer at major contact interfaces in the connection. Concurrently, a database of CBP connection subjected to axial load and uniaxial bending, is constructed from the literature to identify the influential parameters as well as different failure modes of the CBP connection, using Machine Learning (ML) approach. Among nine different ML models, the Decision tree based ML model provides an overall accuracy of 91% for identifying the failure mode whereas base plate thickness, embedment length, and anchor rod diameter are found to be the influential parameters that govern the failure mode of CBP connections. Therefore, a total of 20 different FE models that have different base plate thicknesses and yield strengths, anchor bolt sizes and quantity as well as embedment lengths, grout thicknesses and axial load ratios are developed. Furthermore, a bidirectional symmetric lateral loading protocol is developed and applied with constant axial compressive load in the developed models. The study reveals that the thickness of base plate and anchor rod diameter are the governing parameters for

iii

different base connection behavior such as moment rotation response, maximum bolt tensile force, and yield line pattern of the base plate. Moreover, the rigidity of the base plate connection is found to be in the semi-rigid region under biaxial bending condition. Finally, this study found that the available methods for uniaxial bending overpredicts the connection rotational stiffness compared to the stiffness obtained from numerical analysis considering biaxial bending.

Acknowledgements

Table of Contents

List of Tables

List of Figures

Nomenclature

K_i Initial Stiffness of base connection

t_p Base plate thickness

F_{yp} Base plate yield strength

d Diameter of anchor rod

N No. of anchor rod

L Embedment length of anchor rod

t_g Grout thickness

p Center to center distance between the anchor rods in the direction of the load

M_p Plastic moment capacity

M Column base moment

θ Base rotation

F Lateral force at the column top

H_{col} Column height from the base plate

Δ_{top} Displacement at the top of the column

E_{col} Modulus of elasticity of the column

I_{col} Column's second moment of inertia in the direction of loading

T_u Maximum bolt tensile force

K_θ Base rotational stiffness

F_y Yield strength of column

EI Flexural rigidity

H Height of the column

$K_{y(FEM)}$ Connection stiffness at first yield for biaxial bending from FEM

$K_{y(K)}$ Connection stiffness at first yield for uniaxial bending from Kanvinde et al. (2012)

$K_{y(EU)}$ Connection stiffness at first yield for uniaxial bending from Eurocode 3

$K_{y(J)}$ Connection stiffness at first yield for uniaxial bending from AIJ (2001)

Chapter 1   Introduction

1.1 Background

Column base plate (CBP) connections are one of the most safety-critical components of steel structures since it carries all the vertical forces, shear, and moment from the entire structure and transfers them to the foundation. The components of a typical exposed CBP connection are the base plate, anchor bolts with nuts and washers, grout and concrete pedestal. A typical exposed CBP connection with its various components is shown in Figure 1.1. Failure of any of the components can induce the collapse of the entire structure since they directly contribute to the ductility demand and force distribution of the structure (Grauvilardell et al., 2005). Tremblay et al. (1995) and Midorikawa et al. (2012) outlined several issues with the exposed CBP connections experienced during the Northridge (1994), Kobe (1995), and Tohuku (2011) earthquakes. Exposed CBP connections are mostly used in low-rise steel structures all over the world and considerable research efforts have been made to identify the parameters which affect their strength and serviceability (DeWolf & Sarisley, 1980; Picard et al. 1987; Burda & Itani, 1999; Fahmy et al., 1999). These research outcomes led to the publication of the AISC Design Guide 1 (Fisher and Kloiber, 2006) for column base plate design, which is still widely used in the industry. All these previous studies and design guidelines focused on base plate design under axial load and uniaxial bending moment but very often these base plates are subjected to bidirectional bending moment from lateral loads such as wind and earthquake. Although, the columns are designed and checked under combined axial load and bi-axial bending, when it comes to the base plate connection, only the axial load and major axis bending are considered. Grauvilardell et al. (2005) reported that the performance of exposed CBP connection was not at a desired level in case of any lateral loading event. This means that the characterization of force and deformation demands, as well as the deformation capacities of the connection components and failure mechanisms, are yet to be well established especially when the CBP connection is subjected to combined axial load and biaxial bending. The research presented in this Thesis aims to investigate the behavior of W-shaped steel CBP connection under combined axial load and biaxial bending through extensive parametric numerical analysis. Additionally, this study utilizes the recent advancement of data-driven

Machine Learning (ML) techniques to develop a ML model for identifying the failure mode of CBP connections including its influential parameters.
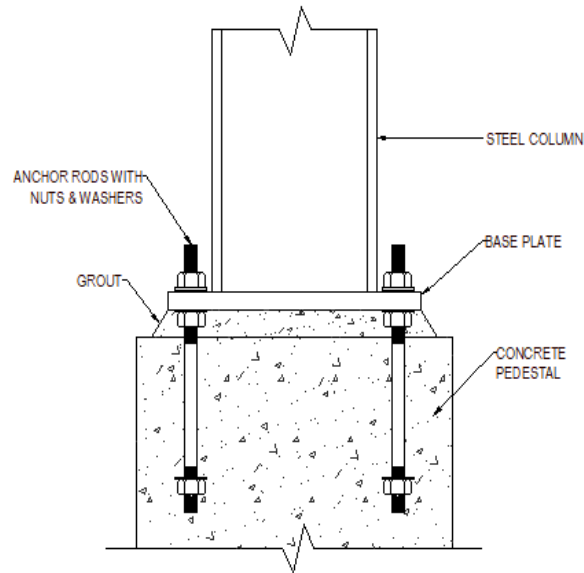
Figure 1.1 Typical exposed column base plate (CBP) connection and its components

1.2 Research Objectives

Severity of CBP connections becomes significant when the structure experiences dynamic loading such as wind or earthquake, which incorporates dynamic effects in the structure that need to be transferred to the foundation. As previous studies related to CBP connections considered only uniaxial bending (major axis) combined with axial load, the main goal of this research study is to obtain the quantitative understanding about the behavioral insight of different components of CBP connections subjected to combined axial load and biaxial bending through numerical parametric study. This is achieved through the pursuit of the following objectives:

1. To develop an accurate Finite Element (FE) model of CBP connections and substantiate the accuracy of the developed model based on the available experimental results.
2. To conduct a comprehensive parametric study through FE analysis considering different components of CBP connections.
3. To understand the behavioral insight of the CBP connections under combined axial load and bi-axial bending.
4. To develop data-driven Machine Learning (ML) model to identify the influential parameters as well as different failure modes of CBP connections.

2

5. To develop an open-source ML model with graphical user interface (GUI) that can be utilized to rapidly identify the failure modes of CBP connections with the scope for future improvement.

1.3 Organization of Thesis

This thesis performs extensive numerical analysis through FE simulations to investigate the behavioral insight of exposed CBP connections under combined axial load and biaxial bending. Additionally, the capability of data-driven ML techniques is explored to identify different failure modes of CBP connections including its influential parameters using different ML algorithms. **Chapter 1** provides a general introduction of exposed column base plate connections together with the scope and objectives of this thesis. **Chapter 2** presents a brief literature review, which overviews the previous experimental and analytical research works on column base plate connections. Moreover, a brief overview of different CBP failure modes and application of ML in structural engineering are discussed. **Chapter 3** details the data-driven ML techniques developed to identify the influential parameters as well as the different failure modes of CBP connections based on past experimental studies. **Chapter 4** describes the FE simulation which replicates the available experimental results from literature. The purpose of these simulation is to validate and generalize the experimental results by providing complete description of the general features of the developed FE model including the contact surfaces, material properties, boundary conditions, loading protocol, geometric imperfection, and mesh definitions. **Chapter 5** presents a numerical parametric study of different base plate connection components by considering the similar FE modeling techniques described in Chapter 4. The chapter concludes by presenting the simulation results and discussing the analytical findings from the FE simulations. **Chapter 6** concludes this Thesis by summarizing the conclusions and providing recommendations for future study on column base plate connections.

Chapter 2　　　Literature Review

2.1 Introduction

In steel moment-resisting frames, evidence of column base plate (CBP) connection damage was first reported after the 1964 Anchorage earthquake (Berg, 1964). Following this event, considerable amount of research on CBP connections was performed all around the world. This chapter provides a review of literature related to exposed CBP connections and motivation for current investigation. In particular, the literature review focuses on both experimental and numerical investigation of exposed CBP connections for flexural response. The chapter covers early-stage research efforts on CBP connections as well as the most recent research. Firstly, a brief overview of exposed CBP connection is provided followed by a detailed review of experimental research conducted on CBP connections to date. Then, numerical investigation on CBP connections is discussed followed by tabular representation of previous studies on CBP connections. Further, different types of failure mode of CBP connections are discussed. Finally, a summary of application of Machine Learning (ML) techniques to identify structural failure mode is provided to elucidate the appropriateness of ML for this research.

2.1 Column Base Plate Classification

Generally, CBP connections can be broadly classified as (a) exposed and (b) embedded, based on their position with respect to the foundation element that traditionally represent 'pinned' and 'fixed' supports, respectively. Although exposed CBP connections are widely used in low-rise steel moment resisting frames, their application in taller structures is infeasible (Grilli and Kanvinde, 2015). Researchers have classified exposed column base connections based on several criteria such as (a) base plate behavior, (b) amount of restraint provided, (c) steel failure mode, (d) concrete failure mode, (e) energy dissipation capacity, and (f) type of frame.

2.1.1 Classification According to Base Plate Behavior

Astaneh et al. (1992) and Fahmy (1999) classified base plate connection according to the thickness required to form a plastic hinge in the base plate. Figure 2.1 illustrates a schematic representation of three types of CBP connections based on base plate behavior and their deformed shapes.
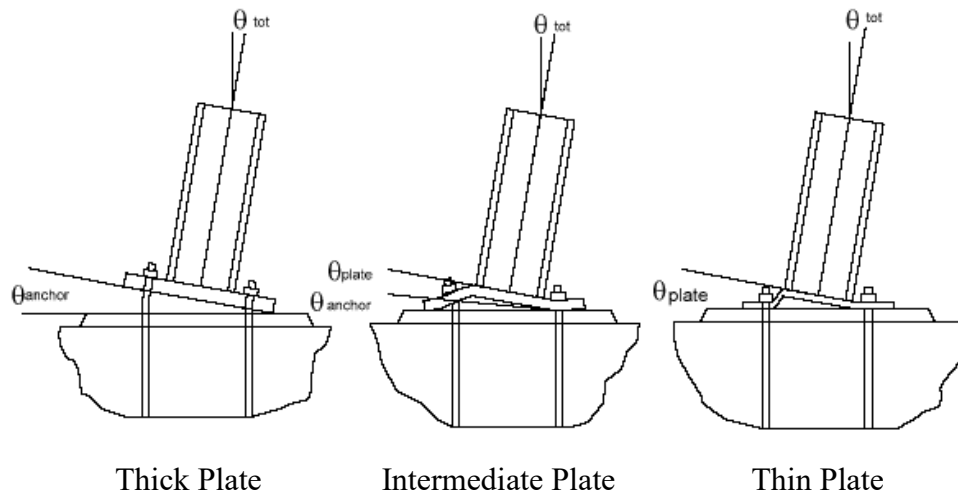
Figure 2.1 Types of base plate behavior (Adapted from Astaneh et al., 1992)

Thick/Rigid Plate: Column base connections with thick base plates are considered as the most rigid among the three types of classification summarized in this section. Although rigid, these type of CBP connections very often experience a non-ductile behavior due to fracture of anchor rods or crushing and spalling of the grout during large rotations (Grauvilardell et al., 2005). Sato (1987) proposed "yield ratio" parameter to achieve a ductile behavior while designing the anchor rod. The "yield ratio" was defined as the ratio between the yield strength and the tensile strength of the bolt. It was reported that behavior of anchor rod became ductile when the ratio between the threaded and the non-threaded cross section area of the bolt was greater than the yield ratio. This indicated that higher area of anchor rods would be able to withstand higher deformation of column base without fracture of the anchor rods. Sato (1987) conducted experiments with stiffer base plate and reported that stiffer base plates could guarantee the rotation of the column resulting from elongation of the anchor rod and concrete compressive deformation only. It was also reported that under cyclic loading, ductile behavior was observed using low yield ratio anchor rods without rupture experiencing higher rotations, whereas anchor rods with higher yield ratio ruptured at lower rotations, although showing ductile behavior.

Intermediate/Semi-rigid Plate: Lee and Goel (2001) expressed their concerns about designing the base plate following AISC provisions stating that it might not behave as expected due to yielding of the base plate. They suggested that the failure of anchor rods in tension needed to be considered, which might be the governing case. Astaneh et al. (1992) claimed that less flexible

base plates along with less bending deformation could cause damage to the grout and result in the tension fracture of the anchor rods.

Thin/Flexible Plate: Column base connections associated with thin base plates are specified as flexible where ductile behavior is achieved through the inelasticity in the base plate itself. Yield lines are expected to form along the flanges of the column. However, very thin base plates can form 45º yield lines at the corners of the base plate (Grauvilardell et al., 2005). The rest of the components of CBP connections such as anchor rods, grout, and concrete foundation are considered as elastic. This type of inelastic deformation of the base plate may help to lessen seismic response by acting as an isolator for the structure during any seismic event.

2.1.2 Classification According to Amount of Restrained Provided

Three type of classifications such as pinned, fixed, and partially restrained are available under this category of CBP connection.

Pinned: Grauvilardell et al. (2005) reported that no exposed base plate had behaved as a pure simple connection. Picard and Beaulieu (1985) demonstrated through experimental investigation that commonly assumed pinned connections with two anchor rods in the CBP connection showed a stable partial restraint behavior. Melchers (1992) derived moment-rotation diagrams to provide designers a formulation to implement in the frame analysis. CBP connections considered as pinned supports have been proven to reduce the response of the structures under seismic actions.

Fixed: Fixed CBP connections can be closely compared with the rigid connection. Fahmy (1999) demonstrated through parametric studies that CBP connections with rigid base plates responded similar to those with fixed supports in terms of drifts and moments. Wald and Jaspart (1998) proposed limiting values which are still in use for Eurocode 3 for the connection's initial stiffness (K_i) to classify rigid CBP connection. Eurocode 3 uses a limiting value of $K_i \geq 30\ EI/L$ to establish a rigid connection and $K_i < 0.5\ EI/L$ for pinned connections where E, I and L are the modulus of elasticity, second moment of inertia, and length of the column, respectively. Column bases with initial stiffness within these two limits are classified as semi-rigid.

Partially Restrained: Column base connections for structures with gravity and moderate lateral loads may present typical simple classifications "fixed" or "pinned." However, Astenah et al. (1992) reported that CBP connections, when subjected to inelastic cycles, could act as a "semi-rigid" connection. Yamada and Akiyama (1997) as well as Kawano and Matsui (1998) had shown

through analytical studies that partially restrained column bases distributed the story drift and formation of plastic hinges more evenly than perfectly fixed ones.

2.1.3 Classification According to Steel Failure Mode

Fahmy (1999) classified three types of steel failure modes based on three regions on the moment –rotation diagram through experimental and numerical investigation. The first region is considered where the behavior remains elastic. The second one is a transition region where the behavior is inelastic and material hardening takes place. The third one is the softening region after the maximum moment of the connection has been reached and rupture occurs at the end.

Weak Column–Strong Connection: These types of connections are specified by the formation of a plastic hinge at the base of the column while rest of the components of the CBP connection remain elastic or exhibit incipient yielding. Fahmy (1999) and Adany et al. (2000) conducted experimental investigation on this type of connection and found plastic hinge only in the column, when all the other components of CBP connections reached yield stress. They also reported that welds could play an important role in this type of connection.

Strong Column–Weak Connection: Strong column-weak connections can resemble a pinned condition as long as the connection is in the nonlinear range (Grauvilardell et al., 2005). Several researchers (DeWolf and Sarisley, 1980; Picard and Beaulieu, 1985; Thambiratnam and Paramisivam, 1986; Astaneh et al., 1992; Burda and Itani, 1999) have reported that the performance of this type of connection can be specified by the inelastic deformation of one or more components of the CBP connection as well as the potential brittle failures such as concrete crushing, anchor rod fracture. Low strength and initial stiffness, pinched hysteresis loops with significant energy dissipation are some of the characteristics of this type of CBP connection.

Balanced Mechanism: This type of connection can be characterized as intermediate mechanism where simultaneous and concurrent behavior can be achieved in between the two types of connections discussed above. In this type of connection, column yields at approximately the same time as one or more of the components of the connection meaning that not only one component is subjected to extreme deformations but all the components undergo moderate inelastic behavior.

2.1.4 Classification According to Concrete Failure Mode

Several researchers (Wald et al., 1995; Balut and Moldovan, 1997; Stamatopoulos and Ermopoulos, 1997) assumed an elastic plastic stress distribution in the concrete to define bearing

stresses that develop underneath the base plate. Three types of failure modes can be classified according to the level of bearing stresses as shown in Figure 2.2 and are characterized by the level of compressive axial force with respect to the ultimate bearing stress in the concrete.

Low Axial Load: The bearing capacity of the concrete is never reached when the axial load is low. Collapse occurs either by yielding of anchor rods or by formation of plastic mechanism in the base plate.

Medium Axial Load: During medium axial loads, the behavior is characterized by anchor rod yielding and the concrete attaining its bearing strength.

High Axial Load: In case of high axial loads, only the concrete bearing capacity is reached at the time of failure.
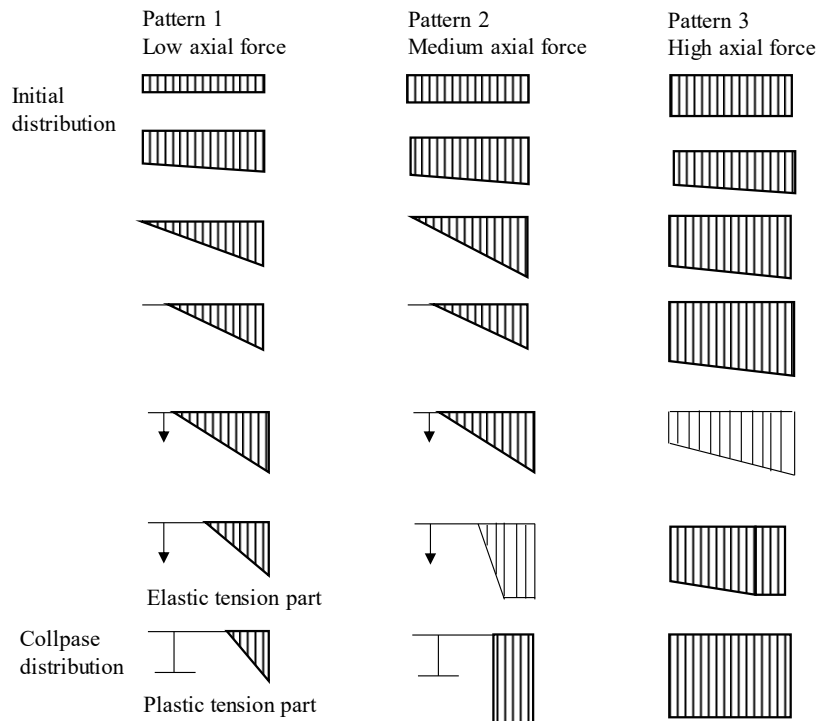
Figure 2.2 Internal force distribution under low, medium and high axial force in initial and collapse stages (Adapted from Grauvilardell et al., 2005)

2.1.5 Classification According to Energy Dissipation Capacity

Fahmy (1999) classified CBP connections according to energy dissipation characteristics. This type of classification becomes important when a capacity design of the CBP connection is carried out.

8

Non-dissipative Mechanism: These types of failure mechanisms do not provide significant energy dissipation. Mechanisms that provide brittle behavior are cracking of welds, fracture of anchor rods and base plates, and crushing of the concrete or grout. For mechanisms that show some form of ductility, excessive local buckling of the column flange is observed which in turn leads to a lower strength capacity in the connection than expected.

Dissipative Mechanism: Dissipative mechanisms provide considerable energy dissipation through yielding of one or more components of CBP connections such as yielding of the base plate, yielding of the anchor rods and plasticisation of the base of the column by forming a plastic hinge.

2.1.6 Classification According to Type of Frame

Variation of overall behavior, as well as the nature of acting forces of the exposed CBP connection largely depends on the attachment of the column base with the type of structure. Two types of attachments are viable such as column bases attached with moment resisting frames and column bases attached with braced frames.

Column Bases Attached to Moment Resisting Frames: This type of CBP connection experiences moments in addition to axial forces and shear. Researchers have focused mainly on this type of connection as it is common practical scenario. These types of CBP connections are challenging when lateral forces are significant with low gravity loads at the sides of the frames.

Column Bases Attached to Braced Frames: No significant research effort was found in the literature dealing with column bases attached to braced frames. Goldman (1983) and Tronzo (1984) have addressed the design of this type of connection analytically focusing on the design of the anchor rods, shear lugs, and the gusset plate. However, none of them accounted the contribution of the gusset plate attached to the base plate.

2.2 Previous Experimental Studies

A. Picard and D. Beaulieu (1985): The objective of this research was to investigate the base connection rigidity under the influence of axial loading. A total of 15 specimens were tested under flexural loading condition and combined axial compression-flexure conditions. The variables were cross section of column, base plate dimension and thickness, number of anchor rods, and load eccentricity. Test results showed that flexural stiffness of the base connection was significantly

improved when axial compression was considered. Furthermore, the method for determining the ultimate moment capacity of the base connection was found to be conservative.

A. Picard and D. Beaulieu (1987): This study was a continuation of the previous study by the same authors, where the main objective was to determine the value of the rigidity ratio of a column base connection at the column base. A total of 14 specimens were tested under constant axial force combined with monotonic lateral loading about both the strong and weak axis of the column. The applicable test variables were the cross section of column, base plate dimension and thickness, number of anchor rods, and level of axial loading. Results from the experiments found that the flexural stiffness of both strong and weak axis connection positively affected the column stability and frame behavior when the column base was considered as pinned connection. Rigidity ratio was found to be significantly higher in the strong axis direction compared to the weak axis direction. This was due to the reduction in the column effective length when there was no relative displacement at the column ends. They also reported that an approximate 30% increase in the column strength was observed for intermediate columns of specific slenderness ratios.

D.P. Thambiratnam and P. Paramasivam (1986): This research experimentally investigated the behavior of base plate under combined axial load and moment by eccentric loading on the column. Test parameters considered in this study were the base plate thickness and eccentricity of the load. All the twelve specimens were tested under monotonic eccentric axial loads. Test results showed that the primary mode of failure was cracking of concrete at the lowest eccentricity level whereas for all other cases yielding of base plate was observed as the primary failure mode. Yielding of the base plate was observed at the column base plate junction on the same side where the load was applied. The interaction curves indicated that the thickest base plate was unable to sustain the largest moments in all cases. They also reported that there was a reduction in strain with increasing base plate thickness at constant loading.

A. Astaneh, G. Bergsma and J.H. Shen (1992): The main objective of the research was to study the non-moment-resisting column base connections under cyclic loading. Six specimens were tested where the applied lateral load was varied in a quasi-static cyclic pattern. Column axial load and the base plate thickness were the two test variables. Wide range of variation was considered for both the variables. The results showed that anchor rod yielding was the primary mode of failure for all the specimens. An increase in the anchor rod tension force was observed with the increase

of base plate thickness. It was found that the level of axial load did not significantly affect the failure mode and the specimens were found to be stiffer with the increase in the axial load level. Specimen with thinner base plates had more energy dissipation capacity than that with thicker base plates. The bending strength of all tested connections was found to be apparently less than the column plastic moment because of the early yielding of anchor rods which significantly reduced the bending capacity of the column base connections. They reported that the reason for such behavior due to the rods in non-moment connections were solely used for erection purposes and not expected to carry any tension forces.

S. Igarashi, **S. Nakashima and T. Imoto (1993):** The objective of this research was to examine the response of full-scale exposed steel square tubular column bases under combined constant axial load and alternate lateral loading. Eleven specimens were tested where the test variables were column size, base plate thickness, number of anchor rods, and axial load ratios. The connection ductility and strength were found to be moderately limited. Base plate slipping was noticed in the hysteresis loop except for specimens with column flanges yielding. Weld fracture was observed between the column and the base plate in two out of eleven specimens. The remaining specimens first yielded at the compression side of the column followed by yielding of the base plate in the compression side then in the tension side. No anchor rod yielding was detected for the specimens where weld fracture did not occur.

J.P. Jaspart and D. Vandegans (1998): This research study examined the behavior of twelve small scale exposed column base connections subjected to axial force and gradually applied monotonic lateral loading. They reported that the sequence of such type of load application was more realistic, considering the fact that during an earthquake the lateral load varies whereas the dead and live load of buildings remain constant. The results of the research indicated that different axial load level did not influence the initial stiffness of the base connection. They also reported that for a chosen base plate thickness, an increase in the axial load and connection strength were related proportionally. Local buckling of the column controlled the connection capacity for thicker base plates indicating that an increase in axial load did not increase the connection strength. Contrarily, the connection capacity was controlled by base plate yielding when thinner base plate was considered.

J. Burda and A. Itani (1999): An extensive experimental investigation was carried out for exposed column base plate connections subjected to large deformations to examine their seismic response. Six one-half scale column base plate connections having different plate sizes and thicknesses were tested under constant axial load and lateral cyclic loading. Fillet welds completely around the column were considered in three of the specimens and the remaining three had CJP groove welds. Test variables were the base plate thickness and the distance between the column flange and the anchor bolts. Test results indicated that weld fracture between the column and the base plate was the primary mode of failure mode for each of the base connections at drift levels ranging from 2% to 13%. Higher ductility was observed in the thinner base plates as compared to the thicker ones. Moreover, significant amount of energy dissipation in the connection was detected due to the bending capability of the thinner base plates.

T. Li, J. Sakai and C. Matsui (2000): The objective of this experimental study was to gain a better understanding of the behavior of steel-concrete composite column bases under seismic loading. Seven specimens were tested under constant axial load and cyclic lateral loading. The cyclic lateral load was applied according to a predetermined sequence of rotation angle cycles of column base. Axial load levels and type of column were the two variables of the experimental investigation. Results showed that the ultimate strength of the specimens increased with an increment in the applied axial load. A similar trend was observed for the rotational stiffness of the composite column bases. They also reported effective results in the ultimate strength obtained from superposed method under high axial loads when the coefficient of bearing stress of concrete was considered.

D.Y. Lee, S. Goel and B. Stojadinovic (2008): The main objective of this study was to scrutinize the global cyclic performance of column base connections bending about weak axis and behavior of major connection elements under large column lateral displacements. Four exposed column base plate connections were tested under the SAC Phase II loading history in the direction of column weak axis. Test variables were the number of anchor bolts as well as different filler metal and welding details. Results showed that only one of the four specimens was able to complete the entire applied loading history without significant strength degradation and formed a plastic hinge at the bottom of the column. Limited ductility in the connection was observed with the other three

specimens. They also claimed that the exposed column base plate connections designed by the D&E method (Drake and Elkin, 1999) was not appropriate in the case of weak axis bending.

I. Gomez, G. Deierlein and A. Kanvinde (2010): This research study mainly focused on characterizing the performance and behavior of exposed column base plate connections subjected to combinations of axial and flexural loading. Seven large scale specimens were tested under different combinations of axial load and flexural loading. Test variables considered were base plate thickness, anchor rod strength, anchor rod layout, axial load level, and loading history. The column base connection specimens were designed and constructed in accordance with the AISC Design Guide 1 (Fisher & Kloiber, 2006) to reflect typical construction practice in North America. They reported three types of base connection failure such as yielding of the base plate, crushing/spalling of the grout pad, and yielding and fracture of the anchor rods. However, no damage was detected on the column as well as on the foundation. All the specimens showed satisfactory ductility by absorbing 6% or greater drift amplitude. Two of the seven specimens experienced sudden failure due to the fracture of the anchor rod.

J.H. Choi and Y. Choi (2013): This study explored the inelastic behavior of exposed steel column bases under axial load and biaxial lateral loading. Six hollow square steel columns were tested using two different base plate thicknesses under biaxial loading protocols. The specimens were tested under two different failure modes: base plate yielding and anchor rod yielding. Test results showed that for anchor rod yielding with thicker base plates experienced significant stiffness degradation. They also reported that the behavior of exposed column base connections under combined axial load and biaxial lateral loading was found to be relatively different compared with other loading cases due to the early yielding of anchor rods.

J. Borzouie (2016): This study experimentally explored the performance of steel column base connections under seismic demands to develop low damage base connections. Test parameters were exposed base plate connections with and without anchor rod preloading, bases with different patterns of asymmetric friction connections, and bases with yielding angles. The results indicated that the proposed details for base connections with friction connections resisted repeated cycles without strength degradation or any requirements for repair or replacement following a seismic event. However, some stiffness degradation was observed in the weak axis direction. It was also reported that bases with friction connections were preferable for low strength loss whereas bases

with yielding angles performed better while prioritizing straightforward detailing and construction practice.

W.Y. Lim, D. Lee and Y.C. You (2017): This study experimentally investigated column base plate strong-axis connections of small-size steel structures subjected to both axial and lateral loadings. Nine specimens were tested where the main parameters were the thickness of base plates, the embedment length of anchor bolts, and the presence of hook and rib plates. They found that the hysteretic behavior of exposed column-base plate strong-axis connections was significantly influenced by the base plate thickness as well as the number and embedment length of anchor bolts. However, they reported that the effect of rib plates on the flexural performance of column-base plate connections was negligible. They also reported that although column-base plate strong-axis connections were properly designed in accordance with design guides, the flexural performance of the connections could be unreliable without sufficient bond capacity between concrete and anchor bolts.

2.3 Previous Numerical Studies

F. Wald (1995): The objective of this study was to estimate the rotational stiffness through analytical simulation of mechanical model components. This analytical model considered the base plate as a rigid bar resting on three springs. One of these springs represented the concrete stiffness and was considered parallel with two other springs which defined the stiffness of anchor rods and the base plate in tension. The analytical model suggested three collapse modes to be critical for rotational stiffness evaluation. Two axial force boundaries were established to separate the three collapse mode. The results of these test series were used to formulate the Eurocode 3 Annex J design models that estimate the rotational stiffness of column base connections.

M. Fahmy (1999): This research study substantiated an experimental investigation through numerical analysis to identify failure modes of column base connection and develop seismic design recommendations for column base connections subjected to combined moment, shear and axial forces. Further, the study was extended into parametric studies with various combinations of independent base connection parameters. Variables considered in the study were column size, base plate, number of anchor rods, amount of axial load applied, and type of weld metal used. Three different base connection failure mechanisms were defined in the study such as weak column-strong connection (plastic hinge formation in the column), balanced mechanism (simultaneous

14

yielding of the column and one or more connection components), and strong column-weak connection (inelastic deformation of one or more connection components i.e., anchor rods, concrete foundation, and/or base plate). Test results indicated that the post-yield deformation could be maximized when considering weak column-strong connection mechanism and therefore, could be implemented as a desirable connection behavior under seismic excitations. To identify the expected failure mode of the column base connection, a strength connection ratio was introduced and verified using plastic analysis. It was also reported that the weld metal type had a significant effect on the base connection behavior.

D.Y. Lee, S. Goel and B. Stojadinovic (2008): An extensive numerical parametric study was conducted on exposed column base plate connections bending about weak axis to investigate effects of the relative strength ratio among the connection elements subjected to larger lateral displacements. For this numerical study, a total of 43 three-dimensional Finite Element Analysis (FEA) models were developed having different base plate thicknesses, anchor bolt sizes, and grout compressive strengths. Test results showed that thinner base plates and stiffer anchor bolts increased the amount of reaction bearing force due to the shortened overall moment arm between the tensile bolt force and reaction bearing force. They recommended avoiding excessively thicker base plate coupled with weaker anchor bolts in order to prevent undesirable crushing of grout beneath the base plate edge on the compression side. They also suggested that minimum base plate thickness should be adopted to overcome high local stress concentration in the anchor bolts before the base connection reaches its ultimate state for any specific anchor bolt size.

A.M. Kanvinde, S.J. Jordan and R.J. Cooke (2013): This research presented a finite element (FE) simulation study to offer behavioral insights into connection response through internal stress distributions. The 3D FE simulations considered different important aspects of base connection behavior such as contact, gapping, and nonlinear constitutive response of various components. The simulation was performed under axial load and major axis bending where the variables for the numerical analysis were base plate thickness and axial load level. Results of the simulations indicated that current strength characterization and design approaches where assuming a rectangular bearing stress block might misrepresent the stress distribution beneath the base plate. Thicker base plates concentrated the stress at the compression zone of the base plate whereas the stresses were concentrated under the compression flange of the column for thinner base plate. They

also reported that no significant effect on the anchor rod force was found despite the variation of the stress profile which was assumed in the design method.

M.A. Shaheen, K.D. Tsavdaridis and E. Salem (2017): The main objective of this study was to investigate the shear capacity of the column base connections based on the grout thickness and strength. Test variables considered for the numerical analysis were the thickness and compressive strength of the grout. Test results demonstrated an improvement in the base connection behavior when grout was considered in the connection. It was also reported that the shear capacity was significantly increased with the thicker grout thickness and minor effect was found due to the change in the grout compressive strength.

C.A. Trautner and T.C. Hutchinson (2018): The objective of this study was to investigate the moment-rotation behavior as well as failure modes of the column base connections through an explicit numerical parametric study under combined axial load and major axis bending. They categorized different base connection components into low, medium, and high categories depending on their sensitivity to the connection behavior. Variables considered in the study were diameter, quantity and embedment length of the anchor rods as well as the base plate dimension, and the distance between the anchor rods on the edge. They reported that the differences in moment rotation behavior and maximum plasticity in the welded region was a function of the anchor size, layout, and embedment length of the base connection.

M.A.K. Fasaee, M.R. Banan and S. Ghazizadeh (2018): This research focused on investigating the response of base plate connections subjected to various biaxial moments and axial loads. They proposed an analytical model to determine the capacity of major and minor axis moment considering the variation of applied axial load only. From the numerical results obtained from the study, they developed an interaction curve for designing exposed unstiffened column base plates under combined axial load and monotonic biaxial bending.

2.4 Summary of Previous Studies on CBP connections

Table 2.1 provides a comprehensive summary of the literature in terms of how researchers all around the world have investigated the behavior of exposed column base connections under different loading scenarios.

Table 2.1 Comprehensive summary of column base connection studies

Investigator	Year	Loading Type	Number of Tests	Main Test Parameters	Main Failure Modes
Akiyama *et al.*	1984	Axial plus moment (cyclic)	5	End detail and depth of anchor rod Shape of column and base plate	Concrete crushing Anchor rod pull-out
Thambiratnam & Parimasivam	1986	Axial plus moment (from eccentricity)	12	Base plate thickness Eccentricity of axial load	Concrete block failure Base plate yielding Anchor rod yielding
Picard & Beaulieu	1987	Axial plus moment	14	Shape of column Baseplate area and thickness Number of anchors	Column buckling in the direction of weak axis
Sato	1987	Axial plus moment (cyclic)	6	Size of base plate Column axial load Yield strength of anchor rod	Anchor rod fracture Concrete failure Anchor rod yielding
Hon & Melchers	1988	Axial plus moment (from eccentricity)	26	Base plate thickness Anchor rod size	Anchor rod failure Base plate yielding
Astaneh *et al.*	1992	Axial plus moment (cyclic)	6	Base plate thickness Column axial load	Column and plate yielding Rod and weld fracture Grout crushing
Igarashi *et al.*	1992	Moment (cyclic)	4	Type of anchor rod	Concrete riser and grout cracking and crushing Anchor rod yielding
Melchers	1992	Moment (cyclic)	10	Base plate thickness Number and size of anchor rod Anchor rod yield strength	Base plate yielding Anchor rod yielding
Targowski *et al.*	1993	Moment	12	Column section Base plate thickness	Base plate yielding Anchor rod elongation
Kallolil *et al.*	1998	Axial plus moment (from eccentricity)	3	Anchor bolt size Base plate thickness Ratio of the moment to the axial load	Yielding and fracture of anchor rods Yielding of base plate
Akiyama *et al.*	1998	Moment (shaking table)	2	Base plate thickness	Anchor rod elongation Base plate yielding

Jaspart & Vandegans	1998	Axial plus moment	12	Base plate thickness Number of anchor rods	Failure of anchor rod and concrete Yielding of base plate and column
Burda & Itani	1999	Axial plus moment (cyclic)	6	Base plate area Base plate thickness	Fracture of the weld between column and base plate
Fahmy	1999	Moment (cyclic)	3	Number of anchor rods Weld material	Fracture of the weld between column and base plate
Adany et al.	2000	Moment (cyclic)	5	End-plate thickness Anchor bolt pre-tensioning	Base plate yielding Anchor rod yielding Column local buckling
Li et al.	2000	Axial plus moment (cyclic)	7	Column section Concrete filling Anchor rod strength	Anchor rod yielding Buckling of steel tube
Lee & Goel	2001	Moment (cyclic)	4	Number of anchor rods Weld material	Fracture of the weld between column and base plate
Miyasaka et al.	2001	Moment	8	Base plate thickness Location of anchor rods	Base plate deformation and yielding
Liu	2001	Moment	8	Base plate thickness Number of anchor rods	Plate yielding Anchor yielding
Somiya et al.	2002	Axial and moment	12	Different initial axial load and load rate Plate and tube thickness	Base plate Yielding Anchor rod yielding
Takamatsu & Tamai	2005	Axial plus moment (cyclic)	9	Number of anchor rods Level of axial load Moment application (monotonic/cyclic) Use of wedge device	Yielding of anchor rods
Kim et al.	2007	Axial plus moment (cyclic)	2	Number of anchor rods Full scale frame	Plastic hinging at column top Inelastic flexural-torsional buckling
Di Sarno et al.	2007	Axial plus moment	4	Axial load level Connection type	Fracture of anchor bolts Plastic hinging of column

Author	Year	Loading	Number of specimens	Parameters	Failure mode
Lee *et al.*	2008	Moment (cyclic)	4	Number of Anchor bolt Relative strength between base plate & anchor rod Weld detail	Plastic hinging of column Weld failure
Myers *et al.*	2009	Moment (cyclic)	5	Weld detail Loading history	Weld failure
Cui *et al.*	2009	Axial plus moment	8	Column embedment type	Fracture of anchor bolts
Gomez *et al.*	2009	(1) Moment (monotonic/cyclic) (2) Axial plus moment (cyclic)	7	Number of anchor rods Anchor rod strength Base plate thickness Level of axial load Cyclic/monotonic moment	Anchor rod Yielding and fracture Grout crushing Plate yielding
Kanvinde *et al.*	2012	Axial load plus moment	9	Base plate size & thickness Axial load level Anchor rod dimension Column size	Base plate yielding Anchor rod yielding
Kanvinde *et al.*	2013	Axial load plus moment	6	Base plate thickness Axial load ratio Moment	Base plate yielding Anchor rod yielding
Choi & Choi	2013	Axial load plus moment	14	Base plate thickness Uniaxial & cyclic Moment	Base plate yielding Anchor rod yielding
Trautner *et al.*	2015	Cyclic load	8	Anchor rod selection Setting arrangement Stretch length	Crack in grout & concrete Base plate yielding Anchor rod yielding
Shaheen *et al.*	2017	Lateral load	-	Grout thickness	Crack in grout Anchor rod yielding
Fasaee *et al.*	2018	Axial load plus biaxial bending	7	Base plate thickness Biaxial moment	Base plate yielding Anchor rod yielding

				Number of anchor	
				rods Anchor rod size	Base plate yielding
Trautner &	2018	Axial & Lateral	6	Base plate thickness	Anchor rod yielding
Hutchinson		load		Cyclic/monotonic	
				moment	

					Local buckling & axial shortening of
Elkady &	2018	Axial load plus	10	Column section	column
Lignos		uniaxial/biaxial		Loading protocol	Plastic hinge
		bending			formation near
					column base

2.5 Column Base Connection Design Provisions and Design Issues

Current approaches widely used in the industry for design of column base connections subjected to axial load and moments are typically based on the AISC Steel Design Guide 1 – Column Base Plates (Fisher & Kloiber, 2006). An elastic approach considering triangular/trapezoidal bearing stress distribution is adopted in its first edition which is further modified in the latest edition where an ultimate approach of rectangular bearing stress distribution is considered by Fisher & Kloiber (2006) to design the CBP connection. Additionally, the AISC Steel Design Guide Series 10 – Erection Bracing of Low-Rise Structural Steel Buildings (Fisher & West, 2003) provides further information relevant to column base design and construction. Several recommendations for the CBP connection design for axial column tension, shear or moment are available in the AISC Steel Construction Manual (15th edition). It is to be noted that all of these design provisions consider only the major axis moments combined with axial loads during the design of the CBP connection. Canadian Institute of Steel Construction (CISC) follows similar procedures described in the AISC Design Guide 1.

Column base design provisions published in ENV1993 Eurocode 3 and the background of these provisions are well described in Wald et al. (1995). According to Eurocode 3, the design for connection strength as well as for stiffness is defined as a component based approach where the connection is considered to be an assembly of individual components.

Extensive research conducted by Architectural Institute of Japan (AIJ) has revealed that variation of different parameters of CBP connections characterizes column base design in high seismic regions. Also, connection details are highly related to seismic behavior and performance

of the CBP connection. According to AIJ, the estimation of the design moments for the column base is done by modeling the rotational stiffness of the CBP connection.

2.6 Column Base Plate Connection Failure Modes

A majority of past studies (Picard & Beaulieu 1985; Picard et al. 1987; Igarashi et al. 1993; Lee et al. 2008; Gomez et al. 2010; Kanvinde et al. 2013; Choi & Choi 2013; Shaheen et al. 2017; Trautner & Hutchinson 2018) found that the ductile behavior of CBP connections could be achieved by either base plate yielding or anchor rod yielding for exposed types of CBP connections. Base connection failures observed during past seismic events (Northridge 1994, Kobe 1995, and Tohuku 2011) are shown in Figure 2.3.

Figure 2.3 Base connection failure observed in past earthquakes

Gomez et al. (2009) and Kavoura et al. (2017) reported the crushing of the concrete pedestal for a few specimens from their experimental studies. However, failure mode for most of their test specimens was associated with either base plate or anchor rod yielding. Grout crushing was observed by Thambiratnam and Parimasivam (1986) due to the use of anchor rod configuration with only two rods for the entire CBP connection. This type of arrangement is no longer valid because it doesn't have adequate stability during the erection procedure of the structure. Fahmy et al. (1999) conducted experimental investigations considering the formation of a plastic hinge in the column above the base plate by using relatively thicker base plates and larger diameter anchor

rods than usual practice. They observed a desirable weak column-strong connection mechanism for CBP connection which could maximize the post-yield deformation behavior as well as the connection strength. It is to be noted that considerable ductile behavior can be obtained by either base plate yielding or anchor rod yielding whereas concrete crushing and column hinging result in limited ductile behavior. Grout crushing has a passive influence on the ductile behavior of the CBP connection by increasing redundancy of the connection through development of multiple plastic hinges in the anchor rods (Shaheen et al. 2017). Figure 2.4 shows typical illustration of different types of CBP failure modes found in literature. It is to be noted that any types of failure associated with anchor rod is considered as anchor rod yielding since this classification is used only for the machine learning part of the concerned study.

(a) anchor rod yielding

(b) base plate yielding   (c) concrete crushing   (d) column hinging   (e) grout crushing
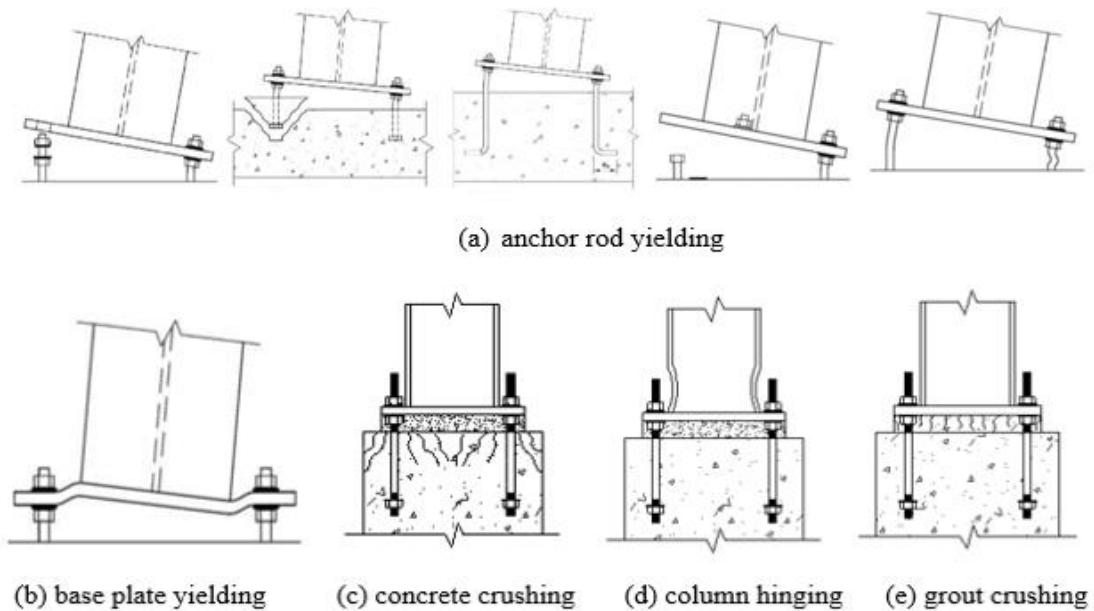
Figure 2.4 Typical failure modes of CBP connection

2.7 Machine Learning for Structural Failure Mode Identification

Artificial intelligence is proving to be an efficient alternative approach to classical modeling techniques which refers to the branch of computer science that develops machines and software with human-like intelligence. Among the different artificial intelligence techniques, machine learning (ML) has recently acquired considerable attention and are establishing themselves as a new class of intelligent methods for use in all engineering domains. In recent years, there has been

a growing interest towards the application of ML techniques in civil engineering practices especially in the structural damage assessment area. For structural engineers and designers, it is of paramount importance to identify the anticipated failure mode of any structure. The strategy currently used to identify the failure mode is based on either experimental investigation or detailed continuum-based finite element models. Such types of detailed analysis are valuable but require considerable amount of computational cost and effort as well as the time and resources to perform the analysis. Practically, after the occurrence of any natural hazard it is desirable to identify the failure mode in the shortest possible time for deciding the damage assessment or retrofitting strategies of the affected structure. In such situation, the application of data-driven ML techniques provides the feasible alternative to the detailed numerical analysis.

Mangalathu and Jeon (2018) developed data driven ML models by assembling an experimental database of reinforced concrete (RC) beam-column joints to identify the failure mode. They proposed a lasso regression-based ML model for rapid assessment of RC beam-column joints. Another study by the same authors (Mangalathu and Jeon, 2018) applied ML techniques to classify circular reinforced concrete columns failure modes and achieved 10% higher accuracy with ANN based model compared to the numerical analysis. Very recently, Mangalathu et al. (2020) performed data driven ML techniques for seismic failure mode identification of RC shear walls and the random forest method was suggested as the most effective ML algorithm. Huang and Burton (2019) implemented ML techniques with limited dataset (114 dataset) to identify the in-plane failure modes of RC frames with infills and found reasonable accuracy for both adaptive boosting and support vector machine algorithms. Das et al. (2020) developed a data-driven physics-informed model for crack prediction in concrete structures. Using real time monitoring data, the proposed method can predict the expected service life of infrastructure before required maintenance. Fu (2020) developed an ML framework for progressive collapse prediction of steel frame buildings under fire event. Within the limited dataset, KNN and Neural Network was identified as the suitable ML techniques. Mangalathu et al. (2020) utilized machine learning techniques to predict earthquake induced building damage by using data from the 2014 South Napa earthquake and Random Forest based ML model outperformed the other ML algorithms. Although there have been significant advancements to identify failure mode and damage assessment of

concrete structures by applying ML techniques, its application in steel structures is found limited while reviewing the current literature.

2.8 Summary

This chapter provides a detailed summary of past experimental and numerical research conducted on exposed CBP connections under different loading scenarios. Furthermore, this study provides an insight into the current practice and applications relating to the design of exposed CBP connections. This chapter systematically summarizes the past studies identifying the loading types, number of specimens tested, main design parameters, and observed failure mode. Additionally, on overview of CBP connection failure modes observed during past major seismic events are discussed along with the most common failure modes described in literature. Finally, this chapter provides an overview of applications of machine learning techniques in structural engineering with a focus on structural failure pattern identification.

Chapter 3 Column Base Connection Failure Mode Identification using Machine Learning

3.1 General

This chapter describes the capability of data-driven ML techniques to identify the failure mode of column base plate (CBP) connection as well as its influential parameters. The chapter begins with providing details of the constructed database on CBP connection for ML application. After that, an overview of various ML algorithms adopted in the study is discussed. Further, the performance of various ML techniques is evaluated using different evaluation metrics for classification based problems as in the concerned study. Furthermore, a sensitivity analysis is performed within different parameters of CBP connection. A comparison among the available experimental results, developed ML model, and available empirical equations available is also performed. The chapter concludes with the development of an easy to use Graphical User Interface (GUI) from the developed ML model.

3.2 Description of Database

3.2.1 Overview of the Constructed Database

Since the data-driven ML model largely relies on the characteristics of the dataset, an experimental dataset composed of 189 specimens for exposed type steel CBP connection is incorporated in this study. The database is constructed based on a rigorous literature review of the available experimental results which contains an up to date existing experimental studies from different parts of the world. Details of the assembled data are provided in the link https://github.com/Md-Asif-Bin-Kabir/CBP-Failure-Mode-Prediction as well as in the appendix-A (Table A1). The database includes the geometric and material properties of the base plate, geometric properties of anchor rod, pattern of the anchor rods connected with the base plate, and the type of column used in the experimental studies with their corresponding failure mode. It is to be noted that this database contains only the primary failure mode of CBP connection and subsequent or combined mode of failure is outside the scope of this study. Since the experimental studies are carried out with the application of either axial load, lateral load or a combination of both, this feature is not included in the database to avoid complexity for any missing values. Among all the specimens, five different

types of failure modes are observed such as anchor bolt yielding (AB), base plate yielding (BP), concrete crushing (CC), grout crushing (GC), and column hinging (CH). The number of specimens with each failure mode is 110, 68, 6, 3, and 2, respectively. As mentioned in the Chapter 2, base plate and anchor rod yielding are the most common types of failure mode for typical CBP connections, concrete or grout crushing can occur due to the insufficient connection strength for transferring the shear force. Column hinging failure is an indication of weak column-strong connection type mechanism for CBP connection. Various parameters of the considered 189 CBP connections have the following ranges:

- Base plate thickness: 6 mm $\leq t_p \leq$ 139 mm
- Base plate yield strength: 240 MPa $\leq F_{yp} \leq$ 576 MPa
- Anchor rod diameter: 12 mm $\leq d \leq$ 51 mm
- No. of anchor rod: $2 \leq N \leq 8$
- Embedment length: 100 mm $\leq L \leq$ 900 mm
- Grout thickness: $0 \leq t_g \leq$ 60 mm
- Pitch Length: 25 mm $\leq p \leq$ 610 mm
- Shape of column section: W or HSS

where, t_p = base plate thickness; F_{yp} = base plate yield strength; d = diameter of anchor rod; N = no. of anchor rod; L = embedment length of anchor rod; t_g = grout thickness; p = center to center distance between the anchor rods in the direction of the applied load. Figure 3.1 illustrates the distribution of the various parameters of CBP connection including the distribution of the failure modes.
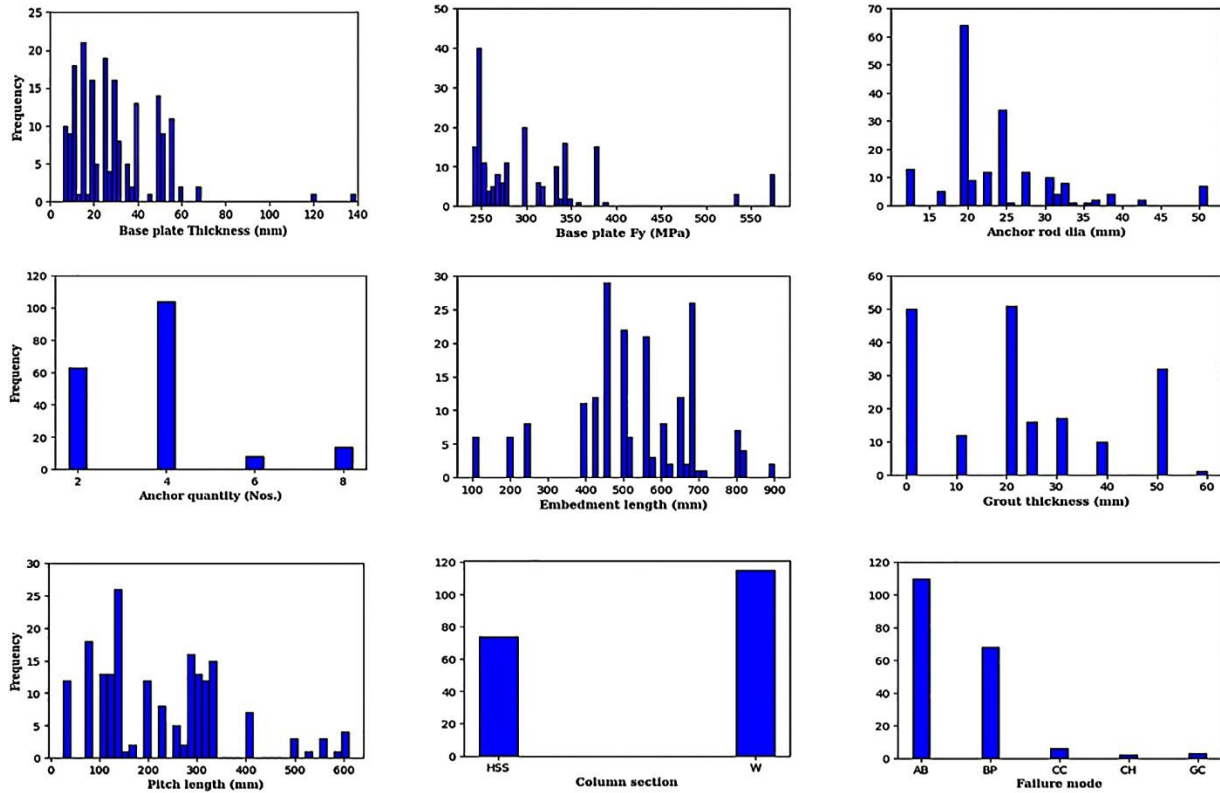
Figure 3.1 Distribution of design parameters and failure modes for base plate connection database

3.2.2 Selection of Input Parameters

Since there are no previous studies on the failure mode identification of CBP connections, this study employs the existing parametric study performed by Trautner and Hutchinson (2018) to select the input parameters from the design parameters described in the previous section. Design parameters are grouped into low, medium, and high categories in the context for the designer to have control for the design of base plate connection. Base plate thickness (t_p), anchor rod size (d), and pattern of anchor rod (N) are considered in the high category since they can be controlled from the design perspective. On the other hand, embedment length (L) and pitch length (p) are considered in the medium category because of their dependency on the high category parameters. Base plate yield strength (F_{yp}), grout thickness (t_g), and shape of the column section are grouped in the low category considering their constant values for a particular design criterion. All the parameters having numerical values are selected for the input parameters. Shape of the column section is not selected as the input parameters since it seems to have no significant influence on

27

failure mode based on statistical analysis of past experimental investigations as shown in Figure 3.2. From Figure 3.2, both W and HSS type column sections have nearly the same percentages of the failure modes irrespective of other parameters. Also, the pitch length is omitted from the study due to a few missing values. Since the missing values can significantly affect the ML models and the way to handle them is an assumptive procedure, this parameter is not considered to avoid such complexity. The selected input parameters for the classification model are summarized in Table 3.1.
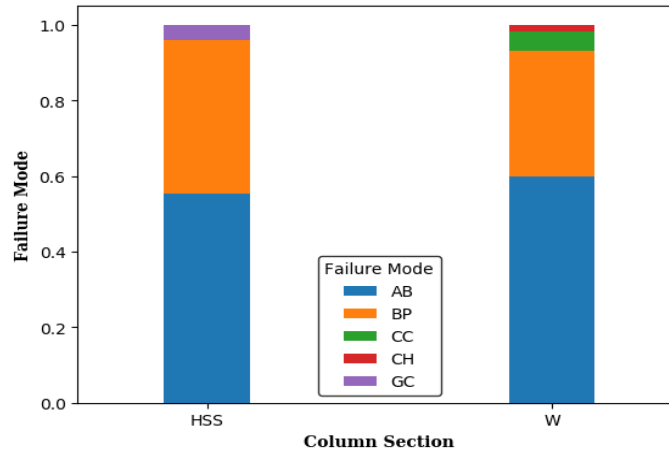
Figure 3.2 Failure mode distribution for HSS and W-column section

Table 3.1 Notation of selected input variables

Input variable	Notation	Unit
Base plate Thickness	t_p	mm
Base plate yield strength	F_{yp}	MPa
Anchor Rod Dia	d	mm
No. of Anchor Rods	N	pcs.
Embedment Length	L	mm
Grout Thickness	t_g	mm

It is well known that the efficiency of the data-driven machine-learning model is completely dependent on the quantity and quality of the data considered for developing the model. Also, it is obvious that the greater amounts of data can provide a prediction that is more accurate. However, the availability of large amounts of data is not always attainable as in the case of this study. Less amount of data with lack of good quality can cause erroneous prediction results. In that case,

exploratory data analysis is required to assess the quality of the data. Previously other researchers have utilized very concise database for developing data driven ML models. For example, Huang and Burton (2019) implemented ML techniques with 114 dataset to identify the in-plane failure modes of RC frames with infills and found reasonable accuracy for both adaptive boosting and support vector machine algorithms. Siam et al. (2019) proposed a ML algorithm for classifying reinforced masonry shear walls using only 97 dataset by deploying both supervised and unsupervised ML domain. Although the dataset constructed in this study from the available literature is very concise, an extensive exploratory data analysis is carried out to ensure the quality of the dataset. Figure 3.3 shows the correlation matrix for the selected input parameters for the classification model. The correlation coefficient is a measure of the relationship strength between any two parameters. A higher value of correlation coefficient indicates a strong relationship which can be either positive or negative whereas a lower value signifies a weak relationship between any two parameters. It can be seen from Figure 3.3 that only the anchor rod diameter (d) has a correlation coefficient of more than 0.5 with base plate thickness (t_p) and all other parameters have a correlation coefficient less than 0.5 which indicates a weak relationship between the parameters. It is to be noted that this study is not concerned with the selection of optimal features and further studies are required to consider all the parameters associated with CBP connection which can have an influential effect on failure mode identification.

	t_p	F_{yp}	d	N	L	t_g
t_p	1.000	0.108	0.619	0.274	0.265	0.338
F_{yp}	0.108	1.000	0.106	0.074	0.309	0.130
d	0.619	0.106	1.000	0.153	0.315	0.155
N	0.274	0.074	0.153	1.000	-0.284	-0.015
L	0.265	0.309	0.315	-0.284	1.000	0.132
t_g	0.338	0.130	0.155	-0.015	0.132	1.000

Figure 3.3 Correlation matrix for selected input parameters

3.2.3 Modification of Failure Modes for Output Response

As mentioned in the previous section, five different types of failure modes are observed from past experimental investigations on exposed CBP connections where almost 94% of the failure modes are either anchor rod yielding (AB) or base plate yielding (BP). Since these two types of failure modes are most likely to occur, concrete crushing (CC), grout crushing (GC), and column hinging (CH) failure modes are considered as a single type of failure mode named as others (OTH) to modify the failure modes into three categories. Figure 3.4 shows the distribution of the modified failure mode which is implemented in the classification model. The modified failure mode dataset contains the same number of failure modes for anchor rod yielding (AB) and base plate yielding (BP) as previous whereas the others (OTH) type of failure mode has a value of 11 which is the summation of concrete crushing (CC), grout crushing (GC), and column hinging (CH) type failure modes.
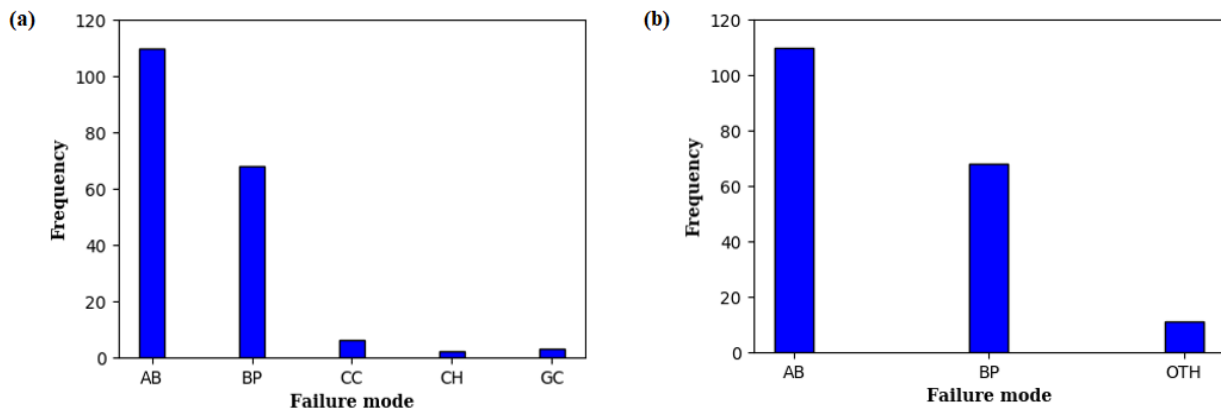
Figure 3.4 Distribution of imbalanced dataset (a) original dataset (b) modified dataset

3.3 Brief Description of Machine Learning Algorithms

In this study, nine different ML algorithms such as Support vector machine, Naïve bayes, K-nearest neighbors, Decision tree, Random forest, Adaboost, XGboost, LightGBM, and Catboost are deployed to classify the failure modes of CBP connection. Many previous studies on structural engineering domain deployed ML techniques like K-nearest neighbors, Decision tree, Naïve bayes, and Random forest (Mangalathu and Jeon, 2018; Huang and Burton, 2019; Das et al., 2020). However, a few recent studies on structural failure utilized less prominent algorithms AdaBoost, LightGBM, XGBoost and CatBoost (Mangalathu et al. 2020). This study includes one additional algorithm support vector machine which is also used in some previous studies in various sectors

of engineering domain (Huang and Burton, 2019; Luo and Paal, 2019). Friedman (2001) described all the algorithms used in this study in detail.

K-Nearest Neighbor: K-nearest neighbors (KNN) is one of the primary non-parametric methods used for classification. It is a lazy learner algorithm which classifies the output variables into the class with the higher number of votes. For any given value of K, the algorithm finds the cluster of data points with k elements, K=1,3,5,7 or 2,4,6,8 etc. Each data point is voted as a member of any existing failure class depending on the similarity or distance-based matrix. A default value of K=5 is usually used to develop any ML model which can be further tuned to find the optimal K value for that particular ML model.

Random Forest: Random forest (RF) is an ensemble of tree based classifiers that uses two independent ML techniques like random feature selection and bagging (Breiman, 2001). Random feature collection constructs decision trees promptly and while bagging constructs each tree independently. Random forest randomly selects the features of the subsets rather than using all the features in the Decision trees. The algorithm takes the mean value of the outputs from the random independent bootstrap training data for predicting the output of a new dataset.

Support Vector Machine: Support vector machine (SVM) is an algorithm used widely in the field of different engineering domains. While KNN is a cluster of values depending on point to point distance, SVM follows a separating line. SVM aims to define a separating hyperplane which ensures the presence of similar class data points at one side of the plane. When the output class is more, it will have more hyperplanes. SVM is useful for classifying both separable and non-separable data (Cortes and Vapnik, 1995). SVM aims at maximizing the margin among various classes. Simultaneously, it takes some errors, which can be regulated later with a penalty parameter (Ahmadi et al., 2018).

Decision Tree: Decision tree (DT) is a machine learning algorithm that follows a transparent decision process to predict binary outcomes. This non-parametric classification method splits the classification into the hierarchy of decisions which depends on one or more input features. One of the ways to build Decision trees is to create non-overlapping regions for the training set space by taking the value of Gini Index as the basis (Breiman et al., 1984). Each tree starts from the same node referred as the root while the branches spread out to the bottom. The computation time is proportional to the height of the tree. However, a tree with immense height is time consuming and

overfitting. Tree pruning is the approach that can be applied to restrain overfitting through cross validation techniques.

Boosting Methods: Boosting methods aim to improve the prediction performance by combining a set of weak classifiers to a robust classifier. Four different boosting methods such as Adaboost (AB), XGboost (XB), LightGBM, and Catboost have been used for classification of failure data. Adaboost initially implies equal weight on all the observations. Then it increases the weight on the incorrectly predicted instances. Thus, the model goes through continuous improvements, learning and modifying the weights of the training dataset. Gradient boosting method works by tuning the losses by performing the regression of gradient vector function at each iteration (Friedman, 2001). A gradient boosting model modifies the sequence of each decision tree starting from the weak decision tree which is taken as the base Decision Tree. XGboost is a slow boosting method that uses sequential model training to reduce misclassification error at each iteration. LightGBM is a boosting method that follows leaf-wise generation of more accurate and complex decision trees for boosting. Catboost is a boosting method that effectively handles both numeric and categorical variables as input. It deals with the variables during the training duration, eventually saving time for preprocessing.

3.4 Performance Evaluation of Different Machine Learning Models

Data-driven ML classification model is established using various ML algorithms outlined in the previous section. Open source sci-kit learn python package (Pedregosa et al., 2011) is used to develop the codes for the classification model with the selected input parameters as mentioned in section 3.2.2. The entire dataset is split into train and test set where 70% of the data (132 samples) is considered to train the classification models and 30% of the data (57 samples) is used to evaluate the developed classification models suggested by Friedman (2001). Splitting of the train and test set is carried out randomly which ensures the performance of the test set from a completely unknown set of data. Also, the train and test set are kept constant for the classification model while applying different ML algorithms. As described in section 3.2.3, the response of the dataset has a highly imbalance feature which can bias the classification model by not giving priority to the minority classes for developing the model. To overcome this issue, an oversampling algorithm SMOTE (Synthetic Minority Oversampling Technique) proposed by Chawla et al. (2002) is implied in the training set data to duplicate randomly selected data from the minority classes

without adding any diversity to the original dataset. Initially, the train set is generated from 70% of the entire dataset which is equal to 132 samples where the distribution of anchor rod yielding (AB), base plate yielding (BP), and others (OTH) type of failure mode is 80, 44, and 8, respectively. However, after the application of SMOTE the train set has a total of 240 samples where all three types of failure modes have an equal amount (80) as shown in Figure 3.6. For each data that belongs to the minority classes, SMOTE gets its nearest neighbors and synthesizes new data of the minority classes at a random location in the line between the current data and its nearest neighbors. It should be noted that this is only applicable to the training set and the test set has no influence with this technique. Evaluation of the developed classification models for each type of ML algorithm is performed with the help of a confusion matrix of actual class versus predicted class which provides a detailed scenario for the classification type problem (Figures 3.5 and 3.6). A confusion matrix is a table which summarizes the correct and incorrect predictions for the classification model where the diagonal and non-diagonal elements represent correct and incorrect predictions, respectively. It contains three types of evaluation metrics such as overall accuracy, precision, and recall. Accuracy is the ratio between the number of diagonal elements to the total number of elements in the confusion matrix. Overall accuracy indicates the number of predictions correctly identified by the classification model. Precision is the ratio between the correctly predicted failure modes by the ML algorithm to the total number of predicted failure modes. On the other hand, recall defines the ratio between the correctly predicted failure modes to the total number of actual failure modes. Higher value of all these evaluation metrics is an indication of accurately predicting the failure mode by the developed classification model. The following inferences can be drawn from Figures 3.5 & 3.6:

- Among the considered ML algorithms, the tree-based models perform better than the non-tree-based models. Decision tree has the highest accuracy with 91% for the test set whereas Random forest, Catboost, and XGboost has an accuracy of 88%, 84%, and 82%, respectively.
- Though anchor rod yielding (AB) and base plate yielding (BP) type failure modes have higher recall value, no ML algorithm can exceed 33% recall value for the others (OTH) type of failure mode. This is due to the lack of actual experimental data for that particular type of failure mode.

(a) Predicted class

Actual class	AB	BP	OTH	Recall
AB	69 (29%)	9 (4%)	2 (1%)	86%
BP	3 (1%)	63 (26%)	14 (6%)	79%
OTH	3 (1%)	2 (1%)	75 (31%)	94%
Precision	92%	85%	82%	86% Accuracy

(b) Predicted class

Actual class	AB	BP	OTH	Recall
AB	52 (22%)	14 (6%)	14 (6%)	65%
BP	17 (7%)	47 (20%)	16 (7%)	59%
OTH	16 (7%)	15 (6%)	49 (20%)	61%
Precision	61%	62%	62%	62% Accuracy

(c) Predicted class

Actual class	AB	BP	OTH	Recall
AB	75 (31%)	3 (1%)	2 (1%)	94%
BP	6 (3%)	66 (28%)	8 (3%)	83%
OTH	2 (1%)	6 (3%)	72 (30%)	90%
Precision	90%	88%	88%	89% Accuracy

(d) Predicted class

Actual class	AB	BP	OTH	Recall
AB	80 (33%)	0 (0%)	0 (0%)	100%
BP	1 (0%)	79 (33%)	0 (0%)	99%
OTH	0 (0%)	3 (1%)	77 (32%)	96%
Precision	99%	96%	100%	98% Accuracy

(e) Predicted class

Actual class	AB	BP	OTH	Recall
AB	80 (33%)	0 (0%)	0 (0%)	100%
BP	1 (0%)	79 (33%)	0 (0%)	99%
OTH	0 (0%)	3 (1%)	77 (32%)	96%
Precision	99%	96%	100%	98% Accuracy

(f) Predicted class

Actual class	AB	BP	OTH	Recall
AB	80 (33%)	0 (0%)	0 (0%)	100%
BP	1 (0%)	79 (33%)	0 (0%)	99%
OTH	0 (0%)	3 (1%)	77 (32%)	96%
Precision	99%	96%	100%	98% Accuracy

(g) Predicted class

Actual class	AB	BP	OTH	Recall
AB	79 (33%)	1 (0%)	0 (0%)	99%
BP	1 (0%)	76 (32%)	3 (1%)	95%
OTH	0 (0%)	4 (2%)	76 (32%)	95%
Precision	99%	94%	96%	96% Accuracy

(h) Predicted class

Actual class	AB	BP	OTH	Recall
AB	80 (33%)	0 (0%)	0 (0%)	100%
BP	1 (0%)	79 (33%)	0 (0%)	99%
OTH	0 (0%)	3 (1%)	77 (32%)	96%
Precision	99%	96%	100%	98% Accuracy

(j) Predicted class

Actual class	AB	BP	OTH	Recall
AB	74 (31%)	6 (3%)	0 (0%)	93%
BP	9 (4%)	64 (27%)	7 (3%)	80%
OTH	0 (0%)	9 (4%)	71 (30%)	89%
Precision	89%	81%	91%	87% Accuracy

Figure 3.5 Confusion matrix of classification models of various ML techniques using the training set: (a) support vector machine, (b) naïve bayes, (c) k-nearest neighbors, (d) random forest, (e) decision tree, (f) XGboost, (g) LightGBM, (h) Catboost, and (j) Adaboost

- Various gradient boosting methods are incapable of improving the performance of the classification model compare to the tree-based models such as Decision Tree and Random forest.

- The performance of the non-tree-based models is found to be unsatisfactory compared to the tree based models. This indicates the non-linear complex decision surfaces between the failure modes.

- Higher accuracy in the training set does not reflect higher accuracy for the test set. For example, Random forest, Decision tree, XGboost, and Catboost have the same accuracy of

98% for the training set but only the Decision tree has a higher accuracy value for the test set. This satisfies splitting the dataset into train and test set for evaluating the performance of the test set from an entirely unknown set of data. Also, use of the entire dataset for performance evaluation might overlook the overfitting tendency of the classification model (Mangalathu and Jeon, 2018; Friedman, 2001).

From Figures 3.5 and 3.6 it can be observed that the performance of Random forest, Decision tree, XGboost, and Catboost is satisfactory compared to the other ML models. Based on the higher values for the evaluation metrics, classification model based on Decision tree algorithm is suggested to identify the failure mode of CBP connection.
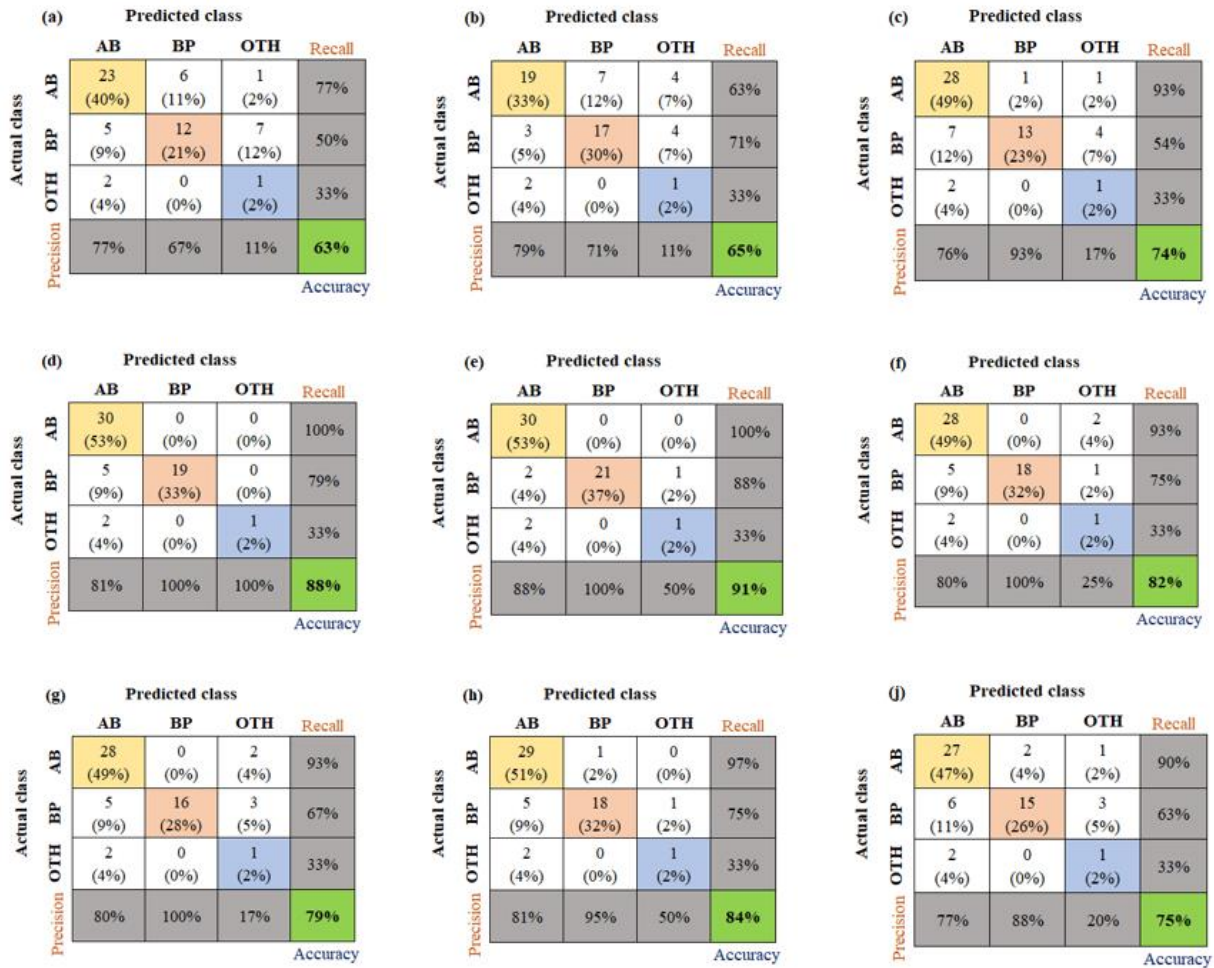
Figure 3.6 Confusion matrix of classification models of various ML techniques using the test set: (a) support vector machine, (b) naïve bayes, (c) k-nearest neighbors, (d) random forest, (e) decision tree, (f) XGboost, (g) LightGBM, (h) Catboost, and (j) Adaboost

35

Furthermore, cost complexity pruning analysis is conducted to check the overfitting criteria of the Decision tree model. This pruning technique involves controlling the tree size by the cost complexity parameter, ccp alpha, where its value is directly proportional to the number of tree nodes to be pruned. Figure 3.7 shows the ccp alpha value with respect to the accuracy for both training and test data. It can be seen from Figure 3.7 that both the training and test set have the highest accuracy corresponding to a zero ccp alpha value which is the default parameter for Decision tree algorithm. This implies that the model has its optimized tree size for the default ccp alpha value and pruning of tree nodes is not required.
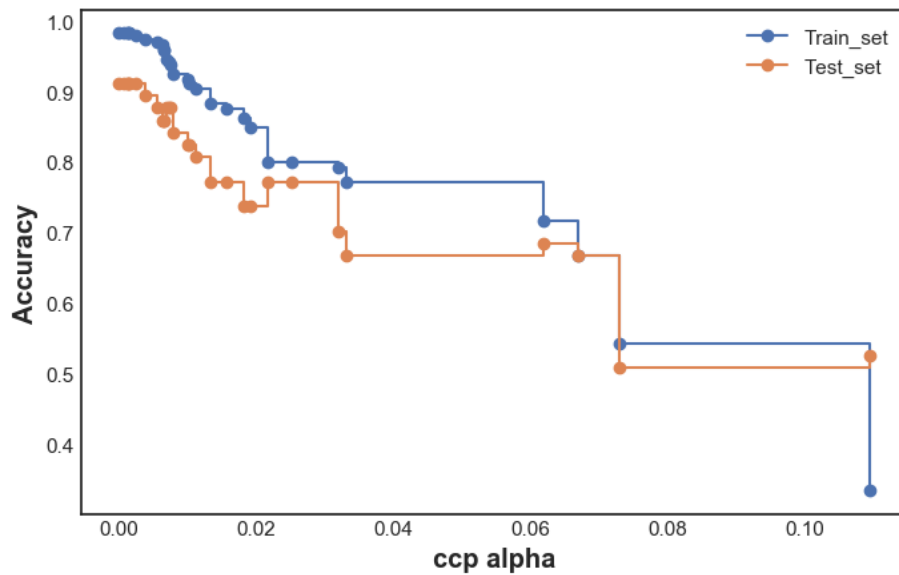
Figure 3.7 Cost complexity pruning of Decision tree model

3.5 Feature Importance of Selected Parameters

Feature importance analysis is performed to evaluate the importance of the selected input features for the Decision tree model. Such type of analysis enables engineers and researchers to identify potential failure modes of CBP connection and thereby adopt adequate measures against such failures. Figure 3.8 shows the relative importance of the input parameters expressed in percentage. Base plate thickness, embedment length, and anchor rod diameter are the critical parameters whereas grout thickness and anchor quantity have lower influence for governing the failure mode of CBP connection as shown in Figure 3.8.
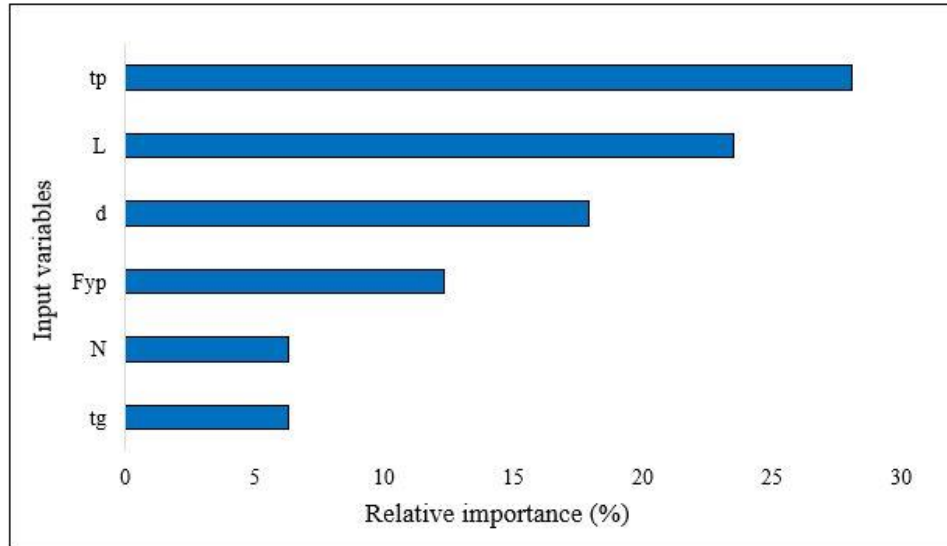
Figure 3.8 Relative importance of input parameters in Decision Tree model

3.6 Sensitivity Analysis of Selected Parameters

Sensitivity analysis is performed in the Decision tree model to find out the interaction between the input variables and the output feature by changing the value of one input variable while keeping the values of the other input variables constant. Recently, Mangalathu et al. (2020) employed SHapley Additive exPlanations (SHAP) approach in ML model for predicting the failure mode of reinforced concrete columns and shear walls to determine the relationship between the input and output variables. Considering the error value, sensitivity of each variables of the developed ML model is shown in Figure 3.9. It shows the changes in the accuracy of failure mode predictions for which the permutation is the shuffling of a set of values among the variables. This permutation method is used to calculate the change in the mean prediction for every possible class of failure, e.g., "AB vs. BP", "AB vs Others", "BP vs. Others", and "Mean (AB vs BP vs Others") change in sensitivity. For instance, if all the variables are kept constant and only the inputs of "t_p" are randomly changed, the model generates a mean change in accuracy of approximately 34%. However, if the model only considers changes in the prediction of failure mode for "AB vs BP", the sensitivity becomes 27%. Thus, the permutation method gives not only the overall change in the mean accuracy but also the associated changes between the prediction accuracies of all the failure modes. The degree of randomness in the permutation is estimated by repeating the procedure with more than one shuffle. This shuffling measures the variation of the overall

37

performance from one reshuffle to another. In other words, it shows the margin of change in the mean prediction value due to reshuffling.
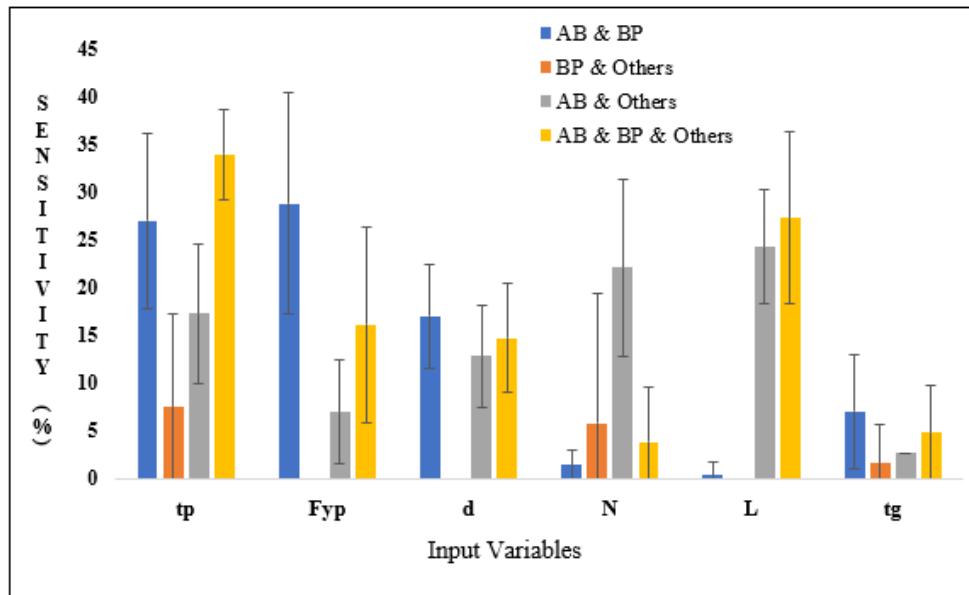
Figure 3.9 Sensitivity of input parameters for prediction accuracy

3.7 Comparison of ML Model with Experimental Results and Empirical Equations

A comparison has been performed among the available experimental results, developed ML model, and empirical equations available in AISC Design Guide 1 (Fisher and Kloiber, 2006). From the constructed dataset, only 53 dataset contains the required parameters to be implied in the empirical equations. Typical calculation details of the empirical equations are provided in Appendix A (Table A2) for 7 experimental results. Figure 3.10 shows the comparison of failure mode prediction by the ML model and empirical equations. It is found from Figure 3.10 that the developed ML model has an accuracy of 74% for identifying the anchor rod type failure mode of column base plate connection whereas the empirical equation is unable to capture any of the anchor rod yielding failure mode observed during the experiment. In the case of identifying the base plate yielding type failure mode, both the ML model and empirical equations overestimate the failure mode by 91% and 109%, respectively from the observed experimental results. The developed ML model performed well enough to identify the others type of failure mode compared to the empirical equations. It is evident from Figure 3.10 that the developed ML model has outperformed the empirical equations to identify all three types of failure mode considered in this study. It should

be noted that the comparison performed in this section is based on the 53 selected dataset since the parameters required to perform the calculations using empirical equations are not available in the rest of the dataset. The overall performance of the developed ML model as evaluated earlier is completely different since only a subset of the 189 dataset are used here for comparison with the empirical equations.
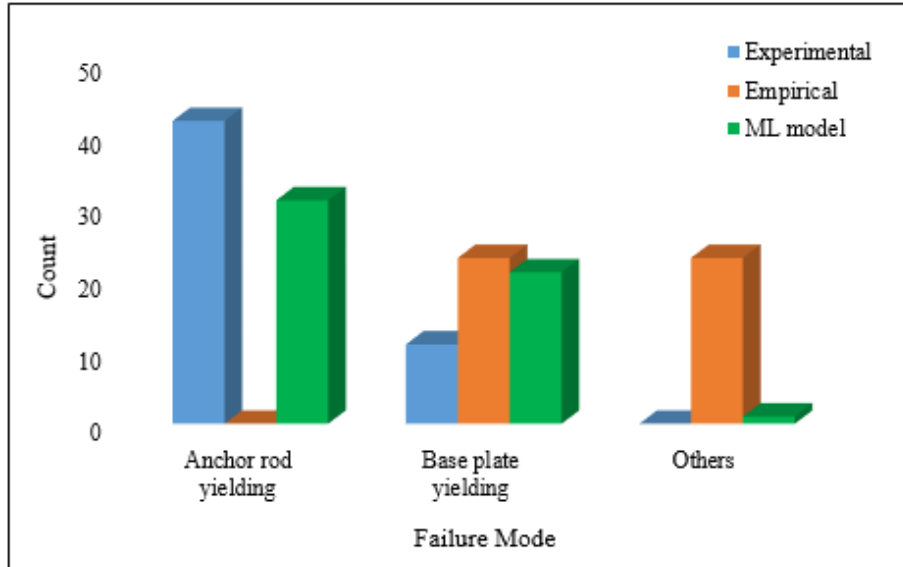
Figure 3.10 Prediction comparison of ML model and empirical equations

3.8 Development of Graphical User Interface (GUI)

This study extends to the development of a graphical user-friendly interface (GUI) tool from the developed ML model by using an open source python library 'Streamlit'. A simple web application of dependent domain is created using the 'Streamlit' library. Figure 3.11 shows the main interface which is simple and easy to use. Users can enter numeric values for the input variables and get the failure mode prediction as the output by clicking on the 'Identify' button. The developed GUI tool has been tested and it is found to be operational and also has the flexibility for future development whenever it is required. Although the GUI tool is functional, further development is required to make it more robust for wider applicability.

Figure 3.11 Data-driven model interactive graphical user-friendly interface (GUI)

3.9 Summary

This chapter introduces a rapid failure mode identification technique for CBP connections by exploring the recent advances in machine learning (ML) techniques. A comprehensive database is assembled with 189 available experimental results for CBP connections including various parameters affecting the CBP behavior. To establish the best classification model, a total of nine different ML algorithms such as Support vector machine, Naïve bayes, K-nearest neighbors, Decision tree, Random forest, Adaboost, XGboost, LightGBM, and Catboost are considered in this study. Comparing the developed ML models, the Decision tree based ML model developed in this study is suggested which has an overall accuracy of 91% for identifying the failure mode of CBP connections. It is also found that base plate thickness, embedment length, and anchor rod diameter are the influential parameters that govern the failure mode of CBP connections. Furthermore, an open-source classification model is provided to rapidly identify the failure mode of CBP connection by allowing modifications for future developments.

Chapter 4   Finite Element Modeling and Validation

4.1 General

This chapter describes the overall methodology used to develop the Finite Element (FE) models of exposed column base plate (CBP) connections followed by the validation of the developed models. A detailed 3D nonlinear FE model is developed using ABAQUS (SIMULIA Inc. 2020) simulation platform. The performance of the FE model depends on the modeling of contacts between different parts of the CBP connections, complexities associated with the geometry of the connection as well as the constitutive response of the material nonlinearity. FE model constructed for validation in this study considered the geometric and material properties of CBP connections experimented by Gomez et al. (2010). Previously, these test results were simulated in ABAQUS by Kanvinde et al. (2013) to observe the internal stress distribution as well as the deformation and forces in the base plate and anchor rod, respectively. A similar approach is adopted in this study to develop and validate the FE model for both cyclic and monotonic loading responses. The FE model is developed and validated in two phases where the model is constructed as a half model first due to the symmetric nature of the specimen under monotonic loading to reduce the simulation time for interpreting a suitable modeling strategy. Later, a full FE model is developed instead of the half-model to simulate the accurate behavior under combined axial load and lateral cyclic loading. The models are validated in terms of anchor rod force, base plate deformation, and hysteresis loop of developed FE model.

4.2 Geometric Details

All the elements are modelled as 3D deformable solid elements except the column in the full model which is defined as shell elements for validating the complex cyclic simulation with the consideration of global and local buckling behavior (Elkady 2016). The column is considered as a W200x71 section and the length of the column is considered as 2350 mm from the top of the base plate which is similar to the experimental analysis performed by Gomez et al. (2010). The cross-sectional dimension of the grout is considered the same as the base plate dimension (356mm x 356mm). A 610x610x610 mm concrete pedestal is considered for the foundation of the CBP connection. Figure 4.1 shows the geometry and dimensions of the specimens used to validate the FE model.
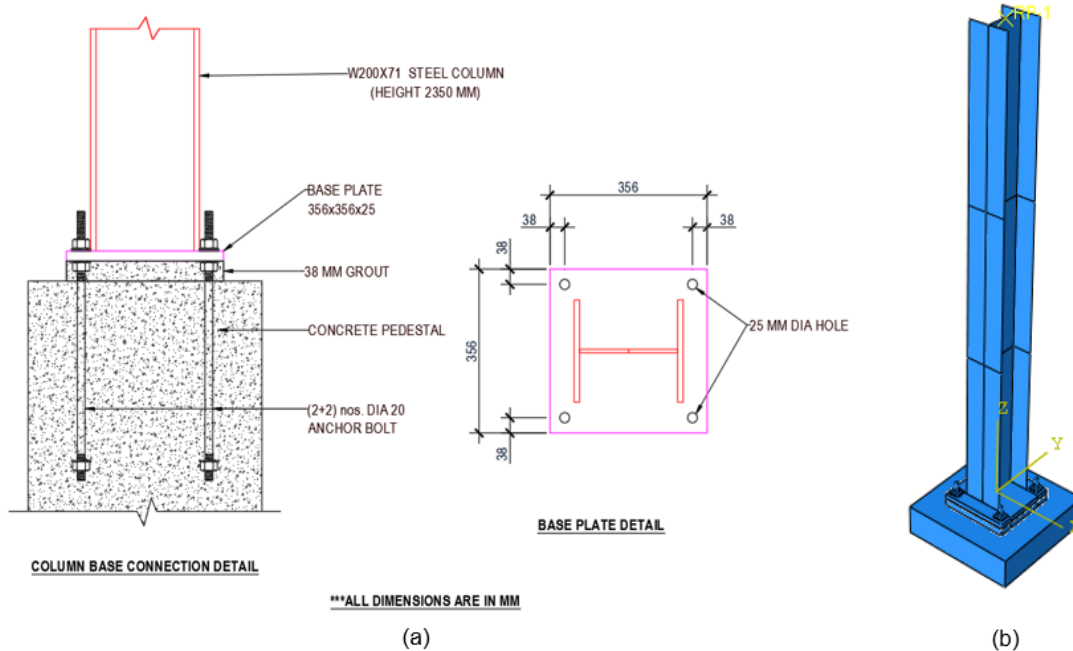
Figure 4.1 (a) Geometric details (b) Developed FE model

4.3 Element Type and Mesh

All the 3D solid elements of the developed model are meshed with hexahedral (C3D8R) element whereas the shell element of the column is meshed with quadratic 4-node doubly curved (S4R) shell elements accumulating a total number of 82000 elements. Geometric nonlinearity (NLGEOM) is considered due to the nonlinear effects of large displacement. Column is meshed by dividing its length into three equal parts for computational efficiency. The bottom part is meshed using 10mm x 10mm elements to neglect the convergence issue with the base plate while the other parts are meshed using a coarser mesh size. Base plate and grout are meshed by a size similar to that of the column bottom part. Anchor rods, nuts, and washers are meshed using a finer element of 2.5mm x 2.5mm to accurately capture the stress behavior of the elements. Since the behavior of footing is not considered in this study, a relatively coarser mesh size of 20mm x 20mm than the other elements is considered for the pedestal. A typical, but not extensive, mesh sensitivity study is conducted to accurately predict the results as well as the computational time efficiency of the developed FE model. As for an example, the column is meshed using three gradually increasing mesh size to reduce the total number of elements where the bottom part contains the similar mesh size as the base plate. Since the upper portion of the column is not critical for this study, relatively

larger mesh size is considered for the upper two parts of the column. Figure 4.2 illustrates the mesh configuration of developed FE model.
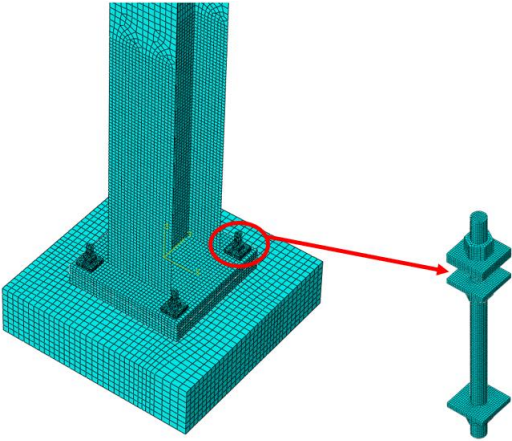
Figure 4.2 Mesh configuration of the developed FE model

4.4 Geometric Imperfection

It is very usual for steel structural elements to contain geometric imperfections as well as residual stresses due to the manufacturing and handling process. Geometric imperfection is introduced to capture the global out-of-straightness imperfections of the column. Separate linear perturbation buckling analysis was performed to obtain different buckling modes of the respective column. A global out-of-straightness limit equal to L/1500 (Elkady 2016) is applied with the first buckling mode of the column during the construction of the full model under cyclic loading as shown in Figure 4.3.
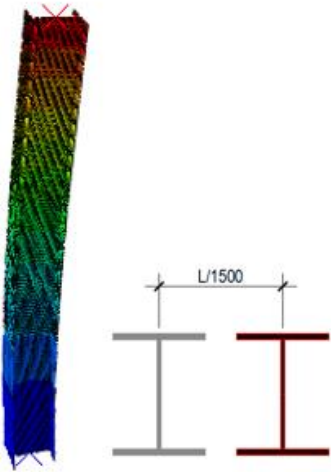
Figure 4.3 First buckling mode for global geometric imperfection

43

4.5 Contact and Interactions

Explicit modeling of component interaction is critical, therefore suitable constraints and interactions need to be implemented as the contact and gapping of CBP connection components control the overall connection response (Kanvinde et al. 2013). Tie constraints are provided between the column-base plate, anchor rods-nuts- washers, and grout-concrete because of their monolithic properties. Although few past studies identified weld fracture as a mode of failure, the connection between column and base plate is considered to be completely fixed with a tie constraint, to substitute for the welds in the experimental specimens. Additionally, it is assumed in this study that the welds are designed to resist fracture following the experimental study by Gomez et al. (2010). Surface to surface contact interactions are defined between the interfaces of the base plate and grout, base plate and both the top and bottom washer, and anchor rod-base plate with the finite sliding formulation. Two different interaction properties are defined for these surface to surface interactions. An isotropic friction formulation is defined using the penalty method (SIMULIA Inc. 2020) for the tangential behavior. A coefficient of friction of 0.45 is used for the base plate and grout whereas 0.80 is used for the other two interactions (Grigoriev et al. 1997). The pressure overclosure for normal behavior is considered as hard contact and separation after contact is allowed whereas the constraint enforcement method is set as default for both the interaction properties (SIMULIA Inc. 2020). No constraints or interactions are defined between the concrete footing and the anchor rods assuming their interfaces to be free as prescribed by Gomez et al. (2010). Figure 4.4 illustrates a schematic description of contact and interactions between different components of CBP connection.
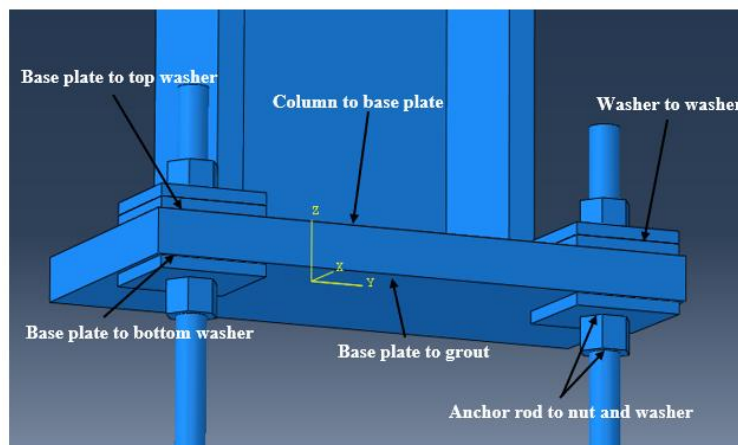
Figure 4.4 Contact and interactions of different components of CBP connection

44

4.6 Boundary Conditions

The bottom of the concrete footing is restrained in all six degrees of freedom to simulate a fixed-base condition. When the FE model is constructed as a half model under monotonic loading, a symmetric boundary condition is provided parallel to the center plane of the column web to simulate its full-scale behavior as shown in Figure 4.5. On the other hand, to accurately capture the flexural yielding and geometric instabilities under cyclic loading with full model, a flexible boundary condition is considered at a reference point defined at the cross-section center of the top of the column. This reference point is tied with the column top surface using rigid body constraint. For the flexible boundary condition under cyclic loading, the out-of-plane rotation, displacement, and the torsional rotation are constrained in the weak axis of the column. Both the monotonic and cyclic lateral loading is applied as in-plane displacement in the developed FE model.
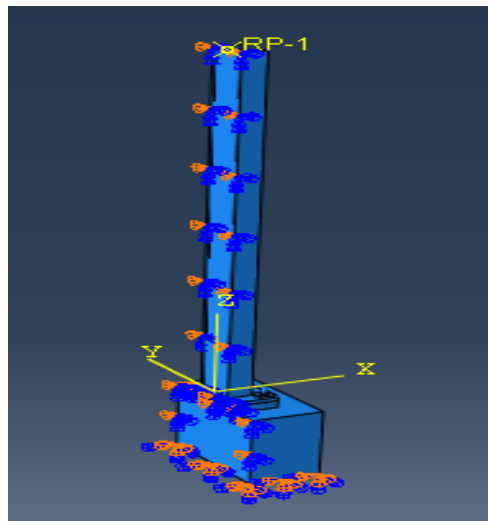
Figure 4.5 Y-axis symmetry for developed half FE model

4.7 Material Modeling

4.7.1 Steel Elements

Von-Mises type of material with a nonlinear isotropic/kinematic hardening material model is used to define the column and base plate. In addition to the modulus of elasticity and yield stress, the nonlinear kinematic and isotropic hardening components (C, γ, Q∞, b) are considered for cyclic loading which are derived from the Chaboche (2008) model. A nonlinear monotonic isotropic hardening is modeled for anchor rod whereas nut and washer are modeled as elastic-perfectly plastic material. The hardening parameters used for these parts are from the results of the ancillary

45

experiments conducted by Gomez et al. (2010). Table 4.1 and 4.2 provides the values used to define different steel materials for validation of developed FE model for monotonic and cyclic loadings, respectively.

Table 4.1 Steel material for monotonic loading

	Yield Stress (MPa)	Modulus of Elasticity (GPa)	Poisson's ratio	Material type
Column	345	200	0.3	nonlinear isotropic hardening
Base Plate	280	200	0.3	nonlinear isotropic hardening
Anchor Rod	786	200	0.3	nonlinear isotropic hardening
Nut & Washer	345	200	0.3	elastic perfectly plastic

Table 4.2 Steel material for cyclic loading

	Yield Stress (MPa)	Modulus of Elasticity (GPa)	Poisson's ratio	C (MPa)	γ	Q∞ (MPa)	b
Column	380	200	0.3	3378	20	90	12
Base Plate	255	216	0.3	6895	25	172	2
Anchor Rod	790	200	0.3	nonlinear isotropic hardening			
Nut & Washer	345	200	0.3	elastic perfectly plastic			

4.7.2 Concrete Elements

Concrete damage plasticity model is developed based on compressive strength for both grout and concrete pedestal. The compressive strengths used for developing concrete damage plasticity model are adopted from the ancillary test results by Gomez et al. (2010) for both footing & grout. For monotonic loading phase, the compressive strength of grout and footing is considered as 51 and 27 MPa, respectively. Similarly, the compressive strength of grout and footing is considered as 64 and 30 MPa, respectively for the cyclic loading case. Default values were used for the other parameters from Shaheen et al. (2017) to define the concrete damage plasticity model as provided in Table 4.3. Figure 4.6 shows typical damage plasticity model used to define concrete elements.

Table 4.3 Concrete damage plasticity parameters

Parameters	Value
Dilation angle (ψ)	36^0
Eccentricity (e)	0.1
fb_0/fc_0	1.16
K	0.6667
Viscosity parameter	0.001
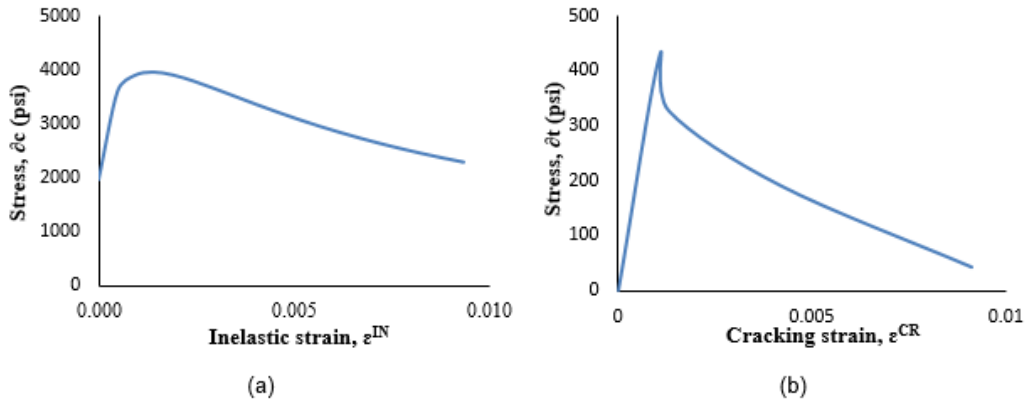
Figure 4.6 Concrete damage plasticity model for (a) compressive stress strain relationship and (b) tensile stress strain relationship

4.8 Loading Protocol

At first, monotonic loading in the form of lateral displacement (10.58% column drift) is applied along the major axis direction with no axial load. After validating under monotonic load, SAC cyclic loading protocol with a maximum drift of 10.6% as shown in Figure 4.7 is applied in the column major axis direction with a constant 410 KN axial compression at the top of the column to validate the model accuracy under combined axial load and uniaxial cyclic loading. The axial compressive and lateral loading are defined in two discrete steps where the axial compressive load is applied entirely before the lateral load is applied. The lateral loading is defined as a displacement boundary condition and is applied on the reference point defined at the cross-section center at the top of the column.
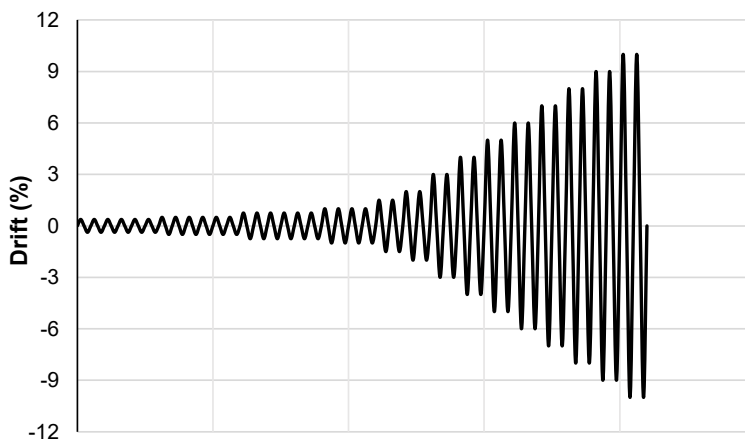
Figure 4.7 SAC cyclic loading protocol

4.9 Validation of Developed FE Model

The developed FE model is validated against experimental results from Gomez et al. (2010) under monotonic and cyclic loading for Test no. 1 and Test no. 5, respectively to check the accuracy of the adopted modeling approach. For monotonic loading, the developed half FE model is validated in terms of anchor rod force and base plate deformation profile as shown in Figure 4.8 and 4.9, respectively. As described by previous researchers (Myers et al. 2009, Kanvinde et al. 2013), an excellent fit of the load-deformation response can't be solely relied upon for accurate prediction of experimental response using FE simulation. To complement the accuracy of the load-deformation response prediction shown in Figure 4.8, the contour plot of the base plate deformation response is also compared in Figure 4.9. From both the Figures, it can be seen that the developed FE model can very well predict the experimental results with reasonable accuracy signifying the suitability of the adopted modeling techniques and material models. Specifically, the maximum anchor rod force is found to be 220.12 kN and 213.24 kN for the numerical and experimental results, respectively having a 3% difference between them whereas the deformation of base plate is observed almost identical in terms of both value and contour plot.
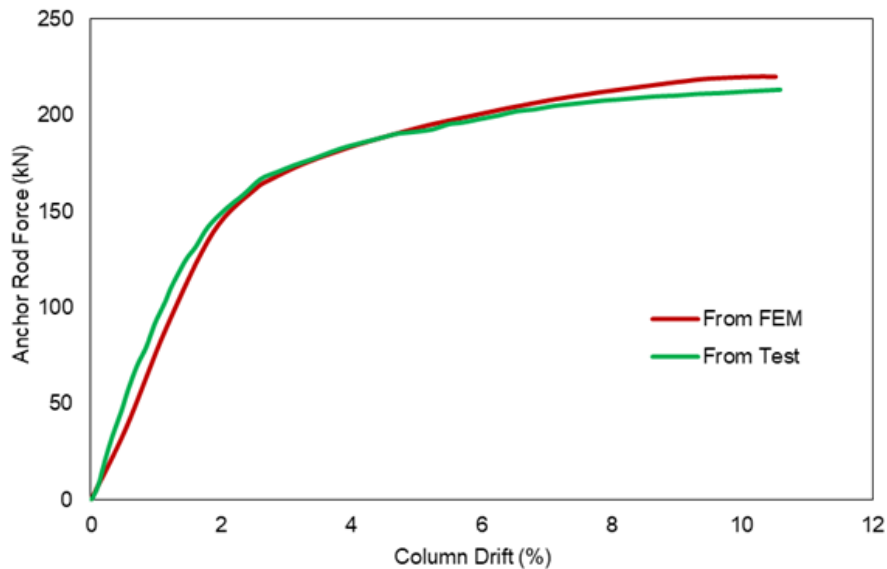
Figure 4.8 Comparison of experimental (Gomez et al. 2010 Test no. 1) and numerical (FE) results
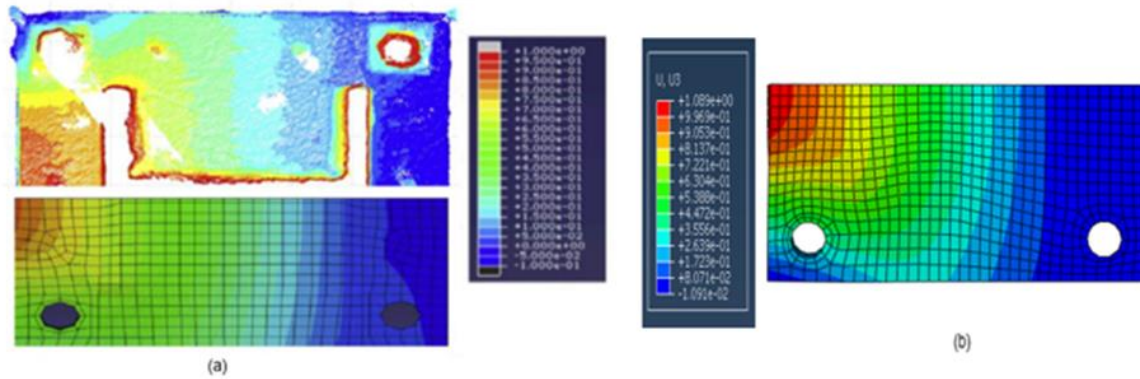
Figure 4.9 Base plate deformation behavior (a) Gomez et al. (2010) Test no.1 (b) developed FE model

Further, the full FE model is validated under cyclic loading protocol in terms of the lateral load-displacement profile as shown in Figure 4.10. It is found that the variation of maximum lateral load is only 3% between the experimental (Test No. 5 of Gomez et al., 2010) and numerical results. Also, it is evident from Figure 4.10 that the hysteresis loop for the developed FE model and experimental results are quite similar except for the slipping behavior which is due to the complexity of the interactions among the various CBP connection elements. All these validation results suggest that the adopted modeling techniques can be applied with a high degree of confidence for further investigation.
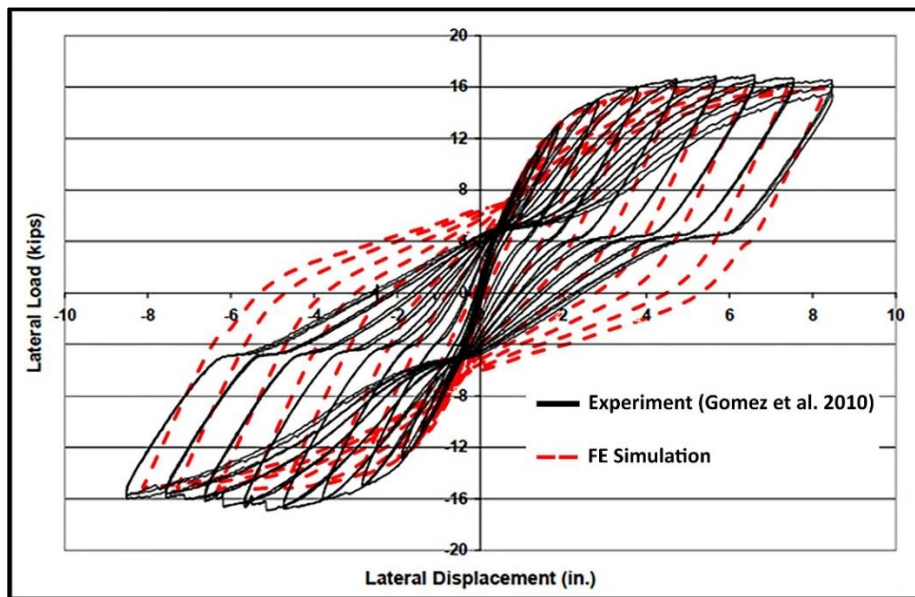
Figure 4.10 Validation of FE model using cyclic loading

49

4.10 Summary

This chapter provides details of the FE modeling approach adopted in this study for modeling the response of CBP connections. The developed FE models are validated by comparing the analytical results against various experimental observations (e.g. anchor rod load deformation curve, base plate deformation, hysteretic response) under lateral monotonic and cyclic loading combined with axial load. This chapter develops an accurate nonlinear FE model of exposed column base plate connections subjected to combined axial load and lateral cyclic loading to investigate the behavior of different base connection components under combined axial load and biaxial bending through an extensive parametric study described in Chapter 5.

Chapter 5   Parametric Study of Column Base Connection under Combined Axial load and Biaxial Bending

5.1 General

This chapter presents the numerical parametric study conducted on exposed column base plate connections to understand the behavioral insights of the CBP connections under combined axial load and biaxial bending using the models validated in the previous Chapter. Since no symmetric plane is available when the specimen is subjected to biaxial bending, a full model is considered in order to simulate the behavior of the CBP connection. The parametric investigation considered base plate thickness and yield strength, anchor rod size, quantity and embedment length, grout thickness as well as axial load ratio. Furthermore, the results that have been scrutinized from the parametric study are the moment-rotation response, maximum bolt tensile force, and the base plate yield line patterns. Moment–rotation curve is a key output to better understand the connection behavior which defines the rigidity, resistance and rotational capacity of any connection. Bolt tensile force is important for designing the capacity of the anchor bolt as well as to check the pullout and breakout strength. Yield line patterns of the base plate indicate the severely stressed section while also determining the required base plate thickness. Connection rigidity in terms of rotational stiffness is also investigated to characterize the type of CBP connection behavior under combined axial load and biaxial bending. Finally, a comparison is performed between the rotational stiffness of CBP connection under biaxial bending with available equations for uniaxial bending.

5.2 Parametric Analysis Cases

Parameters of the analytical investigation are selected from the literature review conducted by Grauvilardell et al. (2005) as well as the previous parametric study done by Trautner and Hutchinson (2018) where they categorized different parameters of CBP connection into a low, medium and high category. This study identified the influential parameters of CBP connection failure using the data-driven machine learning approach explored in Chapter 3. Considering all these studies which utilize different parameters, seven parameters with variable ranges are chosen to be considered in this study. A total of 20 FE models are developed for the parametric study to

understand the behavioral insights of the CBP connections under combined axial load and biaxial bending. Table 5.1 provides the details of the different parameters and simulation matrix considered in this parametric study where the bold numbers indicate the variable values of different parameters. Each of the cases considered only one variable at a time to understand its effect on the base plate connection considering PR-01 as the base model.

Table 5.1 Simulation matrix of the parametric study

| Parameter | Specimen ID | Parameter Values | | | | | | |
		Base Plate Thickness (mm)	Base Plate Yield Strength (Mpa)	Anchor Rod Dia (mm)	Anchor Quantity (No's)	Embedment Length (mm)	Grout Thickness (mm)	Axial Load Ratio
Base Model	PR-01	**25**	**350**	**20**	**4**	**500**	**25**	**0.2**
Base Plate Thickness	PR-02	**16**	350	20	4	500	25	0.2
	PR-03	**20**	350	20	4	500	25	0.2
	PR-04	**30**	350	20	4	500	25	0.2
	PR-05	**38**	350	20	4	500	25	0.2
	PR-06	**50**	350	20	4	500	25	0.2
Base Plate Yield Strength	PR-07	25	**300**	20	4	500	25	0.2
	PR-08	25	**400**	20	4	500	25	0.2
Anchor Rod Dia	PR-09	25	350	**16**	4	500	25	0.2
	PR-10	25	350	**25**	4	500	25	0.2
	PR-11	25	350	**30**	4	500	25	0.2
	PR-12	25	350	**38**	4	500	25	0.2
Anchor Quantity	PR-13	25	350	20	**6**	500	25	0.2
	PR-14	25	350	20	**8**	500	25	0.2
Embedment Length	PR-15	25	350	20	4	**250**	25	0.2
	PR-16	25	350	20	4	**750**	25	0.2
Grout Thickness	PR-17	25	350	20	4	500	**0**	0.2
	PR-18	25	350	20	4	500	**50**	0.2
Axial Load Ratio	PR-19	25	350	20	4	500	25	**0.25**
	PR-20	25	350	20	4	500	25	**0.3**

5.3 General Features of the FE Models

All the developed FE models of the parametric analysis cases have similar geometric and material properties. ASTM A992 Grade 50 W250x73 column section (typical interior first story column) having 2000 mm length (2/3rd of typical first story height of SMRFs) is designed according to the requirements of CSA S16-19 (CSA 2019). Typical design calculations are provided in Appendix

B. The column is designed considering yield strength (F_y) of 345 MPa and modulus of elasticity (E) of 200 GPa. The cross-section is selected to prevent local buckling criteria as well as having an adequate capacity to ensure its effectiveness before the failure of the base plate connection. A rectangular base plate of 407 mm x 407 mm, welded together with the column, having different thicknesses and yield strength is selected for the study. Anchor rods of different sizes, quantities, and embedment lengths are designed using yield strength and modulus of elasticity of 790 MPa and 200 GPa, respectively, following the requirements of CSA S16-19 (CSA 2019) and CSA A23.3-19 (CSA 2019) to prevent any type of failure in the concrete by pullout or breakout strength. Typical arrangement in the base plate for different anchor rod quantities is provided in Appendix C. The nut and washers are selected according to standard geometry for the specific anchor rod. A concrete foundation of 1220 mm x1220 mm of different depths corresponding to different embedment lengths is designed to support all types of loading. Non-shrink grout having a compressive strength of 64 MPa of various thicknesses is also considered between the pedestal and the base plate whereas the compressive strength of footing is considered as 30 MPa.

All the FE models developed for the parametric analysis study have the same configuration of mesh size, geometric imperfection, tie contact, and interaction properties as the validated full FE model. Anchor rod, nuts and washers and concrete material properties of the developed FE models are also the same as the validated model. Since the geometric and material properties of the column section do not change during the parametric analysis study, the hardening parameters for the column remain the same as the validated FE model. Hardening parameters for the base plate vary with the different base plate yield strengths. These parameters are the key to capture the accurate cyclic behavior of the base plate connection and are found through an extensive literature review (Sousa et al. 2020). Table 5.2 provides details of the hardening parameters corresponding to different yield strength and modulus of elasticity of the base plate.

Table 5.2 Hardening parameters for different base plate yield strength

Considered Yield Stress (MPa)	Obtained Yield Stress (MPa)	Modulus of Elasticity (GPa)	C1 (MPa)	$\gamma 1$	C2 (MPa)	$\gamma 2$	Q∞ (MPa)	b
300	306	178	11613	122	1744	8.29	94	5.81
350	339	183	8716	118	1182	5.22	78	9.29
400	376	189	13712	139.7	1147	4.59	29	6.41

5.4 Bidirectional Lateral Loading Protocol

A bidirectional symmetric lateral loading protocol is developed for the numerical investigation in pursuance of evaluating the effect of biaxial bending on the exposed CBP connection. This cyclic loading protocol is developed for a four-story steel frame building following the concepts discussed in Krawinkler (1996) and Elkady (2016). The loading protocol covers a wide range of story drift ratios starting from 0.375% amplitude up to amplitude of 4% radians in the column's strong axis direction as shown in Figure 5.1(a). It also covers story drift ratio ranging from 0.25% to 2% amplitude in the column's weak axis direction as shown in Figure 5.1(b). When combined, it is found that the developed bidirectional loading protocol achieves a maximum drift ratio of 3% in the column's strong axis direction when 2% drift amplitude is reached in the column's weak axis direction as depicted in Figure 5.1(c). Detail procedure of the developed bidirectional loading protocol is described in Elkady (2016).

(a)

(b)

(c)
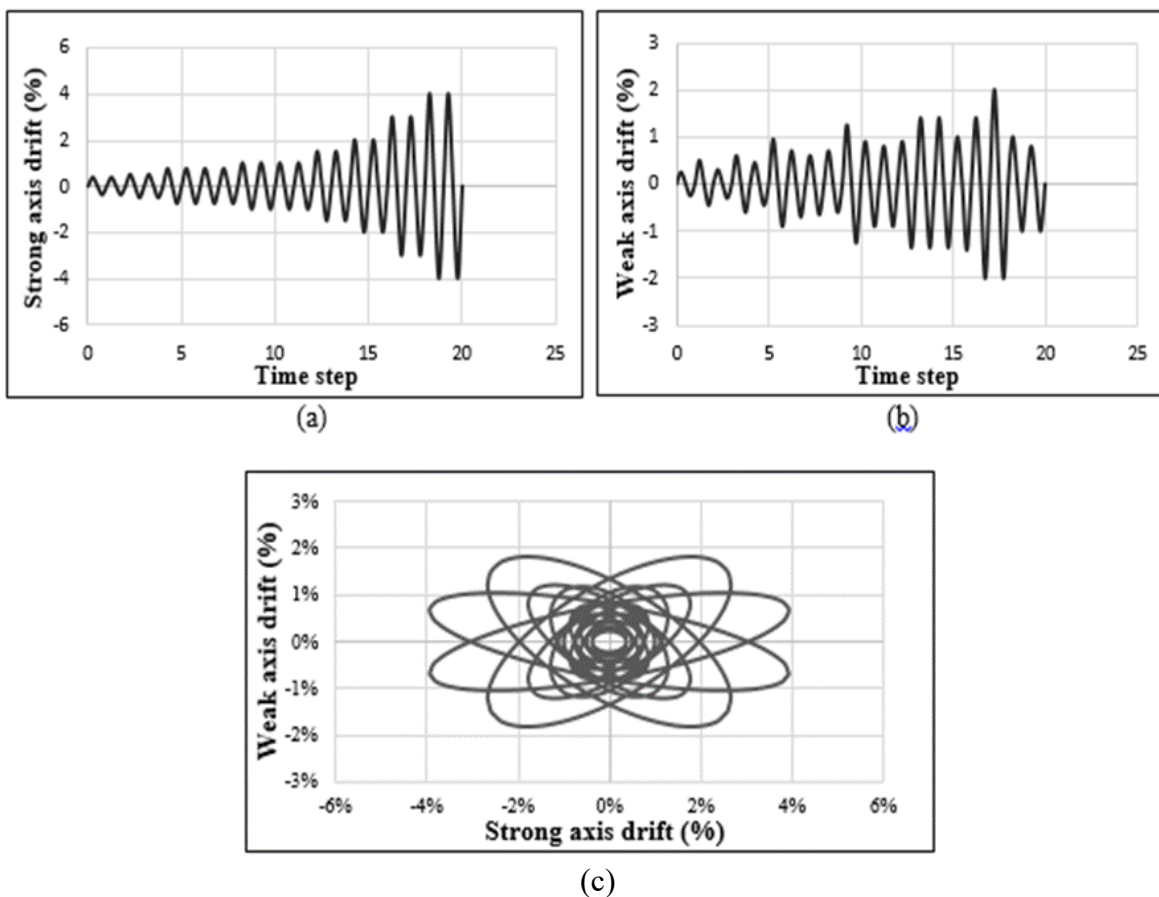
Figure 5.1 Developed bidirectional symmetric lateral loading protocol: (a) history of strong axis drift ratio; (b) history of weak axis drift ratio; (c) history of strong axis vs weak axis drift ratio

5.5 Analysis Results

The analytical results obtained from the parametric study have been used to further understand the behavior of exposed CBP connections subjected to combined axial load and biaxial bending. Table 5.3 provides the summary of the results extracted from the FE models. Results are investigated in terms of moment-rotation response, maximum bolt tensile force, and base plate yield line patterns.

Table 5.3 Summary of FE model results

FE Model ID	Axis	Yield			Ultimate			$K_{\theta(Yield)} / K_{\theta(Ultimate)}$
		M (KN-m)	$\theta \times 10^{-3}$ (rad)	$K_\theta \times 10^3$	M (KN-m)	$\theta \times 10^{-3}$ (rad)	$K_\theta \times 10^3$	
PR-01	X	120.26	13.89	8.66	184.75	33.87	5.45	1.59
	Y	43.28	6.45	6.71	72.20	15.52	4.65	1.44
PR-02	X	49.58	6.68	7.42	78.10	37.38	2.09	3.55
	Y	24.14	3.64	6.63	40.67	16.89	2.41	2.75
PR-03	X	93.22	10.68	8.72	163.81	34.49	4.75	1.84
	Y	40.5	6.57	6.17	63.54	16.07	3.95	1.56
PR-04	X	150.44	12.69	11.85	220.00	32.43	6.78	1.75
	Y	48.68	6.31	7.71	79.43	15.56	5.10	1.51
PR-05	X	155.60	12.65	12.30	244.29	31.40	7.78	1.58
	Y	51.44	6.34	8.11	85.65	15.42	5.55	1.46
PR-06	X	181.52	11.73	15.47	241.43	31.62	7.64	2.03
	Y	53.36	6.27	8.51	89.00	15.25	5.84	1.46
PR-07	X	149.38	21.59	6.92	182.86	33.63	5.44	1.27
	Y	44.52	6.46	6.89	71.91	15.92	4.52	1.52
PR-08	X	154.74	21.67	7.14	195.71	33.09	5.91	1.21
	Y	46.64	6.72	6.94	74.50	15.72	4.74	1.46
PR-09	X	117.20	13.96	8.39	175.71	33.74	5.21	1.61
	Y	37.96	5.19	7.32	71.77	15.81	4.54	1.61
PR-10	X	133.56	13.53	9.87	197.14	33.17	5.94	1.66
	Y	44.98	6.23	7.22	74.64	15.65	4.77	1.51
PR-11	X	132.88	13.48	9.86	205.71	32.89	6.25	1.58
	Y	47.24	6.38	7.41	75.60	15.68	4.82	1.54
PR-12	X	139.34	13.19	10.57	220.00	32.31	6.81	1.55
	Y	46.98	6.42	7.32	76.56	15.59	4.91	1.49
PR-13	X	123.86	13.72	9.03	194.29	33.26	5.84	1.55
	Y	38.6	4.76	8.12	76.56	15.65	4.89	1.66
PR-14	X	124.30	13.33	9.33	200.00	32.95	6.07	1.54
	Y	39.58	4.72	8.38	77.99	15.61	5.00	1.68
PR-15	X	132.74	13.48	9.85	195.71	33.09	5.91	1.67
	Y	47.58	6.43	7.40	73.81	15.80	4.67	1.58
PR-16	X	117.00	13.74	8.51	185.71	33.54	5.54	1.54

	Y	44.02	6.45	6.82	71.77	15.75	4.56	1.50
PR-17	X	123.12	13.76	8.95	188.57	33.32	5.66	1.58
	Y	44.52	6.44	6.91	73.21	15.82	4.63	1.49
PR-18	X	122.12	13.71	8.91	187.14	33.37	5.61	1.59
	Y	43.34	6.50	6.67	72.25	15.85	4.56	1.46
PR-19	X	119.48	13.87	8.61	180.00	33.60	5.36	1.61
	Y	42.92	6.63	6.47	71.77	15.93	4.51	1.44
PR-20	X	123.02	13.81	8.91	181.43	33.55	5.41	1.65
	Y	45.24	6.35	7.12	71.77	15.81	4.54	1.57

5.5.1 Moment Rotation Behavior

For each FE simulation, the hysteretic response in terms of base moment-rotation is plotted as shown in Figure 5.2 and compared within the various values of the specific parameter considered in the analytical study. Further bi-linear moment-rotation curve, considering yield point and ultimate point, is developed for both the strong (x-axis) and weak axis (y-axis) and analyzed separately for convenient visualization. Column plastic moment capacity (M_p) is also shown in the same plot (horizontal line) for both strong $(M_{px} = 346.5$ kN-m) and weak $(M_{py} = 162.4$ kN-m) axis direction. The column base moment (M) and base rotation (θ) are computed from the column lateral force and lateral displacement according to Eq. (5.1) and Eq. (5.2), respectively.

$$M = F \, x \, H_{col} \tag{5.1}$$

$$\theta = (\Delta_{top} - \frac{F \, x \, H_{col}^3}{3 \, x \, E_{col} \, x \, I_{col}}) \, x \, \frac{1}{H_{col}} \tag{5.2}$$

Where, F is the lateral force at the column top, H_{col} is the column height from the base plate, Δ_{top} is the displacement at the top of the column, E_{col} is the modulus of elasticity of the column, I_{col} is the column's second moment of inertia in the direction of loading.
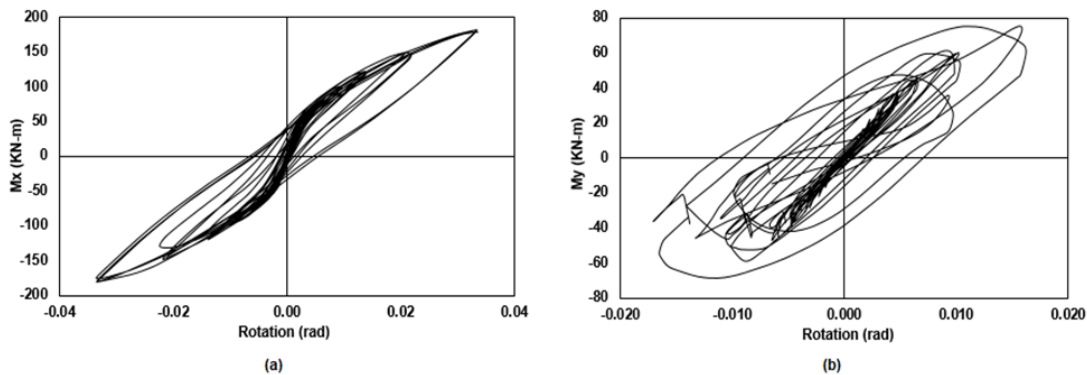
Figure 5.2 Moment-rotation hysteresis curve for PR-01 model (a) Strong axis (b) Weak axis

5.5.1.1 Effect of Base Plate Thickness

Six different base plate thicknesses (PR-01 to PR-06) are considered with values ranging from 16 mm to 50 mm. For the base model (PR-01), the base plate thickness of 25 mm is considered for the study which is widely used in the construction industry. Figure 5.3 illustrates the comparison of bilinear moment-rotation curves for various base plate thicknesses. It is observed from Figure 5.3 that a higher value of base plate thickness increases both the stiffness and the strength of the connection for both strong and weak axis direction. This is plausible since an increase in base plate thickness increases the flexural rigidity as well as bending resistance of the plate. However, it should be noted that the effect of base plate thickness is more pronounced in the strong axis direction compared to the weak axis. The average yield rotation in the major axis direction is 11.39×10^{-3} (rad) and 5.48×10^{-3} (rad) in the minor axis direction. It is to be noted that local buckling in the column is observed near the base plate for 50 mm (PR-06) base plate thickness which is an indication of weak column-strong connection criteria for CBP connection as shown in Figure 5.4. A significant increase in the strength of the connection is observed after yielding for each of the simulation cases except for the PR-02 where the base plate thickness is considered as 16 mm. Early yielding of the base plate of lower thickness significantly hinders the strength gain of the CBP connection. As reported in Table 5.3, the average ratio of yield to ultimate rotational stiffness for various base plate thicknesses is 2.06 and 1.7 in the strong and weak axis direction, respectively. It is also found that the strength of all the base connections with different base plate thicknesses is significantly below the column plastic moment capacity in both the strong and weak axis directions. In brief, as the base plate thickness increases, the strength of the base connection is augmented with the reduction in ductility.
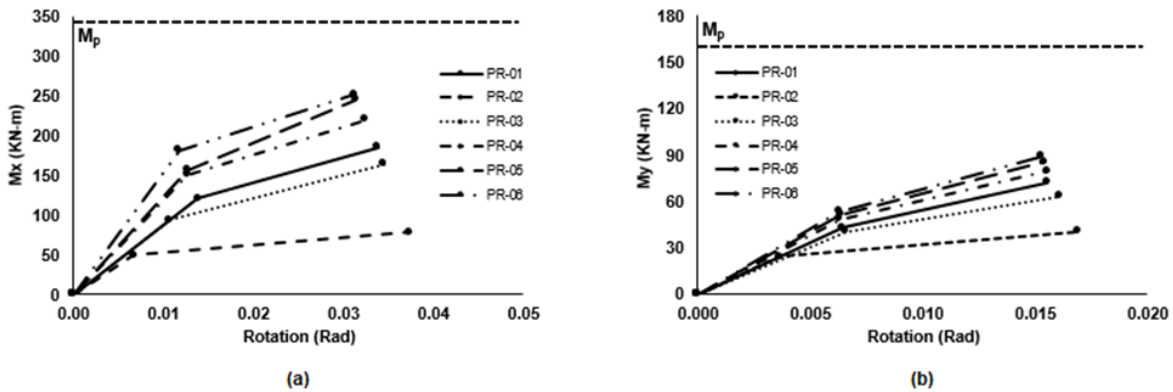
Figure 5.3 Effect of base plate thickness (a) Strong axis (b) Weak axis

57
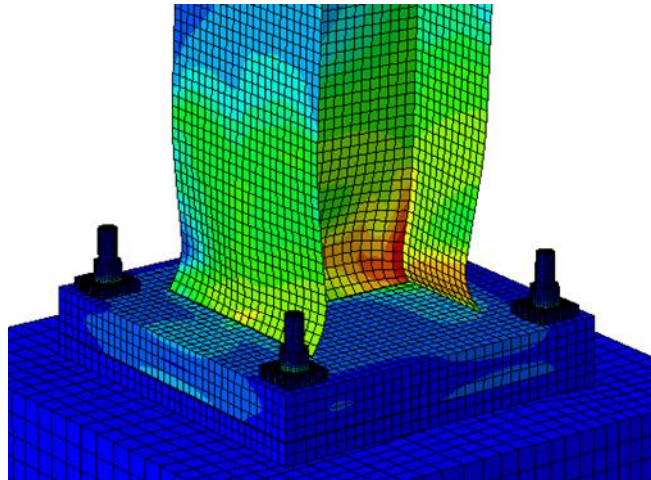
Figure 5.4 Local buckling of column in PR-06 model (50 mm base plate thickness)

5.5.1.2 Effect of Base Plate Yield Strength

Different base plate yield strengths of 300, 350 and 400 MPa (PR-01, PR-07 and PR-08) are considered to understand the effect of base plate yield strength on base plate connection behavior. Although base plate yield strength is not considered in the previous experimental study on CBP connections, it is considered in this study due to its contribution on the design of base plate thickness according to AISC Design Guide 1 (Fisher and Kloiber, 2006). The variations in the base plate strengths are considered based on the most commonly used steel grades in industry. It is to be noted that the considered base plate yield strength is adjusted due to the availability of the cyclic hardening parameters where the yield strength of 300, 350 and 400 MPa are modified to 306, 339 and 376 MPa, respectively as shown in Table 5.2. It can be seen from Figure 5.5 and Table 5.3 that base plate yield strength does not influence the moment-rotation response in the weak axis direction. However, initial stiffness is found to be lower when the base plate yield strength is changed from the base model of 350 MPa in the strong axis direction. Although a gradual variation is expected with the increasing base plate yield strength, the adjustment of the selected base plate yield strength with their corresponding hardening parameters which are derived from literature can impact the actual behavior.
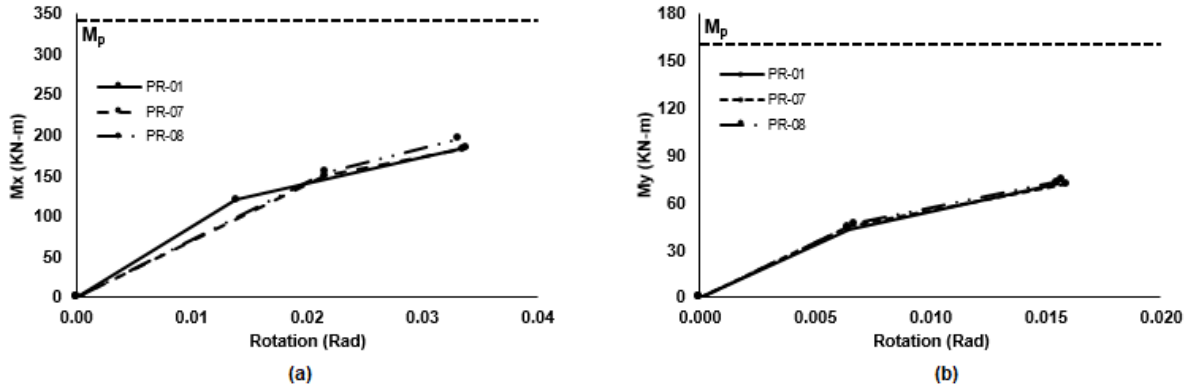
Figure 5.5 Effect of base plate yield strength (a) Strong axis (b) Weak axis

5.5.1.3 Effect of Anchor Rod Diameter

Melchers (1992) reported that CBP connection rotational stiffness increases with an increase of anchor bolt diameter. Different anchor bolt diameters ranging from 16 mm to 38 mm (PR-01, PR-09 to PR-12) are selected to scrutinize the moment-rotation behavior of CBP connections. Figure 5.6 represents the effect of anchor bolt diameter in terms of moment-rotation curves of the base plate connection. It is evident that an increase in anchor bolt diameter increases the initial stiffness as well as the strength in both axes directions. A larger bolt diameter affects the flexibility of the base plate cantilever length by contributing in the base rotation. An increase of 20% is observed for maximum strength in the strong axis direction when the diameter is increased from 20 mm to 38 mm. Conversely, a 6% increment is observed in the weak axis direction for the same configuration. Changes in the initial stiffness are found to be more obvious in the strong axis than the weak axis of the base plate connection. As reported in Table 4, the average ratio of yield to ultimate rotational stiffness is 1.60 and 1.52 in the strong and weak axis direction, respectively.
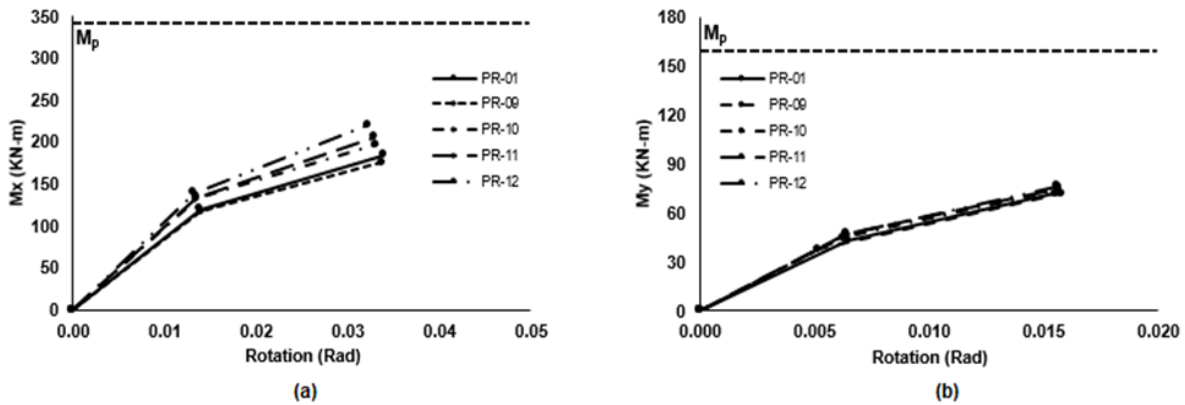
Figure 5.6 Effect of anchor rod diameter (a) Strong axis (b) Weak axis

5.5.1.4 Effect of Anchor Rod Quantity

Anchor bolt quantities of 4, 6, and 8 (PR-01, PR-13 and PR-14) are adopted to explore the behavior of CBP connection for different anchor bolt configurations. Figure 5.7 depicts the moment-rotation behavior of base plate connection for various anchor bolt configurations. Although not very significant, an increase in anchor rod quantity improves both the strength and stiffness of the base connection in both the strong and weak axis direction. An increase in bolt number affected both the elastic and post-yield stiffness in the weak axis direction. However, in the strong axis the effect is observed in post-yield stiffness. Since the bolt quantity is added only in the strong axis direction, the flexibility of the base connection becomes critical in the weak axis direction. As a result, the improvement is more evident in the weak axis with a lower value of yield point than the base model (PR-01).
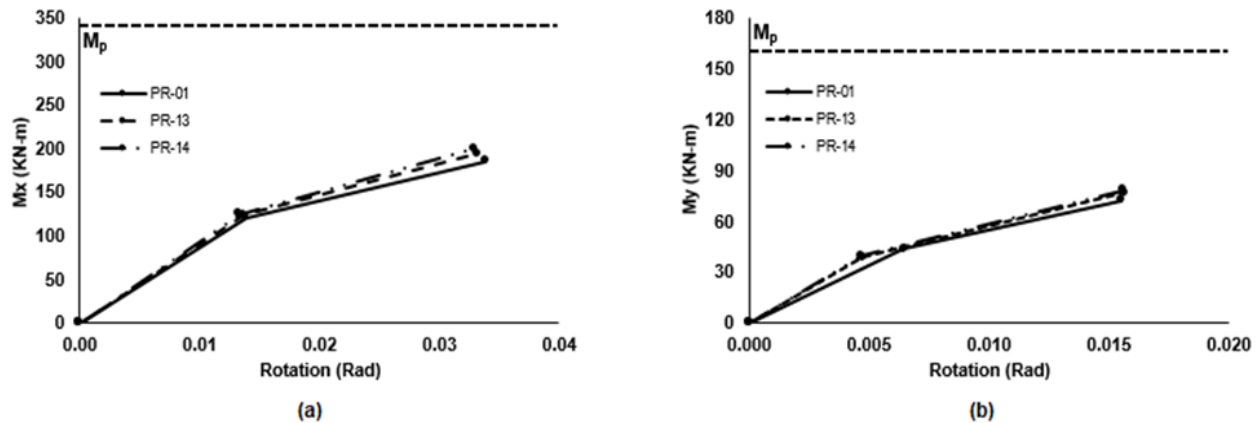
Figure 5.7 Effect of anchor rod quantity (a) Strong axis (b) Weak axis

5.5.1.5 Effect of Embedment Length

Three different embedment lengths of anchor rod such as 250, 500, and 750 mm (PR-01, PR-15 and PR-16) are considered to observe the response of base plate connection. Figure 5.8 illustrates the moment-rotation behavior for different embedment lengths. It is found that a 250 mm embedment length provides both higher strength and stiffness for the base plate connections in both strong and weak axis direction than the other two lengths considered. It should be noted that the 250 mm embedment length is lower than the specified AISC minimum embedment length for the corresponding anchor bolt diameter. No difference is observed when the embedment length considered is beyond the minimum requirement prescribed in the AISC Design Guide 1 (Fisher

and Kloiber, 2006), meaning that consideration of minimum embedment length is mandatory to ensure sufficient bond resistance between the anchor rod and concrete footing.
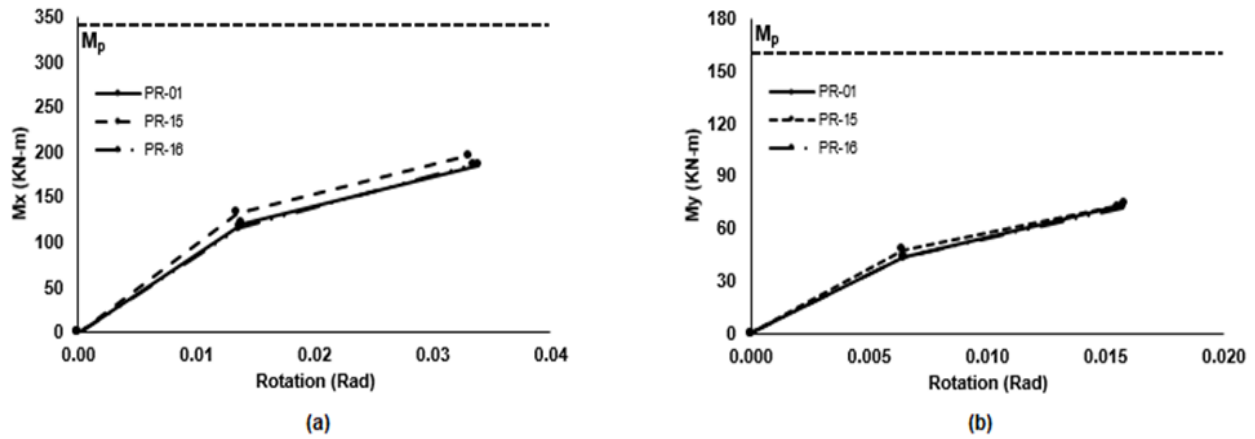
Figure 5.8 Effect of embedment length (a) Strong axis (b) Weak axis

5.5.1.6 Effect of Grout Thickness

Different grout thickness values of 0, 25 and 50 mm (PR-01, PR-17 and PR-18) are adopted to understand the effect of grout thickness on base plate connection behavior. Grout is mainly considered for the suitability of the construction process by ensuring proper contact between the base plate and footing. Consideration of grout enhances the shear strength of base connection up to 40% depending on its thickness (Shaheen et al. 2017). However, it can be seen from Figure 5.9 that grout thickness does not have any influence on the moment-rotation behavior in both the strong and weak axis direction of the base plate connection.
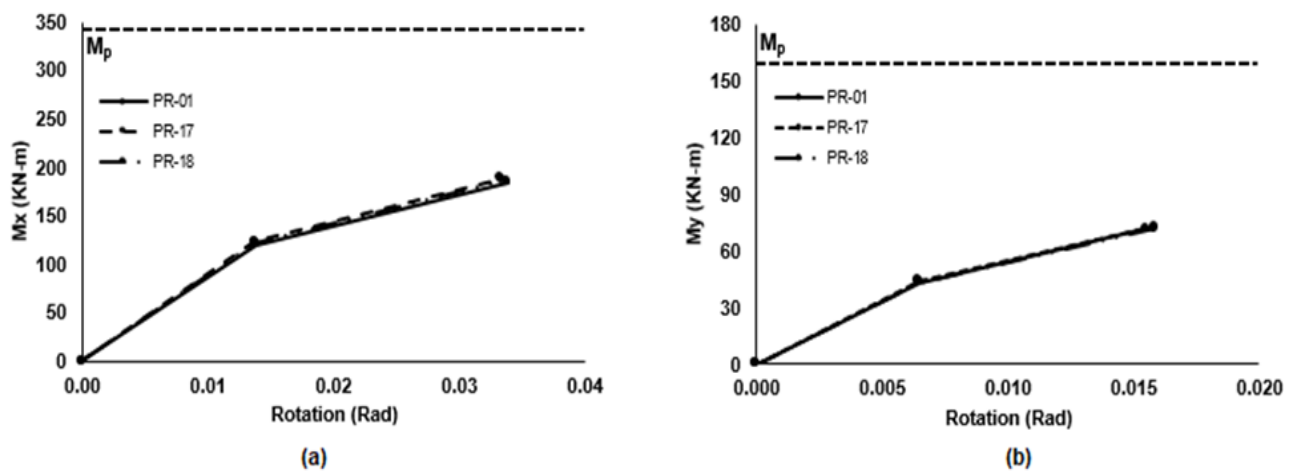
Figure 5.9 Effect of grout thickness (a) Strong axis (b) Weak axis

5.5.1.7 Effect of Axial Load

Axial load ratios of 0.2, 0.25, and 0.3 (PR-01, PR-19 and PR-20) are considered to investigate its influence on the base plate connection behavior. It is noted that the axial load ratio is increased by ensuring the capacity of the column in all design prospects. Since the column is considered unbraced, an axial load ratio higher than 0.3 makes the column critical in lateral torsional buckling criteria. Figure 5.10 depicts the moment rotation behavior for different axial load ratios of the base plate connection. It can be seen from Figure 5.10 that no significant difference is observed when the axial load is increased by 25% and 50% from the base model (axial load ratio of 0.2) in the strong axis direction. However, a slight increase in the strength is observed in the weak axis direction of the base connection when the axial load is increased by 50% from the base model. Although past researchers (Fahmy 1999, Grauvilardell 2005) found that axial load has a significant impact on the strength, ductility as well as failure mode of the CBP connection, they considered the combination of axial load and uniaxial bending only. The mechanism considered suggests that axial load provides resistance in the tension side of the base connection when combined with uniaxial bending. As a result, the increase of the compressive axial load improves connection stiffness (Grauvilardell 2005, Picard et al. 1987, Sato 1987, Li et al. 2000). However, Fahmy (1999) reported that the axial load does not have any influence to significantly change the initial stiffness of the connection which is similar to an experimental study done by Jaspart and Vandegans (1998). Since there are no experimental results available to investigate the effect of axial load on column base connection under combined axial load and biaxial bending, further investigation is required to justify the results obtained from this study.
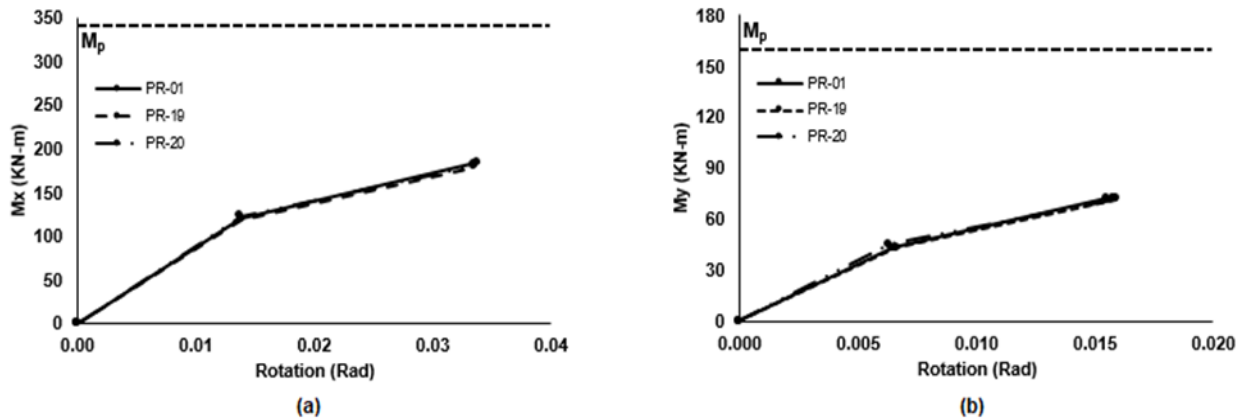
Figure 5.10 Effect of axial load (a) Strong axis (b) Weak axis

5.5.2 Maximum Anchor Rod Tensile Force

The calculated maximum bolt tensile force (T_u) for different parameters of various ranges is illustrated in Figure 5.11. The T_u values are directly calculated from the maximum stress observed at the end of the numerical analysis multiplied by the corresponding anchor rod cross-sectional area. As shown in Figure 5.11, the value of T_u varies considerably with a change in the base plate thickness. A lower value of base plate thickness (16 mm) provides less T_u due to the early yielding of the base plate while other parameters are kept constant. Higher values of base plate thickness (38 and 50 mm) decrease the value of T_u due to the lengthening of the moment arm between the bolt tension force and the resultant force in the base plate region. It is evident from Figure 5.11 that anchor bolt diameter has a significant impact on the bolt tensile force. Higher values of anchor bolt diameter shorten the moment arm between the bolt tension force and the resultant force due to the rotational constraint of the base plate on the tension side (Lee et al. 2008a). This phenomenon increases the bolt tensile force by resisting the same amount of stress within the specific base connection configuration. Base plate yield strength, anchor quantity, embedment length, grout thickness, and axial load ratio found to have a negligible impact on the maximum bolt tensile force of the base plate connection. Figure 5.12 depicts the ratio of maximum bolt tensile force to the anchor rod yield capacity for different base connection parameters under consideration. Since anchor rod yield force is difficult to identify from the numerical analysis, maximum bolt tensile force is considered in lieu of the yield force to understand the anchor rod yielding failure mode. It is evident from Figure 5.12 that the maximum bolt tensile force for a thicker base plate (50 mm) is less than 50% of the anchor rod yielding capacity meaning that anchor rod yielding will not govern for this type of connection. It is also found that the ratio is almost 80% for thinner base plate (16mm) where early yielding of the base plate causing local stress development in the tension side anchor rods. The rest of the cases considered in the study are found to be close to or exceeding the anchor rod yielding limit. This signifies anchor rod yielding of the base connection with respect to the maximum bolt tensile force.
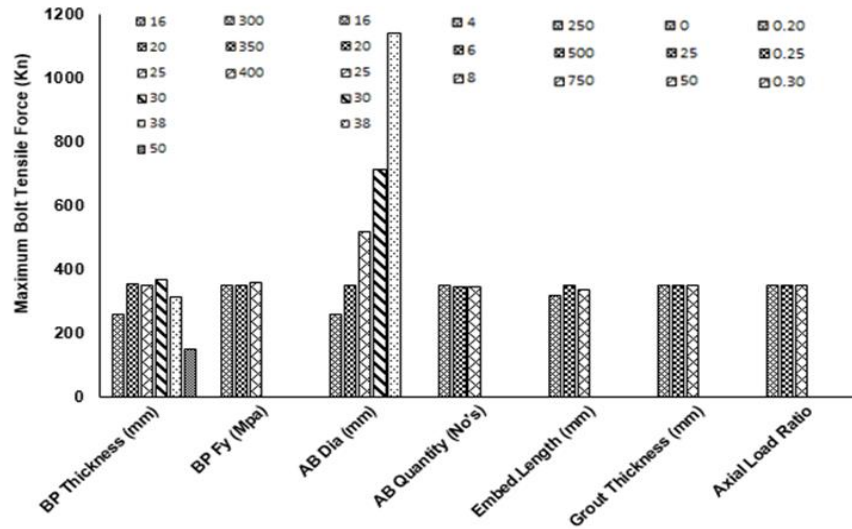
Figure 5.11 Comparison of maximum bolt tensile force
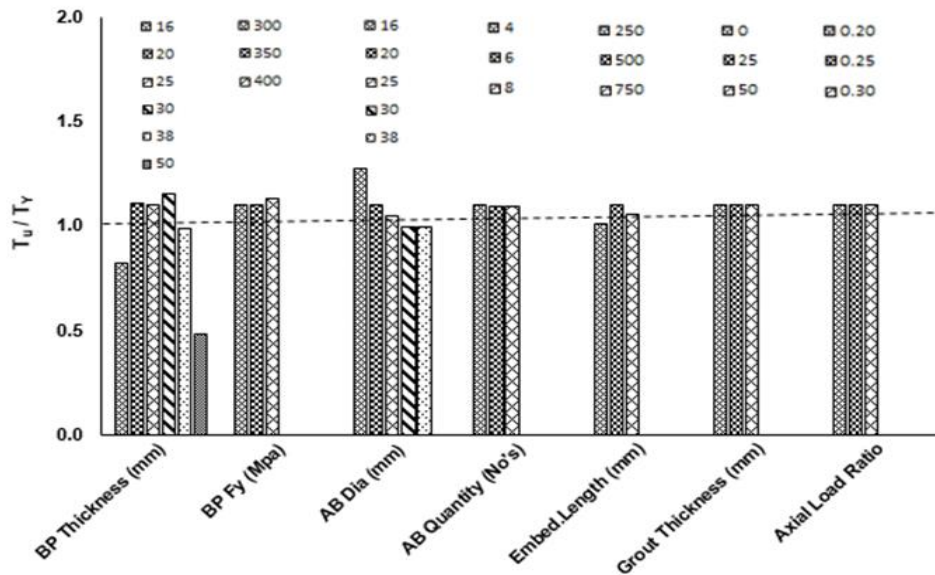
Figure 5.12 Ratio of maximum bolt tensile force to yield capacity of anchor rod

5.5.3 Yielding Pattern in the Base Plate

Equivalent Von Mises stress contours on the base plate surface are presented in Figures 5.13 and 5.14. These stresses are extracted at the end of the numerical analysis where the drift is about 4% and 2% in the strong and weak axis direction, respectively. Comparisons are made for the different parameters of the base plate connection within various ranges of values.

5.5.3.1 Effect of Base Plate Thickness

Previous studies (Thambiratnam and Paramisivam, 1986; Astaneh et al., 1992; Burda and Itani, 1999) showed that thin base plates represent flexible and ductile behavior by developing yield lines along the column flanges. This study also found that the thickness of the base plate has a significant impact on the yield line pattern at the top of the base plate as shown in Figure 5.13. The yielding of the base plate is concentrated at the anchor rod holes when 16 mm plate thickness is considered. The thinner base plate induces local stress on the anchor rod due to the deformation of the base plate on the tension side. Yield lines for 20 mm and 25 mm thick base plates are found similar to the AISC Design Guide 1 (Fisher and Kloiber, 2006) where the yield lines extend both in the tension and compression side of the base plate. Yield lines are found to be diminished for the higher values of base plate thickness such as 50 mm where local buckling in the column is observed near the base plate which signifies weak column-strong connection condition. It is also found that the 30 mm thick base plate has the highest severity of yield pattern on the base plate. With the formation of more yield lines, the connection with 30mm base plate in general showed higher ductility and a higher reduction of the initial stiffness as observed in Figure 5.3(a). A complex interaction between different components of CBP connections can cause such phenomena on the base plate surface.
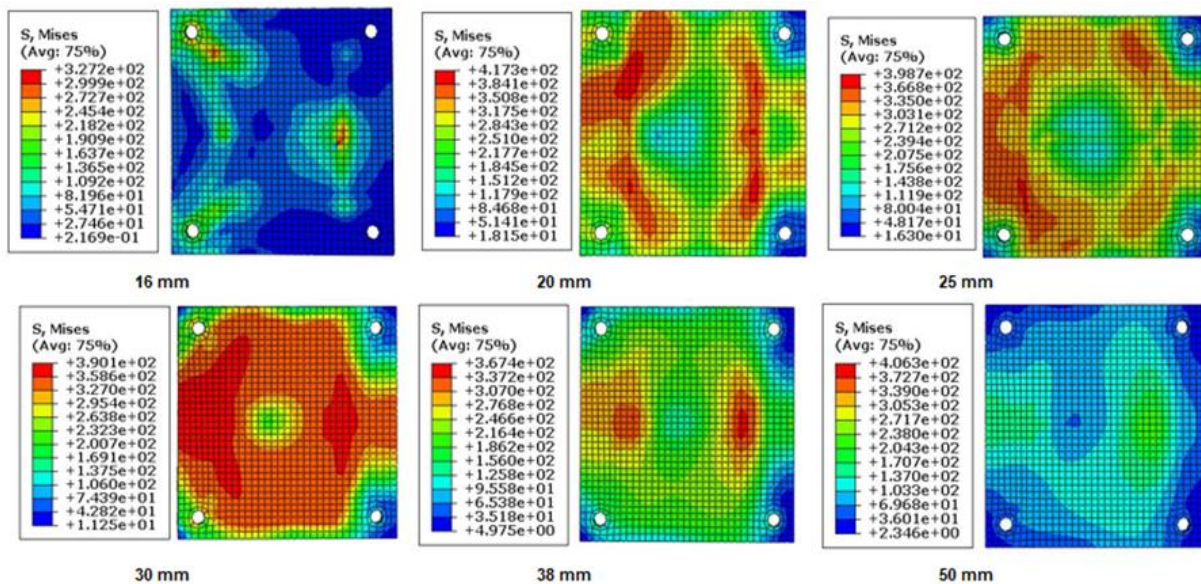
Figure 5.13 Effect of base plate thickness on yield line pattern at the top of the base plate

5.5.3.2 Effect of Anchor Rod Diameter

Anchor bolt diameter is found to have an influential impact on the yield line pattern of the base plate as shown in Figure 5.14. It can be seen from Figure 5.14 that the yield lines for different anchor rod diameters follow the same pattern where the curve-shaped lines are formed around the anchor rod holes in the tension side and straight lines are formed beneath the column flange in the compression side of the base plate. It is observable that anchor bolt diameter of 25 mm and larger values concentrate the yield lines to anchor bolt holes resulting increase in the stress as well as the maximum bolt tensile force.
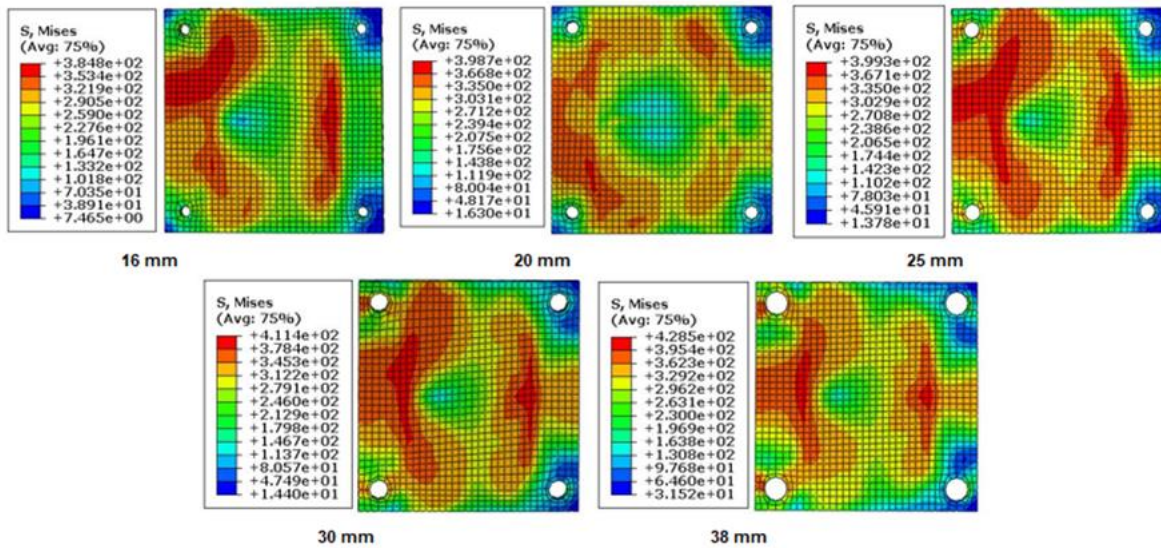
Figure 5.14 Effect of anchor rod diameter on yield line pattern of base plate

5.5.3.3 Effect of Other Parameters

It is observed that no variation in the yield line patterns is distinguished on the base plate surface for the parameters such as base plate yield strength and anchor rod quantity except the differences in the values of Von Mises stress. Remaining parameters such as embedment length, grout thickness and axial load ratio have negligible effect for both the values of Von Mises stress as well as the yield line pattern on the base plate surface.

5.5.4 Rigidity of Base Plate Connection

Exposed CBP connection is typically considered as either rigid or pinned during design consideration (Borzouie 2016). Eurocode 3 (2005) classifies base connection rigidity into three classes as rigid, semi-rigid, and pinned depending on the different base rotational stiffness (K_θ)

limit expressed by Eq. (5.3), (5.4) and (5.5), respectively. Base rotational stiffness can be calculated dividing the base moment (M) by the base rotation (θ). Column base connections having base rotational stiffness of $30(EI/H)$ or greater are considered as fully rigid. It is considered as fully pinned when the base rotational stiffness is less than $0.5(EI/H)$. CBP connections with rotational stiffness between these two limits are considered to be semi-rigid.

$$K_\theta \geq 30 \left(\frac{EI}{H}\right)_{col} \tag{5.3}$$

$$0.5 \left(\frac{EI}{H}\right)_{col} < K_\theta < 30 \left(\frac{EI}{H}\right)_{col} \tag{5.4}$$

$$K_\theta < 0.5 \left(\frac{EI}{H}\right)_{col} \tag{5.5}$$

Here, K_θ is normalized by EI/H, where EI is the flexural stiffness of the column section and H is the height of the column. Figure 5.15 illustrates the rigidity of the base connection of all the developed FE models considered in this study. It is evident from Figure 5.15 that up to the yield point, base plate connection stiffness for all the connection details considered lies within the semi-rigid region in both the strong and weak axis direction. Two of the base plate connections having a lower value of base plate thickness (16 mm and 20 mm) are found to have changed their stiffness from semi-rigid to fully pinned when the ultimate point is considered in the strong axis direction as shown in Figure 5.15(a). When the ultimate point of weak axis direction is considered, almost all the base connections shifted their region from semi-rigid to fully pinned condition as shown in Figure 5.15(b). Figure 5.16 depicts the rigidity of the base connection by plotting moment and rotation using Eq. (5.6) and (5.7) to investigate the biaxial bending effect on the base plate connection behavior.

$$\text{Moment, } M = \sqrt{M_X^2 + M_Y^2} \tag{5.6}$$

$$\text{Rotation, } \theta = \sqrt{\theta_X^2 + \theta_Y^2} \tag{5.7}$$

It is found from Figure 5.16 that up to the yield point base plate connection for all the parameters considered lies within semi-rigid region. However, shifting of the base connection rigidity for a few models is observed when the ultimate point is considered. It is found that if lower values of

base plate thickness and anchor rod diameter are considered, base connection rigidity tends to shift their region from semi-rigid to fully pinned condition when the connection reaches its ultimate point after being yielded. The rest of the parameters considered for base plate connection do not change their rigidity from semi-rigid region for both the yield and ultimate point except the change in values for rotational stiffness. Although most of the cases considered in the parametric study are in the semi rigid region but they remain close to the pinned boundary region. This may be due to the use of unstiffened base plate as well as consideration of low range base plate thickness for the parametric study. Additionally, deformation of the unstiffened base plate, deformation of the concrete under the compression side, and elongation of the anchor bolts can be attributed to the observed flexibilities.
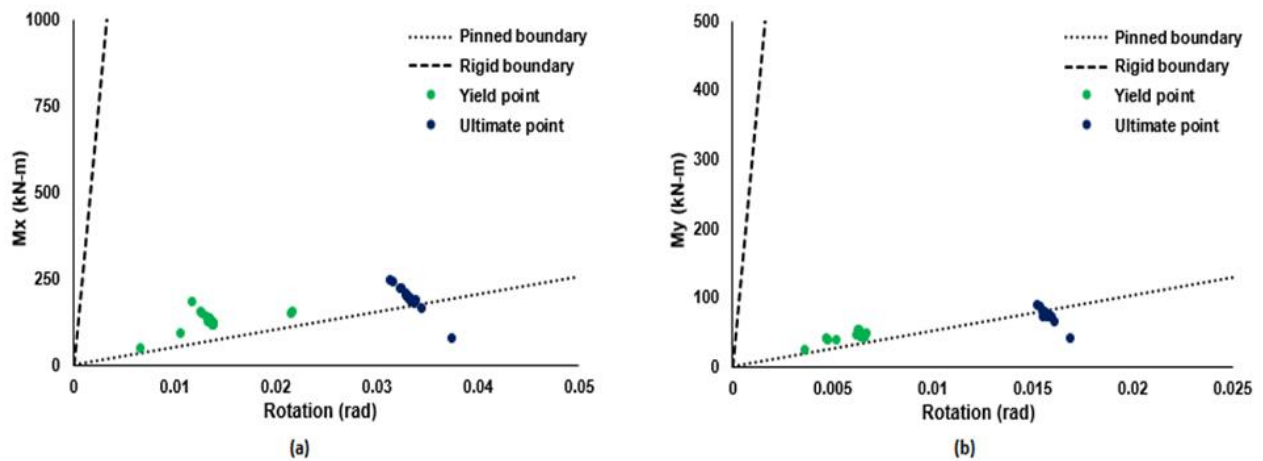
Figure 5.15 Rigidity of the base plate connection (a) strong axis (b) weak axis
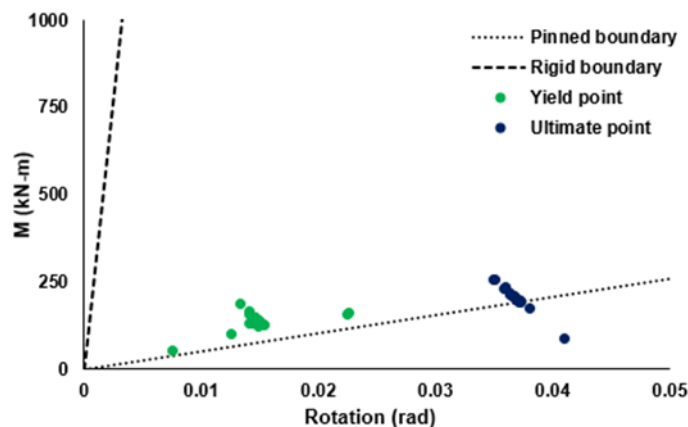
Figure 5.16 Rigidity of the base plate connection for biaxial bending

68

5.5.5 Comparison of Rotational Stiffness under Biaxial Bending with Available Equations for Uniaxial Bending

Rotational stiffness of the CBP connection can significantly affect the response of steel moment frames as suggested by past studies (Fahmy 1999, Aviram et al. 2010, Zareian and Kanvinde 2013). Typically, CBP connections are idealized as fixed or pinned during the design of SMRFs. As discussed in the previous section, Eurocode classified the base fixity into three categories. Several design codes such as Eurocode 3 (2005) and Japanese code (AIJ 2001) provide formulas for estimating CBP connection rotational stiffness. A new approach for calculating the CBP connection was developed by Kanvinde et al. (2012). However, all these equations are based on experimental and numerical studies performed on CBP connections under axial load and uniaxial bending which do not consider the effect of biaxial bending. This study compares the rotational stiffness obtained from the parametric FE analysis of 20 CBP connections subjected to combined axial load and biaxial bending with the rotational stiffness obtained using the methodology described in Kanvinde et al. (2012), Eurocode 3 (2005), and Japanese code (AIJ 2001). Details of the formula for each of the methods are provided in Appendix D. Connection stiffness at first yield $(K_{y(FEM)})$ for biaxial loading is calculated from the FE analysis for the same parametric analysis cases. Table 5.4 summarizes the results from the FEM analysis and the rotational stiffness calculated using three existing methods.

Table 5.4 Results of numerical analysis and available method

FE Model ID	$M_y{}^a{}_{(FEM)}$	$\theta_y{}^a{}_{(FEM)}$	$M_y{}^b{}_{(method)}$	$\theta_y{}^b{}_{(method)}$	$K_y{}^c{}_{(FEM)Bi}$	$K_y{}^d{}_{(K)}$	$K_y{}^c{}_{(EU)}$	$K_y{}^c{}_{(J)}$	$K_y{}^c{}_{(FEM)Uni}$
PR-01	127.8	0.0153	121.0	0.0061	8.35	19.95	30.61	10.75	18.07
PR-02	55.1	0.0076	95.0	0.0089	7.25	10.62	28.27	10.75	27.77
PR-03	101.6	0.0125	105.0	0.0068	8.10	15.51	29.78	10.75	16.58
PR-04	158.1	0.0142	140.0	0.0063	11.15	22.38	31.00	10.75	22.54
PR-05	163.9	0.0142	178.0	0.0076	11.58	23.39	31.27	10.75	25.20
PR-06	189.2	0.0133	248.0	0.0113	14.22	21.91	31.42	10.75	29.93
PR-07	155.9	0.0225	115.0	0.0057	6.92	20.17	30.61	10.75	18.35
PR-08	161.6	0.0227	127.0	0.0064	7.12	19.72	30.61	10.75	20.35
PR-09	123.2	0.0149	121.0	0.0068	8.27	17.73	20.29	6.88	16.97
PR-10	140.9	0.0149	121.0	0.0056	9.46	21.69	45.41	16.80	20.88
PR-11	141.0	0.0149	121.0	0.0053	9.46	22.77	61.57	24.19	20.05

PR-12	147.0	0.0147	121.0	0.0051	10.03	23.78	88.55	38.81	22.49
PR-13	129.7	0.0145	121.0	0.0061	8.93	19.95	30.61	16.13	21.28
PR-14	130.4	0.0141	121.0	0.0061	9.23	19.95	30.61	21.50	18.80
PR-15	141.0	0.0149	121.0	0.0046	9.44	26.37	31.65	21.50	19.45
PR-16	125.0	0.0152	121.0	0.0075	8.23	16.05	29.64	7.17	17.11
PR-17	130.9	0.0152	121.0	0.0061	8.62	19.95	30.61	10.75	19.63
PR-18	129.6	0.0152	121.0	0.0061	8.54	19.95	30.61	10.75	18.51
PR-19	127.0	0.0154	137.0	0.0058	8.26	23.79	30.61	10.75	18.52
PR-20	131.1	0.0152	152.0	0.0058	8.62	26.40	30.61	10.75	18.88

[a] Moment and rotation are calculated using Eq. (6) and (7) for biaxial condition where the units are in kN-m and radian, respectively.

[b] Moment and rotation are calculated from the methodology described in Kanvinde et al. (2012) for uniaxial condition where the units are in kN-m and radian, respectively.

[c] Rotational stiffness is expressed in kN-m/milliradians.

[d] Rotational stiffness calculated using Kanvinde et al. $(K_{y(K)})$, Eurocode $(K_{y(EU)})$ and Japanese code $(K_{y(J)})$ and are expressed in kN-m/milliradians.

Figure 5.17 graphically compares the stiffness obtained from numerical analysis $K_{y(FEM)}$ and the stiffness calculated from three existing methods named Kanvinde et al. as $K_{y(K)}$, Eurocode as $K_{y(EU)}$, and Japanese code as $K_{y(J)}$ for all the parametric analysis cases considered in this study. Figure 5.17(a) shows that the stiffness values predicted from $K_{y(K)}$ considering uniaxial loading are 50% higher for nearly all of the cases than the stiffness values calculated from numerical analysis considering biaxial loading. It can be seen from Figure 5.17(b) that the Eurocode overestimates the stiffness value two times more than the stiffness obtained from numerical analysis which considers biaxial bending. Stiffness calculated from Japanese code is found within roughly 25% limit of the stiffness obtained from numerical analysis for most of the cases as shown in Figure 5.17(c). It is to be noted that the Japanese code considers the parameters associated with anchor rod such as anchor rod area, number of anchor rods in tension as well as embedment length of the anchor rod for calculating base connection stiffness. As a result, changes in any of the parameters associated with the anchor rod provide a significantly higher stiffness value as compared to the numerical analysis. Furthermore, this study compare the stiffness of FE models with the available equations for uniaxial loading as shown in Figure 5.18. SAC cyclic loading protocol is applied in the major axis direction which is the same as considered by Kanvinde et al. (2012) for their experimental analysis. Figure 5.18(a) shows that the stiffness values predicted from $K_{y(K)}$ are very close to the stiffness values calculated from numerical analysis for uniaxial loading. The stiffness

calculated from Eurocode is also found within the considerable ranges when compared with the FE models for uniaxial loading (Figure 5.18(b)). However inconsistency is found for the stiffness values calculated from the Japanese code when compared with the FE models (Figure 5.18(c)) due to the consideration of the parameters associated with anchor rod only for calculating base connection stiffness. In summary, rotational stiffness under uniaxial loading is found to be significantly higher than biaxial loading condition for all the considered base plate connections. Thus, for practical situations under the earthquake and wind loadings where biaxial loading is often present, connection flexibility is overestimated following the existing design codes and other empirical methods where only uniaxial loading is considered. It is to be noted that this study calculates the rotational stiffness considering the first yield moment whereas in design practice first yield moment is considered only for checking the yielding limit of various base plate connection components. This means that the design moment is applied to calculate the rotational stiffness. Since there is no available guideline, this study can shed light on developing future design guidelines for base plate connection subjected to combined axial load and biaxial bending.
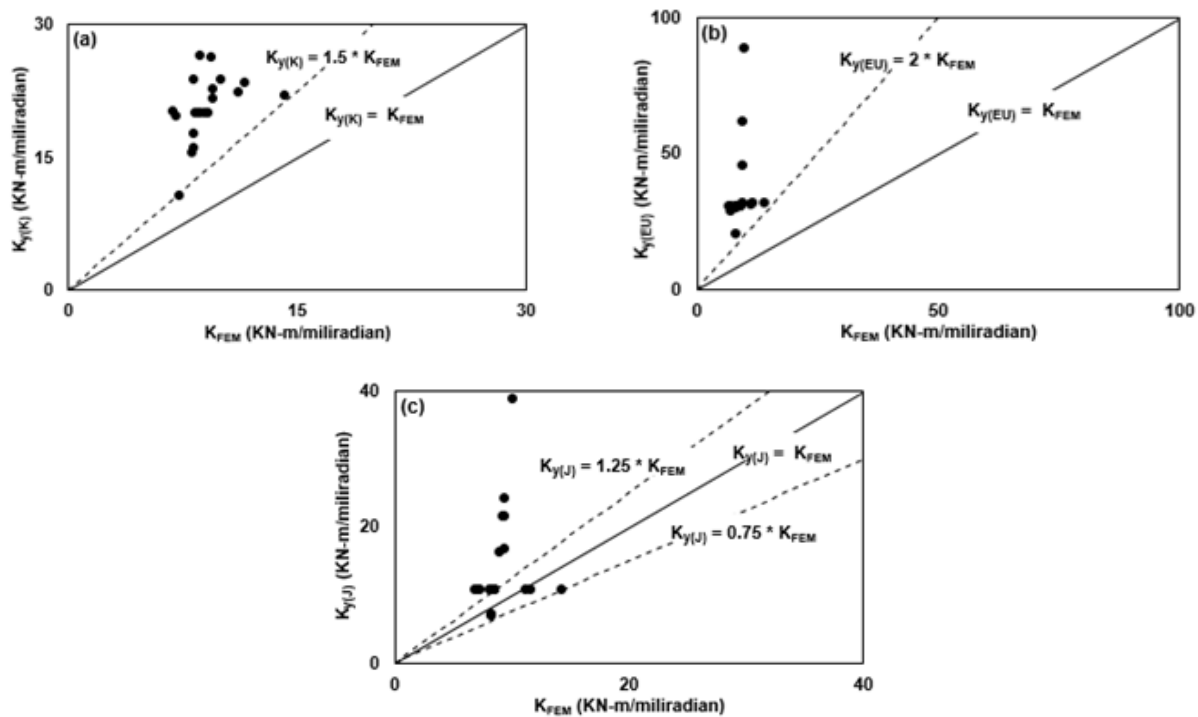
Figure 5.17 Comparison of connection stiffness determined from biaxial FE models and available equations for uniaxial loading (a) Kanvinde et al. (2012), (b) Eurocode 3 (2005) and (c) Japanese code (AIJ 2001)

71
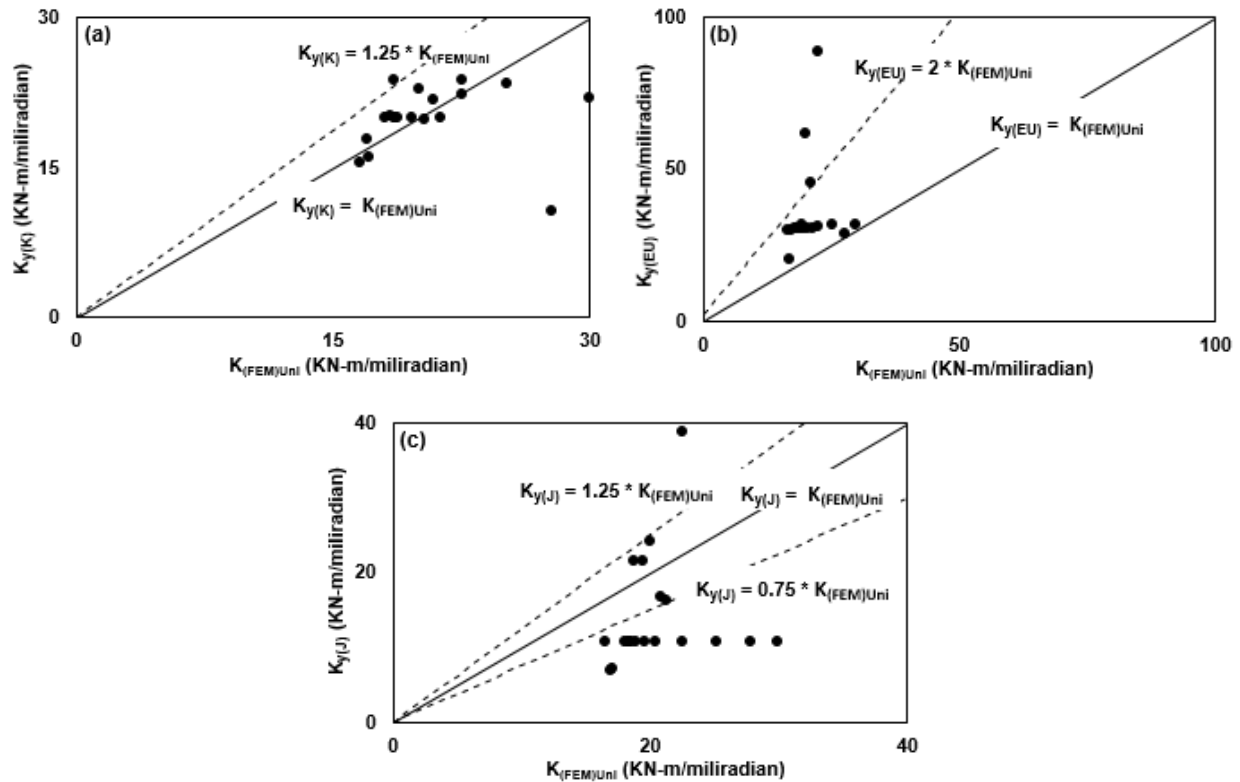
Figure 5.18 Comparison of connection stiffness determined from uniaxial FE models and available equations for uniaxial loading (a) Kanvinde et al. (2012), (b) Eurocode 3 (2005) and (c) Japanese code (AIJ 2001)

5.6 Summary

In design practices, it is a common approach to idealize the column base connections either as pinned or fixed. Predicting the rotational stiffness of the CBP connections as well as the fixity of the CBP connection is very important for properly estimating the connection design forces. Although structural response is sensitive to base flexibility, methods to properly characterize CBP connection flexibility under combined axial load and biaxial bending are not readily available. Motivated by these issues, this chapter investigated the rotational flexibility of exposed column base connections through an extensive numerical parametric study. Results from the numerical analysis show that the connection rigidity represents semi-rigid behavior under biaxial bending. Comparisons are performed with available equations for calculating column base rotation stiffness which showed the inadequacy of available equations in accurately predicting the connection stiffness under biaxial bending.

72

Chapter 6   Conclusion and Future Works

6.1 General

This thesis presented a comprehensive summary of the past experimental and numerical research conducted to investigate the response of exposed column base connections under different loading conditions. Through extensive literature review, gaps are identified in the existing knowledge. This research was aimed at investigating the behavior of the exposed CBP connections under combined axial load and biaxial bending through an extensive numerical parametric study using Finite Element (FE) analysis. In addition, this research study utilized the capability of data-driven Machine Learning (ML) techniques to identify the failure mode as well as various influential parameters affecting the failure pattern of CBP connections.

6.2 Core Contributions

The outcomes of this research work are expected to initiate further investigation and modify design approaches to consider the effect of combined axial load and biaxial bending on exposed CBP connections. The core contributions of this study are:

- Identifying the influential parameters affecting the failure mode of CBP connections.
- Development of a machine learning based GUI for rapid identification of CBP connection failure.
- Development of validated full scale 3D FE models of exposed CBP connection under combined axial load and biaxial bending
- Development of an understanding of the rotational stiffness of CBP connections and comparisons with existing methodologies.

6.3 Conclusions

6.3.1 Column Base Connection Failure Mode Identification using Machine Learning

This study explores the potentiality of data-driven ML techniques for failure mode identification of CBP connection by considering different parameters. Based on the results of this research, the following conclusions can be drawn:

- Among the ML algorithms, Decision Tree based ML model provides the highest accuracy to identify the failure mode.

- Prediction is found difficult for identifying others type (OTH) of failure mode as compared to the anchor rod yielding (AB) and base plate yielding (BP) type failure mode.

- Base plate thickness, embedment length and anchor rod diameter are found to be the governing parameters for failure mode identification of CBP connection.

- From the sensitivity analysis, prediction accuracy is found to be more sensitive between anchor rod yielding and base plate yielding type failure mode for base plate thickness, base plate yield strength, and anchor rod diameter.

- Overall accuracy of the developed ML model outperformed the overall accuracy of empirical equations to identify the failure mode.

6.3.2 Parametric Study of Column Base Connection under Combined Axial load and Biaxial Bending

This study performs an extensive FE analysis to select and validate a suitable modeling strategy that can mimic the experimental response of CBP connections available in literature. A bi-directional symmetrical lateral loading protocol is developed to simulate a real scenario of design basis seismic event for biaxial loading condition. Furthermore, a comprehensive simulation matrix is constructed where a total of 20 full scale FE models consisted of different parameters of various values are analyzed under combined axial load and biaxial bending to investigate the column base connection behavior. Based on the analysis results, the following conclusions are drawn:

- Among the seven different parameters considered in the study, base plate thickness and anchor rod diameter have a significant influence on the moment-rotation response of base plate connection under combined axial compression and biaxial bending. Early yielding of the base plate is observed for the thinner base plate whereas thicker base plate causes strong connection weak column condition. An increase in the anchor rod diameter significantly

increases both the strength and stiffness in the strong axis of the CBP connection. However, anchor rod diameter has little effect in the weak axis of the CBP connection.

- Significant differences are found in the maximum bolt tensile force for various base plate thicknesses and anchor rod diameters. Considerable reduction in the maximum bolt tensile force is observed for the thicker base plates. Early yielding of the thinner base plate resulted in lower values of maximum bolt tensile force. An increase in the anchor rod diameter significantly increases the maximum bolt tensile force by negotiating the moment arm between the bolt tension force and the resultant force.

- The thinner base plate generates yield lines through the anchor rod holes in the tension side whereas no critical yield line is observed for the thicker base plate which signifies strong connection-weak column condition. A lower value of anchor rod diameter generates the curve-shaped yield lines in the tension side and a straight line underneath the column flange in the compression side of the CBP connection. A higher value of anchor rod diameter tends to disseminate the developed yield lines towards the anchor rod holes in the tension side of the CBP connection.

- All the developed CBP connections are found in the semi-rigid region up to the yield point. However, shifting of the base connection rigidity for a few models is observed when the ultimate point is considered. Lower values for base plate thickness and anchor rod diameter are found to be responsible for shifting the base connection rigidity. Although most of the cases considered in the parametric study are in the semi rigid region but they remain close to the pinned boundary region. Therefore, from a design standpoint, the response of CBP connections under combined axial load and bi-axial bending can be classified as pinned.

- Significant overestimation of connection stiffness is observed when it is calculated from the existing methods which consider uniaxial loading and are compared with the results from the numerical analysis considering biaxial loading. Connection stiffness is found to be more than 2 times from Eurocode and 1.5 times from the Kanvinde et al. method for

almost all the FE models. However, overestimation of connection stiffness from the Japanese method is found only when the parameters associated with anchor rod varies for column base connection.

6.4 Recommendations for Future Works

This study deploys Data-driven Machine Learning techniques to identify the influential parameters as well as the failure mode by considering nine ML algorithms. As ML is a growing field of research and there are continuous updates on the algorithms, several other algorithms can be utilized including Deep Learning with a more comprehensive assembled database of CBP connections. This study considers only six input parameters for failure mode identification of CBP connections without considering the optimal parameters. This study is limited to only permutation-based feature importance criteria for identifying influential parameters. A comparison should be made with the other feature importance criteria to get more extensive output.

The present research performs an extensive numerical parametric study to investigate the behavior of CBP connection subjected to combined axial load and biaxial bending. However, experimental studies should be performed to validate the outcomes of this numerical study and gain an in-depth understanding of the CBP connection response. This study considers only elliptical bidirectional lateral loading protocol to simulate the biaxial bending condition. Although, seven different parameters are considered for numerical investigation, the size and section of column, base plate size and pitch length are kept constant for this study. Based on the above discussion, following recommendations are proposed for future work:

- Development of a more comprehensive database with detailed scenarios of column base connection.
- Implementation of Deep Learning as well as several other updated ML algorithms to improve prediction accuracy.
- Selection of optimal parameters from various feature importance criteria with more comprehensive database.
- Experimental investigation of column base plate connection behavior under combined axial load and biaxial bending.

- Comparison of different bidirectional lateral loading protocol to simulate the biaxial bending condition.

- Selection of different column sections such as HSS section with various sizes as well as variation of base plate size and pitch length should be considered to gain in-depth understanding.

- Consideration of weld connection between the column and the base plate to understand more realistic behavior of the column base connection.

References

Akiyama, H., Kurosawa, M., Wakuni, N., and Nishinura, I. (1984). Strength and Deformation of Exposed Type of Steel Column Bases. *Journal of Structural and Construction Engineering, Transactions of AIJ, 342: 46-54.*

Akiyama, H., Yamada, S., Takahashi, M., Katsura, D., Kumura, K., and Yahata, S. (1998). Full Scale Shaking Test of the Exposed-Type Column Bases. *Journal of Structural and Construction Engineering, Transactions of AIJ, No. 514: 185-192.*

Astaneh, A., Bergsma, G., and Shen, J.H. (1992). Behavior and Design of Base Plates for Gravity, Wind and Seismic Loads. *Proceedings of the National Steel Construction Conference, Las Vegas, Nevada, AISC, Chicago, Illinois.*

Adany, S., Calado, L., and Dunai, L. (2000). Experimental Studies on Cyclic Behavior Modes of Base-Plate Connections. *Proceedings of the Third International Conference on the Behavior of Steel Structures in Seismic Areas (STESSA 2000), Montreal, Canada, 97-104.*

American Institute of Steel Construction (AISC). (2017). Load and Resistance Factor Design. *Manual of Steel Construction, 15th Ed., AISC, Chicago, Illinois.*

Architectural Institute of Japan (AIJ). (2001). Recommendations for Design of Connections in Steel Structures. *Architectural Institute of Japan, Tokyo, Japan.*

Ahmadi, E., Jasemi, M., Monplaisir, L., Nabavi, M. A., Mahmoodi, A., and Jam, P. A. (2018). New efficient hybrid candlestick technical analysis model for stock market timing on the basis of the Support Vector Machine and Heuristic Algorithms of Imperialist Competition and Genetic. *Expert System Application, 94: 21-31.*

Aviram, A., Stojadinovic, B., and Kiureghian, A. (2010). Performance and reliability of exposed column base plate connections for steel moment resisting frames. *PEER Rep. 2010/107, Pacific Earthquake Engineering Research Center, Berkeley, CA, USA.*

Berg G.V. (1964). Anchorage and the Alaska earthquake of March 27, 1964. *Technical report, American Iron and Steel Institute, NY, USA.*

Burda, J.J., and Itani, A.M. (1999). Studies of Seismic Behavior of Steel Base Plates. *Report No. CCEER 99-7, Reno (NV): Center of Civil Engineering Earthquake Research, Department of Civil and Environmental Engineering, University of Nevada, NV.*

Balut, N. and Moldovan, A. (1997). A Model for the Behavior of Column Base Connections. *Proceedings of the Second Conference STESSA, Kyoto, Japan.*

Borzouie, J. (2016). Low Damage Steel Base Connections. *PhD Thesis, Department of Civil and Natural Resources Engineering, University of Canterbury, Christchurch, New Zealand.*

Breiman, L. (2001). Random forests. *Machine Learning, 45: 5–32.*

Breiman, L., Friedman, J.H., Olshen, R.A., Stone, C.J. (1984). Classification and Regression Trees. *Boca Raton, FL: Chapman & Hall/CRC*

CSA. (2019). Design of Steel Structures. *CSA-S16-19, Canadian Standards Association, Toronto, ON, Canada.*

CSA. (2019). Design of Concrete Structures. *CSA-A23.3, Canadian Standards Association, Mississauga, ON, Canada.*

Chaboche, J. L. (2008). A review of some plasticity and viscoplasticity constitutive theories. *International Journal of Plasticity, 24(10): 1642–1693.*

Cui, Y., Nagae, T., and Nakashima, M. (2009). Hysteretic Behavior and Strength Capacity of Shallowly Embedded Steel Column Bases. *ASCE Journal of Structural Engineering, 135(10): 1231-1238.*

Cortes, C., Vapnik, V. (1995). Support-vector networks. *Machine Learning, 20: 273-297.*

Canadian Institute of Steel Construction (CISC). (2017). Load and Resistance Factor Design. *Manual of Steel Construction, 11th Ed., CISC, ON, Canada.*

Choi, J. H., and Choi, Y. (2013). An experimental study on inelastic behavior for exposed-type steel column bases under three-dimensional loadings. *Journal of Mechanical Science and Technology, 27(3): 747-759.*

Chawla, N.V., Bowyer, K.W., Hall, L.O., and Kegelmeyer, W.P. (2002). SMOTE: Synthetic Minority Over-sampling Technique. *Journal of Artificial Intelligence Research, 16: 321-357.*

Dewolf, J. T., and Sarisley, E. F. (1980). Column base plates with axial loads and moments. *ASCE Journal of Structural Division, 106(11): 2167–2184.*

Drake R. and Elkin S. (1999). Beam-Column Base Plate Design- LRFD Method. *AISC Engineering Journal, first quarter, 1999.*

Das, S., Dutta, S., Putcha, C., Majumdar, S., and Adak, D. (2020). A data-driven physics-informed method for prognosis of infrastructure systems: theory and application to crack

prediction. *ASCE-ASME Journal of Risk Uncertainty Engineering System, Part A: Civil Engineering, 6(2): 04020013.*

Di Sarno, L., Pecce, M.R., and Fabbrocino, G. (2007). Inelastic Response of Composite Steel and Concrete Base Column Connections. *Behavior of Steel Structures in Seismic Areas 2006. Mazzolani, F.M., editor. Published by A.A. Balkema, a member of Sweets & Zeitlinger Publishers, August.*

Elkady, A. (2016). Collapse Risk Assessment of Steel Moment Resisting Frames Designed with Deep Wide Flange Columns in Seismic Regions. *PhD Thesis, Department of Civil Engineering and Applied Mechanics, McGill University, Montreal, Canada.*

Elkady, A., and Lignos, D. G. (2014). Modeling of the composite action in fully restrained beam-to-column connections: Implications in the seismic design and collapse capacity of steel special moment frames. *Journal of Earthquake Engineering Structural Dynamics, 43(13): 1935–1954.*

Elkady, A., and Lignos, D. G. (2018). Full-scale testing of deep wide-flange steel columns under multiaxis cyclic loading: Loading sequence, boundary effects, and lateral stability bracing force demands. *ASCE Journal of Structural Engineering, 144(2):04017189*

Eurocode 3. (2005). EN 1993-1-8; Design of steel structures – Part 1– 8: Design of Joints. *CEN, European Committee for Standardization, Brussels, Belgium.*

Fahmy, M., Stojadinovic, B., and Goel, S. C. (1999). Analytical and experimental behavior of steel column bases. *Proceedings of 8th Canadian Conference on Earthquake Engineering, Canadian Association for Earthquake Engineering, Ottawa, ON, Canada.*

Fahmy, M. (1999). Seismic Behavior of Moment-resisting Steel Column Bases. *Ph.D. Dissertation, Department of Civil and Environmental Engineering, University of Michigan, Ann Arbor, Michigan, USA.*

Fisher, J.M., and Kloiber, L.A. (2006). Design Guide 1: Base Plate and Anchor Rod Design. *2ⁿᵈ Ed. American Institute of Steel Construction (AISC), Chicago, USA.*

Fasaee, M.A.K., Banan, M.R., and Ghazizadeh, S. (2018). Capacity of Exposed Column Base Connections Subjected to Uniaxial and Biaxial Bending Moments. *Journal of Constructional Steel Research, 148: 368–370.*

Fisher, J.M., and West, M.A. (2003). Design guide 10: Erection Bracing of Low-Rise Structural Steel Buildings. *American Institute of Steel Construction (AISC), Chicago, USA.*

Fu, F. (2020). Fire induced progressive collapse potential assessment of steel framed buildings using machine learning. *Journal of Constructional Steel Research, 166: 105918.*

Friedman, J.H. (2001). Greedy function approximation: a gradient boosting machine. *Annals of Statistics, 29: 1189–1232.*

Grauvilardell, J.E., Lee, D., Hajjar, J.F., and Dexter, R.J. (2005). Synthesis of design, testing and analysis research on steel column base plate connections in high seismic zones. *Structural Engineering Rep. No. T-04-02, Dept. of Civil Engineering, University of Minnesota, Minneapolis, USA.*

Grilli, D.A., and Kanvinde, A.M. (2015). Embedded Column Base Connections Subjected to Flexure and Axial Load: Tests and Strength Models. *Final Report (3-11) University of California, Davis, CA, USA.*

Goldman, C. (1983). Design of Column Base Plates and Anchor Bolts for Uplift and Shear. *Structural Engineering Practice, 2(2): 103-115.*

Gomez, I., Deierlein, G., and Kanvinde, A. (2010). Exposed column base connections subjected to axial compression and flexure. *Final Report Presented to the American Institute of Steel Construction (AISC), Chicago, USA.*

Gomez, I.R., Kanvinde, A., Smith, C., and Deierlein, G.G. (2009). Shear Transfer in Exposed Column Base Plates. *Technical Report submitted to the American Institute of Steel Construction (AISC), Chicago, USA.*

Grigoriev, I.S., Meĭlikhov, E.Z., and Radzig, A.A. (1997). Handbook of Physical Quantities. *CRC Press, Boca Raton, FL, 1997.*

Huang, H., and Burton, H.V. (2019). Classification of in-plane failure modes for reinforced concrete frames with infills using machine learning. *Journal of Building Engineering, 25: 100767.*

Hon, K.K., and Melchers, R.E. (1988). Experimental Behavior of Steel Column Bases. *Journal of Constructional Steel Research, 143(9): 35-50.*

Igarashi, S., Kadoya, H., Nakashima, S., and Suzuki, M. (1993). Behavior of Exposed-Type Fixed Column Base Connected to Riser Foundation. *Proceedings of the Tenth World Conference on Earthquake Engineering, Madrid, Spain.*

Jaspart, J. P. and Vandegans, D. (1998). Application of Component Method to Column Bases. *Journal of Constructional Steel Research, 48: 89-106.*

Kawano, A. and Matsui, C. (1998). On the Effect of Restoring Force Characteristics of Column-Base on Inelastic Response Behavior of Weak-Beam Steel Frame under Earthquake Ground Motion. *Journal of Structural and Construction Engineering, Transactions of AIJ, 507: 139-146.*

Kanvinde, A.M., Jordan, S. J., and Cooke, R. J. (2013). Exposed column baseplate connections in moment frames—Simulations and behavioral insights. *Journal of Constructional Steel Research, 84: 82–93.*

Kavoura, F., Gencturk, B., and Dawood, M. (2017). Reversed Cyclic Behavior of Column-to-Foundation Connections in Low-Rise Metal Buildings. *ASCE Journal of Structural Engineering, 143. https://doi.org/10.1061/(ASCE)ST.1943-541X.0001821*

Krawinkler, H. (1996). Cyclic loading histories for seismic experimentation on structural components. *Earthquake Spectra, 12(1): 1–12.*

Kanvinde, A.M., Grilli, D.A., and Zareian, F. (2012). Rotational stiffness of exposed column base connections - experiments and analytical models. *ASCE Journal of Structural Engineering, 138(5): 549–60.*

Kallolil, J.J., Chakrabarti, S.K., and Mishra, R.C. (1998). Experimental Investigation of Embedded Steel Plates in Reinforced Concrete Structures. *Engineering Structures, 20 (1-2): 105-112.*

Kim, S.E., Lee, D.H., and Cuong, N.H. (2007). Shaking Table Tests of a Two-Story Unbraced Frame. *Journal of Constructional Steel Research, 63(3): 412-421.*

Lee, D. and Goel, S. C. (2001). Seismic Behavior of Column-Base Plate Connections Bending about Weak Axis. *Report No. UMCEE 01-09, Department of Civil and Environmental Engineering, University of Michigan, Ann Arbor, Michigan, USA.*

Li, T., Sakai, J., and Matsui, C. (2000). Seismic Behavior of Steel-Concrete Composite Column Bases. *Proceedings of the 12th World Conference on Earthquake Engineering, 1072.*

Liu, T.C. (2001). Investigation of Rotational Characteristics of Column 'Pinned' Bases of Steel Portal Frames. *Steel and Composite Structures, 2(1): 187-200.*

Lee, D.Y., Goel, S.C. and Stojadinovic, B. (2008a). Exposed Column-Base Plate Connections Bending about Weak Axis: I. Numerical Parametric Study. *International Journal of Steel Structure, KSSC, 8(1): 11–27.*

Lee, D.Y., Goel, S.C. and Stojadinovic, B. (2008b). Exposed column-base plate connections bending about weak axis: II. Experimental Study. *International Journal of Steel Structure, KSSC, 8(1): 29–41.*

Lim, W.Y., Lee, D., and You, Y.C. (2017). Exposed column-base plate strong-axis connections for small-size steel construction. *Journal of Constructional Steel Research, 137: 286–296.*

Luo, H., and Paal, S.G. (2019). A locally weighted machine learning model for generalized prediction of drift capacity in seismic vulnerability assessments. *Journal of Computer Aided Civil Infrastructure Engineering, 34: 935–950.*

Miyasaka, H., Arai, S., Uchiyama, M., Yamada, T., and Hashimoto, A. (2001). Elasto-Plastic Behavior of Structural Elements Consist in Exposure Fixed-Type Steel Column Base. Part I – Behavior to Bending Moment. *Journal of Structural and Construction Engineering, Transactions of AIJ, 550: 167-174.*

Midorikawa, M., Nishiyama, I., Tada, M., and Terada, T. (2012). Earthquake and tsunami damage on steel buildings caused by the 2011 tohoku japan earthquake. *International Symposium on Engineering Lessons Learned from the 2011 Great East Japan Earthquake, March. Tokyo, Japan.*

Melchers, R.E. (1992). Column-base response under applied moment. *Journal of Constructional Steel Research, 23(1–3): 127–143.*

Mangalathu, S., and Jeon, J-S. (2018). Classification of Failure Mode and Prediction of Shear Strength of Concrete Beam-Column Joints using Machine Learning Techniques. *Engineering Structures, 160: 85-94.*

Mangalathu, M., and Jeon, J-S. (2019). Machine learning-based failure mode recognition of circular reinforced concrete bridge columns: comparative study. *Journal of Structural Engineering 145: 04019104*

Mangalathu, S., Jang, H., Hwang, S-H., and Jeon, J-S. (2020). Data-driven Machine Learning based Seismic Failure Mode Identification of Reinforced Concrete Shear Walls. *Engineering Structures, 208: 110331.*

Mangalathu, S., Sun, H., Nweke, C.C., Yi, Z., and Burton, H.V. (2020). Classifying earthquake damage to buildings using machine learning. *Earthquake Spectra, 36(1): 183-208.*

Mangalathu, S., Hwang, S. H., Jeon, J-S. (2020). Failure mode and effects analysis of RC members based on machine learning-based SHapley Additive exPlanations (SHAP) approach, *Engineering Structures, 219: 110927.*

Myers, A.T., Deierlein, G.G., and Kanvinde, A.M. (2009). Testing and probabilistic simulation of ductile fracture initiation in structural steel components and weldments. *Blume center technical report TR-170, Stanford University, Stanford, CA, USA.*

Picard, A., Beaulieu, D., and Perusse, B. (1987). Rotational Restraint of a Simple Column Base Connection. *Canadian Journal of Civil Engineering, 14: 49-57.*

Picard, A., and Beaulieu, D. (1985). Behaviour of a Simple Column Base Connection. *Canadian Journal of Civil Engineering, 12: 126-136.*

Patil, T.R., and Sherekar, S.S. (2013). Performance analysis of Naive Bayes and J48 classification algorithm for data classification. *International Journal of Computer Science and Application, 6: 256–261.*

Pedregosa, F., Varoquaux, G., Gramfort, A., Michel, V., Thirion, B., and Grisel, O. (2011). Scikitlearn: Machine learning in Python. *Journal of Machine Learning Research, 12: 2825–2830.*

Sato, K. (1987). A Research on the Aseismic Behavior of Steel Column Base for Evaluating Its Strength Capacity and Fixity. *Report No. 69, Kajima Institute of Construction Technology, Tokyo, Japan.*

Stamatopoulos, G. and Ermopoulos, J. (1997). Interaction Curves for Column Base-Plate Connections. *Journal of Constructional Steel Research, 44(1-2): 69-89.*

Somiya, Y., Fukuchi, Y., and Chin, B. (2002). Experimental Study on Elasto-Plastic Behavior and Strength Estimation of Exposed-Type Column Base with Variable Axial Force. *Journal of Structural and Construction Engineering, Transactions of AIJ, 562: 137-143.*

Shaheen, M.A., Tsavdaridis, K.D., and Salem, E. (2017). Effect of Grout Properties on Shear Strength of Column Base connections: FEA and Analytical Approach. *Engineering Structures, 152: 307–319.*

SIMULIA Inc. (2020). ABAQUS user's manual. *Version 6.20. Providence, RI, USA*.

Sousa, A.C., Inamasu, H., and Lignos, D.G. (2019). An Explicit Model for Exposed Column Base Connections and its Parameter Sensitivity. *Proceeding of 12th Pacific Structural Steel Conference, Tokyo, Japan.*

Siam, A., Ezzeldin, M., and El-Dakhakhni, W. (2019). Machine learning algorithms for structural performance classifications and predictions: application to reinforced masonry shear walls. *Structures, 22: 252–265.*

Tremblay, R., Filiatrault, A., Timler, P., and Bruneau, M. (1995). Performance of steel structures during the 1994 Northridge earthquake. *Canadian Journal of Civil Engineering, 22(2): 338–360.*

Thambiratnam, D.P., Paramasivam, P. (1986). Base Plates under Axial Loads and Moments. *Journal of Structural Engineering, 112: 1166-1181.*

Tronzo, T. M. (1984). Design of Heavy Steel Column Bases: Handling Forces- Some Practical Procedures. *Structural Engineering Practice, 2(4): 279-300.*

Targowski, R., Lamblin, D., and Guerlement, G. (1993). Base Plate Column Connection under Bending: Experimental and Numerical Study. *Journal of Constructional Steel Research, 27: 37-54.*

Takamatsu, T., and Tamai, H. (2005). Non-Slip-Type Restoring Force Characteristics of an Exposed-Type Column Base. *Journal of Constructional Steel Research, 61(7): 942-961.*

Trautner, C. A., Hutchinson, T. C., Grosser, P., and Silva, J. (2015). Effects of detailing on the cyclic behavior of steel baseplate connections designed to promote anchor yielding. *ASCE Journal of Structural Engineering, 142(2): 04015117.*

Trautner, C. A., and Hutchinson, T. C. (2018). Parametric Finite-Element Modeling for Exposed Steel Moment Frame Column Baseplate Connections Subjected to Lateral Loads. *ASCE Journal of Structural Engineering, 144(6): 04018049.*

Wald, F. and Jaspart, J. (1998). Stiffness Design of Column Bases. *Journal of Constructional Steel Research, 46(1-3): 135*

Wald, F., Sokol, Z., and Steenhuis, M. (1995). Proposal of the Stiffness Design Model of the Column Bases. *Proceedings of the Third International Workshop on Connections in Steel Structures, Trento, Italy.*

Wald, F. (1995). Column-Bases. *1ˢᵗ ed., CVUT, Praha, Czech Republic.*

Yamada, S. and Akiyama, H. (1997). Influence of the Rigidity of Column Bases on the Ultimate Earthquake Resistance of Multi-Story Steel Moment Frames. *Journal of Structural and Construction Engineering, Transactions of AIJ, 496: 113.*

Zareian, F., and Kanvinde, A. (2013). Effect of column-base flexibility on the seismic response and safety of steel moment-resisting frames. *Earthquake Spectra, 29(4): 1537–1559*

Appendices

Appendix A

Table A1 Details of assembled database

Investigator	Number of Tests	Base plate Thickness (mm)	Base plate Fy (Mpa)	Anchor Rod Dia (mm)	No. of Anchor Rods	Embedment Length (mm)	Grout Thickness (mm)	Pitch Length (mm)	Column Section	Failure Mode
Trautner & Hutchinson (2018)	7	51	248	38	6	100	50	305	W	Anchor rod yielding
		51	248	38	6	560	50	305	W	Anchor rod yielding
		51	248	51	4	100	50	305	W	Base plate yielding
		51	248	38	6	560	50	254	W	Anchor rod yielding
		51	248	38	6	560	50	406	W	Anchor rod yielding
		51	248	51	4	100	50	305	W	Base plate yielding
		51	248	51	4	100	50	254	W	Base plate yielding
Shaheen et al. (2017)	2	25	278	19	4	520	25	279	W	Anchor rod yielding
		25	278	19	4	520	60	279	W	Anchor rod yielding
Choi & Choi (2013)	2	9	270	12	8	100	0	230	HSS	Anchor rod yielding
		19	250	12	8	100	0	230	HSS	Anchor rod yielding
Kanvinde et al. (2013)	5	25	345	20	4	560	50	284	W	Base plate yielding
		38	345	20	4	560	50	284	W	Base plate yielding
		25	345	20	4	560	50	284	W	Base plate yielding
		51	345	20	4	560	50	284	W	Base plate yielding
		25	345	20	4	560	50	284	W	Base plate yielding
	12	16	241	19	2	432	10	25	HSS	Grout crushing

Thambiratnam & Parimasivam (1986)		16	241	19	2	432	10	25	HSS	Base plate yielding
		16	241	19	2	432	10	25	HSS	Base plate yielding
		16	241	19	2	432	10	25	HSS	Base plate yielding
		16	241	19	2	432	10	25	HSS	Base plate yielding
		19	241	19	2	432	10	25	HSS	Grout crushing
		19	241	19	2	432	10	25	HSS	Base plate yielding
		19	241	19	2	432	10	25	HSS	Base plate yielding
		19	241	19	2	432	10	25	HSS	Base plate yielding
		22	241	19	2	432	10	25	HSS	Grout crushing
		22	241	19	2	432	10	25	HSS	Base plate yielding
		22	241	19	2	432	10	25	HSS	Base plate yielding
Picard (1987)	14	18	300	19	2	450	25	125	W	Anchor rod yielding
		25	300	19	2	450	25	125	W	Anchor rod yielding
		26	300	19	2	450	25	125	W	Anchor rod yielding
		25	300	19	4	450	25	160	W	Anchor rod yielding
		25	300	19	4	450	25	70	W	Anchor rod yielding
		26	300	19	4	450	25	250	W	Anchor rod yielding
		22	300	19	2	450	25	125	W	Anchor rod yielding
		22	300	19	2	450	25	70	W	Anchor rod yielding
		29	300	19	2	450	25	125	W	Anchor rod yielding
		27	300	19	2	450	25	125	W	Anchor rod yielding
		29	300	19	4	450	25	250	W	Anchor rod yielding
		27	300	19	4	450	25	250	W	Anchor rod yielding
		27	300	19	4	450	25	160	HSS	Anchor rod yielding
		27	300	19	4	450	25	70	HSS	Anchor rod yielding
Picard (1985)	15	11	250	19	2	450	20	70	W	Anchor rod yielding
		11	250	19	2	450	20	70	W	Anchor rod yielding

		11	250	19	2	450	20	70	W	Anchor rod yielding
		11	250	19	2	450	20	70	W	Anchor rod yielding
		11	250	19	2	450	20	70	W	Anchor rod yielding
		11	250	19	2	450	20	70	W	Anchor rod yielding
		11	250	19	2	450	20	70	W	Anchor rod yielding
		29	250	19	4	450	20	70	W	Anchor rod yielding
		29	250	19	4	450	20	70	W	Anchor rod yielding
		29	250	19	4	450	20	70	W	Anchor rod yielding
		29	250	19	4	450	20	70	W	Anchor rod yielding
		29	250	19	4	450	20	70	HSS	Anchor rod yielding
		29	250	19	4	450	20	70	HSS	Anchor rod yielding
		29	250	19	4	450	20	70	HSS	Anchor rod yielding
		29	250	19	4	450	20	70	HSS	Anchor rod yielding
Fahmy (1999)	2	68	248	31	6	900	50	406	W	Column hinging
		68	248	50	4	900	50	406	W	Column hinging
Igarashi (1992)	4	36	380	30	4	600	30	280	HSS	Anchor rod yielding
		36	380	30	4	600	30	280	HSS	Anchor rod yielding
		36	380	30	4	600	30	280	HSS	Anchor rod yielding
		36	380	32	4	600	30	280	HSS	Anchor rod yielding
Targowski (1993)	12	6	275	24	4	650	0	200	HSS	Base plate yielding
		6	275	24	4	650	0	200	HSS	Base plate yielding
		6	275	24	4	650	0	200	HSS	Base plate yielding
		6	275	24	4	650	0	200	HSS	Base plate yielding
		6	275	24	4	650	0	200	HSS	Base plate yielding
		6	275	24	4	650	0	200	HSS	Base plate yielding
		12	311	24	4	650	0	200	HSS	Base plate yielding
		12	311	24	4	650	0	200	HSS	Base plate yielding

		12	311	24	4	650	0	200	HSS	Base plate yielding
		12	311	24	4	650	0	200	HSS	Base plate yielding
		12	311	24	4	650	0	200	HSS	Base plate yielding
		12	311	24	4	650	0	200	HSS	Base plate yielding
Miyasaka (2001)	8	20	333	27	4	575	0	500	HSS	Base plate yielding
		30	346	36	4	615	0	550	HSS	Base plate yielding
		40	333	27	4	575	0	520	HSS	Base plate yielding
		40	333	27	4	575	0	500	HSS	Base plate yielding
		40	333	33	4	600	0	500	HSS	Base plate yielding
		50	346	36	4	615	0	550	HSS	Anchor rod yielding
		60	340	42	4	665	0	580	HSS	Anchor rod yielding
		60	340	42	4	665	0	550	HSS	Anchor rod yielding
Lee (2008)	4	56	248	50	4	815	50	406	W	Base plate yielding
		56	248	50	4	815	50	406	W	Base plate yielding
		56	248	31	6	815	50	406	W	Base plate yielding
		56	248	31	6	815	50	406	W	Base plate yielding
Gomez (2009)	7	50	345	19	4	515	31	610	W	Anchor rod yielding
		50	345	31	4	515	25	610	W	Anchor rod yielding
		50	345	19	4	515	38	610	W	Concrete Crushing
		50	345	19	4	515	38	610	W	Concrete Crushing
Gomez (2010)	7	25	278	19	4	560	50	280	W	Anchor rod yielding
		25	278	19	4	560	50	280	W	Anchor rod yielding
		25	278	19	8	560	50	280	W	Base plate yielding
		38	255	19	4	560	50	280	W	Anchor rod yielding
		25	278	19	4	560	50	280	W	Base plate yielding
		51	265	19	4	560	50	280	W	Anchor rod yielding

90

		25	278	19	4	560	50	280	W	Anchor rod yielding
Trautner (2015)	8	32	248	19	4	250	38	330	W	Anchor rod yielding
		32	248	19	4	250	38	330	W	Anchor rod yielding
		32	248	19	4	250	38	330	W	Anchor rod yielding
		32	248	19	4	250	38	330	W	Anchor rod yielding
		32	248	19	4	250	38	330	W	Anchor rod yielding
		32	248	19	4	250	38	330	W	Anchor rod yielding
		32	248	19	4	250	38	330	W	Anchor rod yielding
		32	248	19	4	250	38	330	W	Anchor rod yielding
Hon (1988)	26	20	320	24	2	680	20	140	W	Anchor rod yielding
		16	345	24	2	680	20	140	W	Base plate yielding
		16	345	24	2	680	20	140	W	Base plate yielding
		16	345	24	2	680	20	140	W	Base plate yielding
		20	320	24	2	680	20	140	W	Anchor rod yielding
		25	270	24	2	680	20	140	W	Anchor rod yielding
		30	255	24	2	680	20	140	W	Anchor rod yielding
		25	270	24	2	680	20	140	W	Anchor rod yielding
		25	270	24	2	680	20	140	W	Anchor rod yielding
		30	255	24	2	680	20	140	W	Anchor rod yielding
		30	255	24	2	680	20	140	W	Anchor rod yielding
		12	280	24	2	680	20	140	W	Base plate yielding
		16	280	24	2	680	20	140	W	Base plate yielding
		20	320	24	2	680	20	140	W	Anchor rod yielding
		16	390	24	2	680	20	140	W	Base plate yielding
		25	270	20	2	680	20	140	W	Anchor rod yielding
		30	255	20	2	680	20	140	W	Anchor rod yielding

91

		12	280	20	2	680	20	140	W	Base plate yielding
		16	240	20	2	680	20	140	W	Base plate yielding
		12	280	24	2	680	20	140	W	Base plate yielding
		16	240	24	2	680	20	140	W	Base plate yielding
		30	255	24	2	680	20	140	W	Anchor rod yielding
		20	320	24	2	680	20	140	W	Anchor rod yielding
		16	345	24	2	680	20	140	W	Base plate yielding
		20	320	24	2	680	20	140	W	Base plate yielding
		20	240	24	2	680	20	140	W	Base plate yielding
Melchers (1992)	10	6	533	12	2	500	20	100	W	Base plate yielding
		10	300	12	2	500	20	100	W	Anchor rod yielding
		12	300	12	2	500	20	100	W	Anchor rod yielding
		6	573	16	2	500	20	100	W	Base plate yielding
		10	300	16	2	500	20	100	W	Base plate yielding
		12	300	16	2	500	20	100	W	Base plate yielding
		6	533	12	4	500	20	100	W	Base plate yielding
		10	300	12	4	500	20	100	W	Anchor rod yielding
		6	533	16	4	500	20	100	W	Base plate yielding
		10	300	16	4	500	20	100	W	Base plate yielding
Li (2000)	7	55	576	30	4	800	50	330	HSS	Anchor rod yielding
		55	576	30	4	800	50	330	HSS	Anchor rod yielding
		55	576	30	4	800	50	330	HSS	Anchor rod yielding
		55	576	30	4	800	50	330	HSS	Anchor rod yielding
		55	576	30	4	800	50	330	HSS	Anchor rod yielding
		55	576	30	4	800	50	330	HSS	Anchor rod yielding
		55	576	30	4	800	50	330	HSS	Anchor rod yielding

		39	258	22	4	500	30	310	HSS	Anchor rod yielding
		39	258	22	4	500	30	310	HSS	Anchor rod yielding
		39	258	22	4	500	30	310	HSS	Anchor rod yielding
		39	258	22	4	500	30	310	HSS	Anchor rod yielding
		40	335	22	4	500	30	310	HSS	Anchor rod yielding
		40	335	22	4	500	30	310	HSS	Anchor rod yielding
Somiya (2002)	12	40	335	22	4	500	30	310	HSS	Anchor rod yielding
		40	335	22	4	500	30	310	HSS	Anchor rod yielding
		40	335	22	4	500	30	310	HSS	Anchor rod yielding
		40	335	22	4	500	30	310	HSS	Anchor rod yielding
		36	360	22	4	500	30	310	HSS	Anchor rod yielding
		45	345	22	4	500	30	310	HSS	Anchor rod yielding
		50	261	27.5	4	560	0	300	W	Anchor rod yielding
		50	261	27.5	4	600	0	300	W	Anchor rod yielding
		50	261	27.5	4	560	0	300	W	Anchor rod yielding
		50	261	27.5	4	600	0	300	W	Anchor rod yielding
Takamatsu (2005)	9	50	254	27.5	2	560	0	300	HSS	Anchor rod yielding
		50	254	27.5	2	560	0	300	HSS	Anchor rod yielding
		50	254	27.5	2	560	0	300	HSS	Anchor rod yielding
		50	254	27.5	2	560	0	300	HSS	Anchor rod yielding
		50	254	27.5	2	600	0	300	HSS	Anchor rod yielding
Inamatsu (2019)	2	120	345	35	8	710	0	-	W	Anchor rod yielding
		139	345	51	8	690	0	-	W	Anchor rod yielding
		15.9	379	19	4	400	0	101	W	Anchor rod yielding
Kavoura (2017)	11	15.9	379	19	4	400	0	152	W	Anchor rod yielding
		15.9	379	25	4	400	0	101	W	Base plate yielding

		15.9	379	32	4	400	0	127	W	Base plate yielding
		9.5	379	32	4	400	0	127	W	Base plate yielding
		15.9	379	32	4	400	0	127	W	Base plate yielding
		15.9	379	32	6	400	0	127	W	Concrete Crushing
		15.9	379	32	8	400	0	127	W	Concrete Crushing
		15.9	379	32	8	400	0	127	W	Concrete Crushing
		19.1	379	32	8	400	0	127	W	Concrete Crushing
		12.7	379	19	4	400	0	101	W	Anchor rod yielding
Choi & Ohi (2003)	6	9	270	12	8	205	0	230	HSS	Base plate yielding
		9	270	12	8	205	0	230	HSS	Base plate yielding
		9	270	12	8	205	0	230	HSS	Base plate yielding
		19	250	12	8	205	0	230	HSS	Base plate yielding
		19	250	12	8	205	0	230	HSS	Anchor rod yielding
		19	250	12	8	205	0	230	HSS	Anchor rod yielding

Table A2 Calculation details for empirical equations

Parameter							
Base plate Thickness, t_p (mm)	25	51	25	38	25	25	25
Base plate Fy, F_{yp} (Mpa)	278	265	278	255	278	278	278
Anchor Rod Dia, d (mm)	19	19	19	19	19	19	19
No. of Anchor Rods, N (No's)	4	4	4	4	8	4	4
Embedment Length, L (mm)	560	560	560	560	560	560	560
Grout Thickness, t_g (mm)	50	50	50	50	50	50	50
Axial Load, P (KN)	678	410	410	410	0	0	0
Base Moment, M (KN-m)	201.6	185.8	177.3	127.6	141	122	125.4
BP Length, N (mm)	356	356	356	356	356	356	356
BP Width, B (mm)	356	356	356	356	356	356	356
Column Flange Width, bf (mm)	206	206	206	206	206	206	206
Column Depth, dc (mm)	216	216	216	216	216	216	216
D_{edge} (mm)	38	38	38	38	38	38	38
AB Ultimate Strength, Fub (Mpa)	1010	1010	1010	491	1010	1010	1010
Concrete Compressive Strength, f'c (Mpa)	30.3	29.9	29.7	29.2	28.5	27.6	27.3
Failure Mode (Experimental)	Anchor rod yielding	Anchor rod yielding	Base plate yielding	Anchor rod yielding	Base plate yielding	Anchor rod yielding	Anchor rod yielding
Base Plate Yielding Limit State (Empirical)	Base plate yielding	Base plate yielding	Base plate yielding	Base plate yielding			
Anchor Rod Yielding Limit State (Empirical)							
Concrete Crushing Limit State (Empirical)	Others	Others	Others	Others			

* All the parameters and failure mode (experimental) is adopted from Gomez et al. (2010)
* Limit state empirical equations for base plate yielding, anchor rod yielding and concrete crushing are calculated from equations (1), (2) and (3), respectively.

(i) Base plate yielding limit state $= \dfrac{F_{yp} \cdot (t_p)^2}{4} \geq \left(\dfrac{P}{NB} + \dfrac{M}{\left(\frac{1}{6}\right) BN^2} \right) * \left(\dfrac{l^2}{2} \right)$ (1)

Here,

$$l = \dfrac{(B - 0.8\, b_f)}{2}$$

(ii) Anchor rod yielding limit state $= \left(0.75 * \dfrac{N}{2} * F_{ub} * \dfrac{\pi d^2}{4} \right) \geq (0.85 k f'_c\, BL - P)$ (2)

Here,

$k = 2$ (assuming that the area of the supporting foundation is sufficiently large)

$$L = (N - d_{edge}) - \sqrt{(N - d_{edge})^2 - 2\,\dfrac{P\,(M/P + N/2 - d_{edge})}{0.85 k f'_c\, B}}$$

(iii) Concrete crushing limit state $= 0.85 k f'_c \geq \left(\dfrac{P}{NB} + \dfrac{M}{\left(\frac{1}{6}\right) BN^2} \right)$ (3)

Appendix B

Typical design calculation for column subjected to combined axial load and biaxial bending

W Shape Column Capacity Design		(Axial Compression + Bi-axial Bending)	

Designation	W250X73		
Grade	ASTM A992 A572 Gr. 50	K	2.00 (Support Condition)
F_y	345 MPa	L	2000 mm
E	200000 MPa	Frame	Unbraced
G	77000 MPa		

Dimensional Properties (From CISC)

A	9290 mm²	h	225.6 mm
d	254 mm	b	254 mm
t	14.2 mm	w	8.64 mm
r_x	110 mm	r_y	64.5 mm
I_x	113000000 mm⁴	I_y	38900000 mm⁴
Z_x	990000 mm³	Z_y	464000 mm³
S_x	895000 mm³	S_y	306000 mm³
J	579000 mm³	C_w	5.56E+11 mm⁶

Input Data / **Column End Moments**

Max. Comp. Axial Force, C_f	400 kN	m_1 =	0 kN-m
Max. Major Axis Moment, M_{fx}	175 kN-m	m_2 =	175 kN-m
Max. Minor Axis Moment, M_{fy}	50 kN-m	Note: $m_1 < m_2$	

Flange Slenderness Check

b/2t   8.94

Allowable limit for Beam-Column

$145/\sqrt{F_y}$	7.81		Class 1
$170/\sqrt{F_y}$	9.15	Governs	Class 2

Allowable limit for Column only

$200/\sqrt{F_y}$ 10.77

Web Slenderness Check

h/w   26.11

Bi-axial Criteria

$(M_{fy}/S_y)/(0.9*M_{fx}/S_x)$ 0.93

Case -I   GOVERNS
Allowable limit for Beam-Column

Class 1	56.02	Governs	Class 1: $(1100/\sqrt{F_y})*(1-(0.39*(C_f/\Phi F_y A)))$
Class 2	83.78		Class 2: $(1700/\sqrt{F_y})*(1-(0.61*(C_f/\Phi F_y A)))$

Case -II

525/√Fy   28.27   Same for both Class 1 & Class 2

Allowable limit for Column only

670/√Fy   36.07

Compressive Load Capacity for Column only

KL/r_x	36.36		
KL/r_y	62.02	Governs	
λ	0.82		$λ= (KL/r)_{max}*\sqrt{(F_y/\pi^2*E)}$
n	1.34		From Literature
Comp. Resistance, C_r	2043.3 kN		$C_r= (\Phi A F_y)/(1+λ^{2n})^{1/n}$

97

Beam-Column Capacity

Flexural Strength Check

Moment Resistance, M_{rx}	**307.4** kN-m		$M_{rx} = \Phi Z_x F_y$
Moment Resistance, M_{ry}	**144.1** kN-m		$M_{ry} = \Phi Z_y F_y$
Limiting Equation	**0.92**	OK	$(M_{fx}/M_{rx}) + (M_{fy}/M_{ry})$

Cross Sectional Strength Check

Comp. Resistance, C_r	**2884.5** kN		$C_r = \Phi A F_y$
k	0.0		$k = (m_1/m_2)$
w_1	0.6		$W_1 = 0.6 - 0.4k >= 0.4$
C_{ex}	55764 kN		$c_{ex} = \pi^2 E I_x / L^2$
U_{1x}	1.00		$U_{1x} = w_1/(1-(c_f/c_{ex}))$
C_{ey}	19196 kN		$c_{ey} = \pi^2 E I_y / L^2$
U_{1y}	1.00		$U_{1y} = w_1/(1-(c_f/c_{ey}))$
Interaction Equation	**0.83**	OK	$(C_f/C_r) + (0.85 \cdot U_{1x} \cdot M_{fx})/M_{rx} + (0.6 \cdot U_{1y} \cdot M_{fy})/M_{ry}$

Overall In Plane Strength Check

Strong Axis Condition

KL/r_x	36.36		
λ	0.48		$\lambda = (KL/r_x) \cdot \sqrt{(F_y/\pi^2 \cdot E)}$
n	1.34		From Literature
Comp. Resistance, C_r	**2615.1** kN		$C_r = (\Phi A F_y)/(1+\lambda^{2n})^{1/n}$
U_{1x}	1.00		$U_{1x} = w_1/(1-(c_f/c_{ex}))$
Interaction Equation	**0.64**	OK	$(C_f/C_r) + (0.85 \cdot U_{1x} \cdot M_{fx})/M_{rx}$

Weak Axis Condition

KL/r_y	62.02		
λ	0.82		$\lambda = (KL/r_y) \cdot \sqrt{(F_y/\pi^2 \cdot E)}$
n	1.34		From Literature
Comp. Resistance, C_r	**2043.3** kN		$C_r = (\Phi A F_y)/(1+\lambda^{2n})^{1/n}$
U_{1y}	1.00		$U_{1y} = w_1/(1-(c_f/c_{ey}))$
λ	0.41		$\lambda = (L/\pi r_y) \cdot \sqrt{(F_y/E)}$
β	0.76		$\beta = 0.6 + 0.4\lambda_y <= 0.85$
Interaction Equation	**0.46**	OK	$(C_f/C_r) + (\beta \cdot U_{1x} \cdot M_{fy})/M_{ry}$

Lateral Torsonal Buckling Strength Check

Comp. Resistance, C_r	**2043.3** kN		Weak Axis Resistance
U_{1x}	1.00		From Literature (Kulak pg -270)
U_{1y}	1.00		$W_2 = 1.75 + 1.05k + 0.3k^2$
w_2	1.75		
M_u	4330.28 kN-m		$M_u = \dfrac{w_2 \pi \cdot \sqrt{EIyGJ + \left(\frac{\pi E}{L}\right)^2 \cdot I_y C_w}}{L}$
M_p	341.55 kN-m		$M_p = Z_x F_y$
M_{rx}	**307.40** kN-m		
Interaction Equation	**0.94**	OK	$(C_f/C_r) + (0.85 \cdot U_{1x} \cdot M_{fx})/M_{rx} + (\beta \cdot U_{1y} \cdot M_{fy})/M_{ry}$

RESULTS SUMMARY

Compressive Load Capacity for Column only		U. Ratio
Comp. Resistance, C_r	**2043.3** kN	**0.20**

Beam-Column Capacity		
Moment Resistance, M_{rx}	**307.4** kN-m	**0.92**
Moment Resistance, M_{ry}	**144.1** kN-m	

Cross Sectional Strength		
Comp. Resistance, C_r	**2884.5** kN	**0.83**

Overall In Plane Strength		
Strong Axis Condition		**0.64**
Comp. Resistance, C_r	**2615.1** kN	
Weak Axis Condition		**0.46**
Comp. Resistance, C_r	**2043.3** kN	

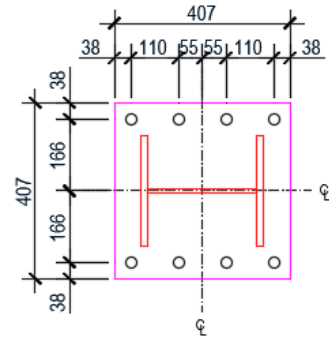| Lateral Torsonal Buckling Strength		
Comp. Resistance, C_r	**2043.3** kN	
M_u	**4330.28** kN-m	**0.94**
$0.9*M_p$	**307.40** kN-m	
M_{rx}	**307.40** kN-m	

Appendix C

Typical arrangement in the base plate for different anchor rod quantities
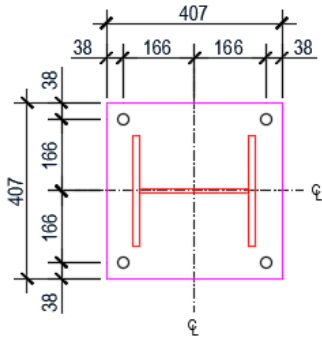
BASE PLATE WITH 4 ANCHOR BOLTS   BASE PLATE WITH 6 ANCHOR BOLTS   BASE PLATE WITH 8 ANCHOR BOLTS
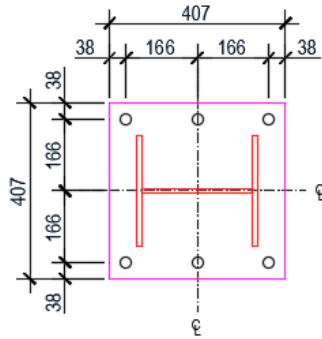
TYPICAL ARRANGEMENT FOR DIFFERENT ANCHOR ROD QUANTITY

Appendix D

Rotational Stiffness formula from Kanvinde et al. (2013)

Eccentricity, $e = M/P$

$$e_{crit} = \frac{N}{2} - \frac{P}{2.B.f_{mx}}$$

$$M_{crit} = P * e_{crit}$$

$$f = \frac{P^2}{P.B.N - 2.M.B}$$

$$Y = N - \frac{2.M}{P} \quad \text{(when } e < e_{crit}\text{)}$$

$$Y = (N - d_{edge}) - \sqrt{(N - d_{edge})^2 - 2\frac{P(M/P + N/2 - d_{edge})}{0.85kf_c' B}} \quad \text{(when } e > e_{crit}\text{)}$$

$$k = \sqrt{\frac{A_2}{A_1}}$$

$$T = f_{mx}.B.Y - P$$

$$f_{mx} = 0.85 f_c' k \le 1.7 f_c'$$

$$\Delta_{rod} = (T_{rod} \times L_{rod})/(A_{rod} \times E_{rod})$$

$$T_{rod} = T_{tension}/2$$

$$\Delta_{tension\ plate} = (T \times (L^3_{tension}/3) \times E_{plate} \times I_{plate}) + (T \times L_{tension}/A^s_{plate} \times G_{plate})$$

$$I_{plate} = B \times t^3_p/12$$

$$A^s_{plate} = (5/6) \times B \times t_p$$

When, $Y \ge m$

$$\Delta_{compression\ plate} = f_{mx} \cdot B \cdot \left(\frac{m^4}{8. E_{plate}. I_{plate}} + \frac{m^2}{2. A^s_{plate}. G_{plate}}\right)$$

When, $Y < m$

$$\Delta_{compression\ plate} = \left(\frac{f_{mx}.B}{8. E_{plate}. I_{plate}}\right)\{m^4 - (1/3)(m-Y)^3 (3m + Y)\} + \frac{f_{mx}.B.Y}{A^s_{plate}. G_{plate}}(m - Y + Y^2/2)$$

$$\Delta_{concrete} = \frac{f_{mx}}{E_{concrete}} \times d_{footing}$$

$$E_{concrete} = 4700\sqrt{f_c'}$$

When, $M_{crit}/M_y < 1$

$\theta_y = (\Delta_{rod} + \Delta_{tension\ plate} + \Delta_{compression\ plate} + \Delta_{concrete})/(s+N/2)$

When, $M_{crit}/M_y > 1$

$\theta_y = d_{footing} \times (\varepsilon_{toe\ concrete} - \varepsilon_{rod\ concrete})/(s+N/2)$

$\varepsilon_{toe\ concrete} = f/E_{concrete}$

$\varepsilon_{rod\ concrete} = \varepsilon_{toe\ concrete}\ (1 - M_y / M_{crit})$

Rotational Stiffness, $K_{y(K)} = M_y/\theta_y$

Here,

A_1 = Bearing area of plate

A_2 = Area of supporting foundation

A_{plate} = Plan area of base plate

A^s_{plate} = Shear area of base plate

A_{rod} = Area of anchor rods

B = Width of base plate

$d_{footing}$ = Depth of concrete footing

d_{edge} = Edge distance of anchor rods

$E_{concrete}, E_{plate}, E_{rod}$ = Elastic modulus of various components

e_{crit} = Critical eccentricity;

f = Bearing stresses in concrete

f_{mx} = Maximum bearing stresses in concrete

f'_c = Concrete compressive strength

G_{plate} = Shear modulus of base plate

I_{plate} = Moment of inertia of plate in bending

L_{rod} = Length of anchor rod

$L_{tension}$ = base plate edge distance

M = Applied moment

M_{crit} = Critical moment at which plate uplifts

M_y = Moment at which first yield occurs

m = Base plate edge distance

N = Length of base plate

P = Applied compressive axial load

s = Base plate edge distance

T = Total anchor rod force

$T_{tension}$ = Tensile forces in anchor rods

t_p = Thickness of base plate

Y = Bearing length for rectangular stress block

$\Delta_{concrete}$, Δ_{rod}, $\Delta_{tension\ plate}$, $\Delta_{compression\ plate}$ = Deformations of various components

$\varepsilon_{rod\ concrete}$, $\varepsilon_{toe\ concrete}$ = Strains in concrete

θ_y = rotation of base connection at yield

Rotational Stiffness formula from Eurocode 3 (2005)

Stiffness of plate, $K_1 = 0.425 * \dfrac{L_{eff}.t_c^3}{m^3}$

Stiffness of concrete, $K_2 = 0.5 * \dfrac{a_p.b_p.E_c}{E_s.h}$

Stiffness of anchor bolts, $K_3 = 2 * \dfrac{A_b}{L_{eff}}$

Where, L_{eff} is the effective length of the rod, t_c is the plate thickness, m is the rod to weld distance, E_c and E_s is the modulus of elasticity of concrete and steel, respectively, a_p is the length of the base plate, b_p is the width of the base plate, h is the depth of the foundation, A_b is the area of the rod.

Rotational Stiffness, $K_{y(EU)} = \dfrac{E_s.Z^2}{\mu.\sum(\frac{1}{K})}$

Where, Z is the distance between the resultant of the compression force and the tension in the rod, μ is the ratio between rotational stiffness and $\sum(1/K)$ is the summation of $(1/K_1)$, $(1/K_2)$ and $(1/K_3)$.

Rotational Stiffness formula from AIJ (2001)

Base Rotational Stiffness, $K_{y(J)} = \dfrac{E_s.\ n_t.\ A_b(d_t+d_c)^2}{2L_b}$

Where, E_s is the modulus of elasticity of steel, n_t is the number of anchor rods on the tension side, A_b is the cross section area of the anchor rods, d_t is the distance between the center of the column to the tension bolt center, d_c is the half of column depth, L_b is the embedded length of the anchor rods.